ABSTRACT

TRANSCEIVER DESIGN AND SYSTEM OPTIMIZATION FOR ULTRA-WIDEBAND COMMUNICATIONS

by
Hongsan Sheng

This dissertation investigates the potential promises and proposes possible solutions to the challenges of designing transceivers and optimizing system parameters in ultra-wideband (UWB) systems. The goal is to provide guidelines for UWB transceiver implementations under constraints by regulation, existing interference, and channel estimation.

New UWB pulse shapes are invented that satisfy the Federal Communications Commission spectral mask. Parameters are designed to possibly implement the proposed pulses. A link budget is quantified based on an accurate frequency-dependent path loss calculation to account for variations across the ultra-wide bandwidth of the signal.

Achievable information rates are quantified as a function of transmission distance over additive white Gaussian noise and multipath channels under specific UWB constraints: limited power spectral density, specific modulation formats, and a highly dispersive channel. The effect of self-interference (SI) and inter-symbol interference (ISI) on channel capacity is determined, and modulation formats that mitigate against this effect is identified. Spreading gains of familiar UWB signaling formats are evaluated, and UWB signals are proved to be spread spectrum. Conditions are formulated for trading coding gain with spreading gain with only a small impact on performance. Numerical results are examined to demonstrate that over a frequency-selective channel, the spreading gain may be beneficial in reducing the SI and ISI resulting in higher information rates.

A reduced-rank adaptive filtering technique is applied to the problem of interference suppression and optimum combining in UWB communications. The reduced-rank combining method, in particular the eigencanceler, is proposed and compared with a minimum mean square error Rake receiver. Simulation results are evaluated to show that

the performance of the proposed method is superior to the minimum mean square error when the correlation matrix is estimated from limited data.

Impact of channel estimation on UWB system performance is investigated when path delays and path amplitudes are jointly estimated. Cramér-Rao bound (CRB) expressions for the variance of path delay and amplitude estimates are formulated using maximum likelihood estimation. Using the errors obtained from the CRB, the effective signal-to-noise ratio for UWB Rake receivers employing maximum ratio combining (MRC) is devised in the presence of channel path delay and amplitude errors. An exact expression of the bit error rate (BER) for UWB Rake receivers with MRC is derived with imperfect estimates of channel path delays and amplitudes.

Further, this analysis is applied to design optimal transceiver parameters. The BER is used as part of a binary symmetric channel and the achievable information rates are evaluated. The optimum power allocation and number of symbols allocated to the pilot are developed with respect to maximizing the information rate. The optimal signal bandwidth to be used for UWB communications is determined in the presence of imperfect channel state information. The number of multipath components to be collected by Rake receivers is designed to optimize performance with non-ideal channel estimation.

TRANSCEIVER DESIGN AND SYSTEM OPTIMIZATION FOR ULTRA-WIDEBAND COMMUNICATIONS

by
Hongsan Sheng

A Dissertation
Submitted to the Faculty of
New Jersey Institute of Technology
in Partial Fulfillment of the Requirements for the Degree of
Doctor of Philosophy in Electrical Engineering

Department of Electrical and Computer Engineering

May 2005

APPROVAL PAGE

TRANSCEIVER DESIGN AND SYSTEM OPTIMIZATION FOR ULTRA-WIDEBAND COMMUNICATIONS

Hongsan Sheng

4/26/2005

Dr. Alexander M. Haimovich, Dissertation Advisor — Date
Professor, Department of Electrical and Computer Engineering, NJIT

4/26/05

Dr. Ali Abdi, Committee Member — Date
Assistant Professor, Department of Electrical and Computer Engineering, NJIT

4/26/04

Dr. Yeheskel Bar-Ness, Committee Member — Date
Distinguished Professor, Department of Electrical and Computer Engineering, NJIT

4/26/05

Dr. Larry J. Greenstein, Committee Member — Date
Visiting Professor, WINLAB, Rutgers University

4/26/05

Dr. Roy You, Committee Member — Date
Assistant Professor, Department of Electrical and Computer Engineering, NJIT

BIOGRAPHICAL SKETCH

Author: Hongsan Sheng

Degree: Doctor of Philosophy

Date: May 2005

Undergraduate and Graduate Education:

- Doctor of Philosophy in Electrical Engineering,
  New Jersey Institute of Technology, Newark, NJ, 2005
- Master of Science in Electrical Engineering,
  Xidian University, Xi'an, China, 1995
- Bachelor of Science in Electrical Engineering,
  Xidian University, Xi'an, China, 1992

Major: Electrical Engineering

Presentations and Publications:

H. Sheng and A. M. Haimovich, "Coding, Spreading, and Rate Scaling in UWB Systems," *submitted to IEEE Transactions on Communications*, Apr. 2005.

H. Sheng, L. Zhao, and A. M. Haimovich, "On Coding and Bandwidth Scaling in Ultra-Wideband Communications," *in Proc. the 39th Annual Conference on Information Sciences and Systems (CISS'05)*, Baltimore, Maryland, 16-18 Mar. 2005.

A. Molisch, Y. Li, Y.-P. Nakache, P. Orlik, M. Miyake, Y. Wu, S. Gezici, H. Sheng, S.Y. Kung, H. Kobayashi, H. V. Poor, A. Haimovich, and J. Zhang, "A Low-Cost Time-Hopping Impulse Radio System for High Data Rate Transmission," *EURASIP Journal on Applied Signal Processing: Special Issue on UWB - State of the Art*, vol. 2005, no. 3, pp. 397-412, Mar. 2005.

H. Sheng and A. M. Haimovich, "Impact of Channel Estimation on Ultra-Wideband Communications," *submitted to IEEE Transactions on Wireless Communications*, Jan. 2005.

H. Sheng, R. You, and A. M. Haimovich, "Performance Analysis of Ultra-Wideband Rake Receivers with Channel Delay Estimation Errors," *in Proc. the 38th Annual Conference on Information Sciences and Systems (CISS'04)*, Princeton, New Jersey, 17-19 Mar. 2004, pp. 921-926.

H. Sheng, A. M. Haimovich, A. F. Molisch, and J. Zhang, "Optimum Combining for Time Hopping Impulse Radio UWB Rake Receivers," *in Proceedings of IEEE Conference on Ultra Wideband Systems and Technologies (UWBST)*, Reston, Virginia, Nov. 2003, pp. 224-228. [Student Achievement Award]

A. F. Molisch, Y.-P. Nakache, P. Orlik, J. Zhang, Y. Wu, S. Gezici, S. Y. Kung, H. V. Poor, Y. G. Li, H. Sheng, and A. Haimovich, "An Efficient Low-Cost Time-Hopping Impulse Radio for High Data Rate Transmission," *in the 6th International Symposium on Wireless Personal Multimedia Communications (WPMC)*, Yokosuka, Kanagawa, Japan, Oct. 2003.

H. Sheng and A. M. Haimovich, "Impulse Radio Ultra-Wideband: Requirements and Implementation," *in CIE-USE/GNYC 2003 Annual Convention Student Poster Session*, Newark Airport Marriott Hotel, Sept. 27, 2003. [Poster Contest Performance Award]

H. Sheng, P. Orlik, A. M. Haimovich, L. J. Cimini, Jr., and J. Zhang, "On the Spectral and Power Requirements for Ultra-Wideband Transmission," *in Proceedings of IEEE 2003 International Conference on Communications (ICC)*, vol. 1, Anchorage, AK, May 2003, pp. 738-742.

A. F. Molisch, Y.-P. Nakache, P. Orlik, J. Zhang, S. Y. Kung, Y. Wu, H. Kobayashi, S. Gezici, H. V. Poor, Y. G. Li, H. Sheng, and A. Haimovich, (May 5th, 2003) "Mitsubishi Electric's Time-Hopping Impulse Radio Standards Proposal," *Response to Call for Contributions on Ultra-wideband Systems for IEEE P802.15 Working Group for Wireless Personal Area Networks (WPANs)*, [Online]. Available: http://www.ieee802.org/15/pub/2003/May03/03112r2P802-15_TG3a-Mitsubishi-CFP-Document.doc.

To Ying, my parents, and Jeff.

ACKNOWLEDGMENT

First and foremost, I take this opportunity to thank my advisor, Professor Alex Haimovich for his constant help, support, encouragement, and guidance regarding this dissertation and the research that went into generating it. It has truly been a great privilege to work with him. The discussions I have had with him stimulated many of the ideas presented in this dissertation. His wide knowledge and unique viewpoints made this research topic most interesting. I am grateful to him for showing me how to write and present highly technical subjects in plain English words.

Many thanks are due to my committee members for reviewing my dissertation and sharing their time and expertise. In particular, I would like to express my appreciation to Dr. Yeheskel Bar-Ness. He created a fabulous CCSPR that allowed me to interact easily with other researchers and to improve my technical knowledge and research skills. I would like to thank Dr. Ali Abdi who always brought in the right references for my research. His lectures solidified my background and proved to be very useful for my dissertation. I am also very lucky to have had Dr. Larry Greenstein as my committee member. He gave me constructive feedback and helpful comments for improving the quality of this dissertation. My special gratitude goes to Dr. Roy You with whom I co-authored one publication. He is acknowledged for many interesting discussions and for the nice moments we spent together.

I owe much to the members of Mitsubishi Electric Research Laboratories (MERL). Especially, I would like to thank Dr. Jinyun Zhang for her support and for giving me the chance to be involved with some real research projects. I enjoyed the wonderful discussions with Dr. Philip Orlik, who always found time to share his knowledge and gave me suggestions for improving my simulation scripts. Sincere thanks also go to Drs. Andy Molisch, Giovanni Vannucci, and Yves-Paul Nakache for all their invaluable help. I appreciate having had the chance to get to know them and enjoy their countless new

ideas about various research efforts. Distinguished thanks are due to Dr. Len Cimini who helped me to write my first academic paper.

Credit must also be given to Ms. Marlene Toeroek for her care and help with many practical issues. I wish to thank Ms. Clarisa González-Lenahan and Dr. Ronald Kane in the Office of Graduate Studies for their help over the years. I am also thankful to the faculty and staff of the Department of Electrical and Computer Engineering and the Office of International Students and Faculty for their constant support.

I am grateful to my colleagues in CCSPR, the intelligent people with whom I could always talk: Xinmin Deng, Dr. Li Zhao, Jason Dabin, Jianming Zhu, Nikolaus Lehmann, Hong Zhao, Dr. Debang Lao and, of course, others who work with me day and night.

My deepest gratitude goes to my wife, Ying, for her love, understanding, patience, constant encouragement, and for sharing the joys and the disappointments. Thanks for helping me believe in myself and for making my dreams come true. I cannot thank my lovely son, Jeff, enough. His coming makes my life more complete and enjoyable. He is my lucky star that speeds up my Ph.D. studying.

Finally, I wish to offer the utmost appreciation to my parents. They brought me up at a very hard time and provided me with unconditional love throughout my life. Their positive attitude towards education encouraged me to pursue a higher education that they, themselves, did not know much about.

TABLE OF CONTENTS

TABLE OF CONTENTS
(Continued)

TABLE OF CONTENTS
(Continued)

Chapter **Page**

LIST OF TABLES

LIST OF FIGURES

LIST OF FIGURES
(Continued)

Figure **Page**

LIST OF FIGURES
(Continued)

Figure **Page**

LIST OF FIGURES
(Continued)

Figure **Page**

CHAPTER 1

INTRODUCTION

Ultra-wideband (UWB) radio is a promising technology with uniquely attractive features inviting major advances in wireless communications, networking, radar, imaging, and position raging systems. This chapter overviews the current development status of UWB systems, discusses the potentials and challenges, and summarizes the outline of the dissertation.

1.1 Current Development Status

1.1.1 Regulations

Ultra-wideband technology has received increasing interest recently at both the theoretical as well as the practical implementation levels [1, 2, 3, 4, 5, 6, 7, 8, 9, 10]. Adminstration organizations have been developing regulations to permit the introduction of ultra-wideband devices. Worldwide regulatory activities are focused on the ITU-R Task Group 1/8. In Europe, the European Telecommunications Standards Institute (ETSI) drafted European rules for UWB emissions. In the USA, the Federal Communications Commission (FCC) issued the rules, referred to as the First Report and Order, in February 2002 [11].

By the FCC's emission limits in the form of a spectral mask, a UWB system can use the FCC Part 15 rules from 3.1 GHz to 10.6 GHz with a peak value of -41.3 dBm/MHz. Outside of this band, the transmitted power must be decreased. From 0.96 GHz to 1.61 GHz, the reduction in admissible transmitted power is necessary to protect GPS transmissions. To protect PCS transmission for outdoor systems in the band from 1.99 GHz to 3.1 GHz, the required backoff is 20 dB, rather than the 10 dB for indoor systems.

1.1.2 Major UWB Schemes

At first, a UWB was conveyed as a carrierless and baseband communication technique known as impulse radio (IR) [12]. According to the new FCC regulation, an intentional UWB device is defined as one that has a bandwidth equal to or greater than 20% of the center frequency, or that has a bandwidth equal to or greater than 500 MHz. Given the recent spectral allocation and the new definition of UWB, any technology that uses more than a 500 MHz spectrum can be regarded as UWB as long as it is within current emission restrictions. New methods emerging today use technologies by direct sequence spread spectrum, referred to as DS-UWB [13, 14], or multiband orthogonal frequency division multiplexing (MB-OFDM) [15, 16, 17].

Impulse radio underlies the physical layer recently proposed for low-rate applications because of the relatively low implementation complexity associated with carrierless pulses. The IR UWB systems operate across a wide range of the frequency spectrum by sending sequences of sub-nanosecond short pulses. Due to the short duration of the pulses, the spectrum of the UWB signal can be several gigahertz wide. From a hardware implementation perspective, an IR transceiver has inherently lower complexity given the fact that RF carriers are eliminated [18].

Ultra-wideband technologies have been proposed as alternative air interfaces for emerging wireless personal area networks (WPAN's) and wireless body area networks (WBAN's). In particular, IEEE 802.15.3a has been established to investigate potential solutions for high data rate, short range communications [19], while IEEE 802.15.4a is focused on low data rate, low power, and longer range communications as well as high precision ranging/location [20].

1.1.3 UWB Channels

An attractive feature of UWB is its ability to resolve multipath. Numerous investigations have confirmed that the UWB channel can be resolved into a significant number of distinct multipath components [21, 22, 23, 24].

The key features of the UWB channel model are summarized below. The path loss is by a law of d^{-n}, where d is the transmitter-receiver distance, and n is the path loss exponent. A line-of-sight (LOS) path loss exponent ranges from 1 in a corridor to about 2 in an office environment. Non-line-of-sight (NLOS) exponents typically range from 3 to 4 for soft NLOS, and from 4 to 7 for hard NLOS [22]. Due to the frequency dependence of propagation effects in a UWB channel, over a wide bandwidth, the pathloss is a function of frequency as well as of distance.

A modified Saleh-Valenzuela (SV) channel model is widely used to model the impulse response of the UWB multipath channel [25]. Measurements show that the UWB channel has an inherently sparse structure [26]. The arrival of paths is in clusters. The distributions of the cluster arrival times and ray arrival times are assumed as Poisson random processes. The power delay profile (PDP) of a cluster and a ray is assumed to be a decaying exponential. The distribution of the small-scale amplitudes is assumed to be a lognormal fading in [21]. The standard deviation of a cluster and ray fading term is 3.3941 dB. The amplitude is also assumed to be Nakagami distributed in [22]. The Nakagami fading parameter m is a lognormal random variable, with delay-dependent mean and variance. These two channel models above are from different measurement techniques (frequency or time domain sounding), different signal bandwidth, and different environment [27]. Block fading is assumed to model the time-varying channel with a low moving speed.

1.2 Ultra-Wideband Systems: Promises and Challenges

Due to limits imposed by regulatory restrictions, a UWB device is authorized to operate in a wide bandwidth under the constraints of a low power spectral density and a specific spectral mask. The wide bandwidth of UWB signals with low power spectral density (PSD) implies that such systems have potential that promises to provide a high data rate for short range communications. Large bandwidth also enables not only large spreading ratios, but very low coding rates. The spectral mask challenges the design of UWB pulse waveforms employed by impulse radio UWB systems.

A core novelty underlying the use of UWB is the ability to optimally cohabit in the frequency band currently occupied by existing applications without causing harmful interference. This opens promising opportunities for a variety of applications including a possible physical layer for emerging WPAN's and WBAN's. However, narrowband interference emitted by existing networks in close proximity has to be suppressed.

One promise of UWB is that a very large bandwidth results in fine resolution of multipath arrivals, since the impulse nature of the transmitted waveforms prevents significant overlap [28]. This in turn leads to reduced fading per resolved path. One attractive feature of UWB is the ability to resolve the multipath components. A Rake receiver with maximum ratio combining (MRC) can be employed to exploit the multipath diversity. However, practical Rake receivers require knowledge of multipath delays and amplitudes. In practice, this is estimated through pilot aided channel estimation, producing imperfect channel state information (CSI), which leads to degraded performance.

Therefore, transceiver implementations for UWB systems are particularly challenging due to regulation, interference, and channel estimation issues. This dissertation investigates the potential promises and proposes possible solutions to the above challenges. The goal is to provide guidelines for the design of optimal transceiver parameters by capturing the specific characteristics of UWB systems.

1.3 Outline of the Dissertation

The main topics of this dissertation are:

1. Pulse waveform design for UWB transmission
2. UWB channel capacity computation as a function of distance
3. Interference suppression and optimum combining for UWB
4. Impact of channel estimation on UWB performance and transceiver design

The first topic is covered in Chapter 2, the second, in Chapter 3, the third, in Chapter 4, and the fourth, in Chapters 5 and 6. The chapter outlines are as follows:

Chapter 2 proposes a new UWB pulse shape that satisfies the FCC spectral mask. A possible implementation of this pulse is presented based on a general Gaussian pulse passed through a highpass filter. Using this pulse, the link budget is calculated to quantify the relationship between data rate and distance. The proposed pulses will be used in discussions in the rest of the chapters.

Chapter 3 evaluates achievable information rates of a single-user UWB system under specific UWB constraints: limited PSD, specific modulation formats, and a highly dispersive channel. The information rates of several modulation formats are evaluated as a function of transmitter-receiver separation for the additive white Gaussian noise (AWGN) and the UWB multipath channel. Conditions are formulated for trading coding gain with spreading gain with only a small impact on performance.

Chapter 4 applies a reduced-rank adaptive filtering technique to the problem of interference suppression in UWB communications. The reduced-rank optimum combining method, in particular the eigencanceler, is compared with minimum mean square error (MMSE) Rake receiver. Simulation is performed to show that the eigencanceler is effective in suppressing interference and requires a shorter data record than MMSE.

Chapter 5 investigates the impact of non-idea estimates on system performance when path delays and path amplitudes are jointly estimated. Pilot symbols are transmitted over

a multipath channel to estimate path delays and path amplitudes. The Cramér-Rao bounds (CRB's) of the variance of the estimate of path delays and path amplitudes are derived. Using the errors obtained from the CRB, the average signal-to-noise ratio (SNR) and bit error rate (BER) are analyzed for a Rake receiver employing MRC. The effective SNR and exact BER are expressed in terms of the number of paths and the number of pilot symbols.

Chapter 6 designs transceiver parameters such as the fraction of a transmitted packet constituted by the pilot symbols, signal bandwidth, and the number of diversity paths used at the receiver, when the path estimation errors are taken into account. To achieve this goal, the derived BER in Chapter 5 is used as part of a binary symmetric channel (BSC), and the achievable information rates are evaluated.

Chapter 7 summarizes the observations throughout this dissertation and proposes future potential research topics.

CHAPTER 2

PULSE WAVEFORM DESIGN FOR UWB TRANSMISSION

Impulse radio UWB systems communicate using a baseband signal composed of sequences of short duration pulses. Spectral masks imposed by the regulatory restrictions challenge the design of UWB pulse waveforms. In this chapter, a new pulse waveform is proposed that satisfies the FCC spectral mask. Using this pulse, the link budget is calculated to quantify the relationship between data rate and distance. It is shown that UWB can be a good candidate for high rate transmission over short ranges with the capability for reliably transmitting 100 Mbps over distances of about 10 meters.

2.1 Introduction

Ultra-wideband technology has been proposed as an alternative air interface for WPAN's because of its low power spectral density, high data rate, and robustness to multipath fading. The FCC has permitted UWB devices to operate using spectrum occupied by existing radio services as long as emission restrictions, in the form of spectral masks, are met [11].

Impulse radio UWB does not use a sinusoidal carrier to shift the signal to a higher frequency, but instead communicates with a baseband signal composed of subnanosecond pulses (referred to as *monocycles*) [12]. Impulse radio systems employ a pulse train with pulse amplitude modulation (PAM) or pulse-position modulation (PPM). Previously, the UWB systems using PAM [29] and PPM [30] have been analyzed, with particular attention to distance as a function of throughput. However, the standard monocycles used in [29] and [30] do not satisfy the FCC spectral rules. Here, the transmission range is analyzed as a function of data rate using a new pulse shape that meets the FCC regulations.

In Section 2.2, the PSD of the Gaussian-based monocycle which does not satisfy the regulatory rules is computed. A new pulse that does meet the FCC emission key is

proposed in Section 2.3. This pulse is based on higher-order derivatives of the Gaussian pulse. In Section 2.4, the transmission range and data rate of a UWB system using the proposed pulse is presented. A possible implementation of the proposed pulse is presented in Section 2.5. Conclusions are drawn in Section 2.6.

2.2 Gaussian Pulse and Spectrum

A Gaussian pulse is one candidate for the monocycle in UWB impulse radio systems. Due to the large bandwidth (occupied from DC to several GHz), antennas used in UWB systems need to be optimized for a wide range of frequencies, and the pulse waveform distortion by the antennas has to be considered [31]. The characteristics of UWB antennas are complicated. In this dissertation, it is useful to model the effect of the antenna system in the UWB transmitted pulse approximately as a derivative operation [32]. Due to the derivative characteristics of the antenna, if a Gaussian pulse is transmitted, the output of the transmitter antenna can be modelled by the first derivative of the Gaussian pulse. Therefore, if a general Gaussian pulse is given by

$$x(t) = \frac{A}{\sqrt{2\pi}\sigma} \exp(-\frac{t^2}{2\sigma^2}), \tag{2.1}$$

then the output of the transmitter antenna will be

$$x^{(1)}(t) = -\frac{At}{\sqrt{2\pi}\sigma^3} \exp(-\frac{t^2}{2\sigma^2}), \tag{2.2}$$

where the superscript $^{(n)}$ denotes the n-th derivative. The pulse at the output of the receiver antenna is then given by

$$x^{(2)}(t) = A(\frac{t^2}{\sqrt{2\pi}\sigma^5} - \frac{1}{\sqrt{2\pi}\sigma^3}) \exp(-\frac{t^2}{2\sigma^2}). \tag{2.3}$$

A UWB transmitted signal using PAM, with uniformly spaced pulses over time can be represented as

$$s(t) = \sum_{k=-\infty}^{\infty} a_k x^{(n)}(t - kT), \tag{2.4}$$

where T is the pulse-spacing interval and the sequence $\{a_k\}$ represents the information symbol. The PSD of the transmitted signal, $S(f)$, is [33, p. 207]

$$S_t(f) = \frac{\sigma_a^2}{T} |X_n(f)|^2 + \frac{\mu_a^2}{T^2} \sum_{k=-\infty}^{\infty} \left| X_n(\frac{k}{T}) \right|^2 \delta(f - \frac{k}{T}), \tag{2.5}$$

where $X_n(f)$ is the Fourier transform of the n-th derivative of a Gaussian pulse, σ_a^2 and μ_a are the variance and mean, respectively, of the symbol sequence $\{a_k\}$, and $\delta(\cdot)$ is the Dirac delta function. The second term in (2.5) is composed of discrete spectral lines and will vanish if the information symbols have zero means. In what follows, it is assumed that this is true and also that $\sigma_a^2 = 1$. Strictly speaking, the duration of the Gaussian pulse and all of its derivatives is infinite. Here, the pulse width, T_p, is defined as the interval in which 99.99% of the energy of the pulse is contained. Using this definition, it can be shown that $T_p \approx 7\sigma$ for the first derivative of the Gaussian pulse.

The FCC has issued UWB emission limits in the form of a spectral mask for indoor and outdoor systems [11]. In the band from 3.1 GHz to 10.6 GHz, UWB can use the FCC Part 15 rules with a peak value of -41.3 dBm/MHz. Outside of this band, the PSD must be decreased. From 0.96 GHz to 1.61 GHz, the reduction in admissible transmitted power is necessary to protect GPS transmissions. To protect PCS transmission for outdoor systems in the band from 1.99 GHz to 3.1 GHz, the required backoff is 20 dB, rather than the 10 dB for indoor systems.

In Figure 2.1, the normalized PSD for the first derivative ($n = 1$) of the Gaussian pulse is plotted for several values of the pulse width, T_p. The normalization factor is the peak value allowed by the FCC, -41.3 dBm/MHz. It is clear that the PSD of the first derivative pulse does not meet the FCC requirement no matter what value of the pulse

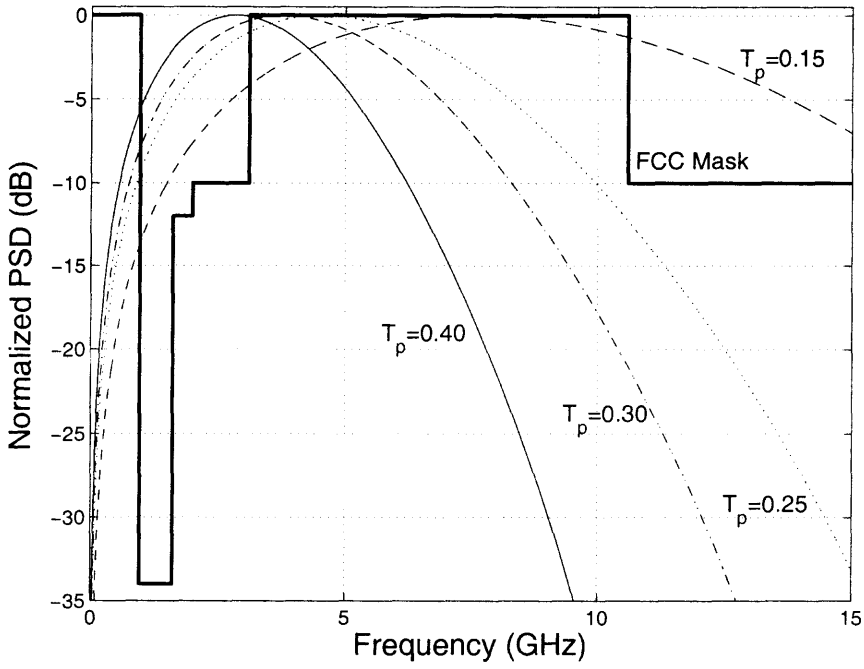

Figure 2.1 Power spectral density for the first-derivative Gaussian pulse for various values of the pulse width. The FCC spectral mask for indoor systems is shown for comparison.

width is used. Therefore, a new pulse shape must be found that satisfies the FCC emission requirements.

One possibility is to shift the center frequency and adjust the bandwidth so that the requirements are met. This could be done by modulating the monocycle with a sinusoid to shift the center frequency and by varying the values of σ. For example, by shifting the center frequency of the monocycles by 3 GHz, for a pulse width $T_p = 0.3$ ns, the PSD will fall completely within the spectral mask for the range $3.1 - 10.6$ GHz. In Figure 2.2, two different modulated monocycles, with center frequencies of 5.2 GHz and 8.5 GHz, are illustrated. Impulse UWB, however, is a carrierless system; modulation will increase the cost and complexity. Therefore, alternative approaches are required for obtaining a pulse shape which satisfies the FCC mask.

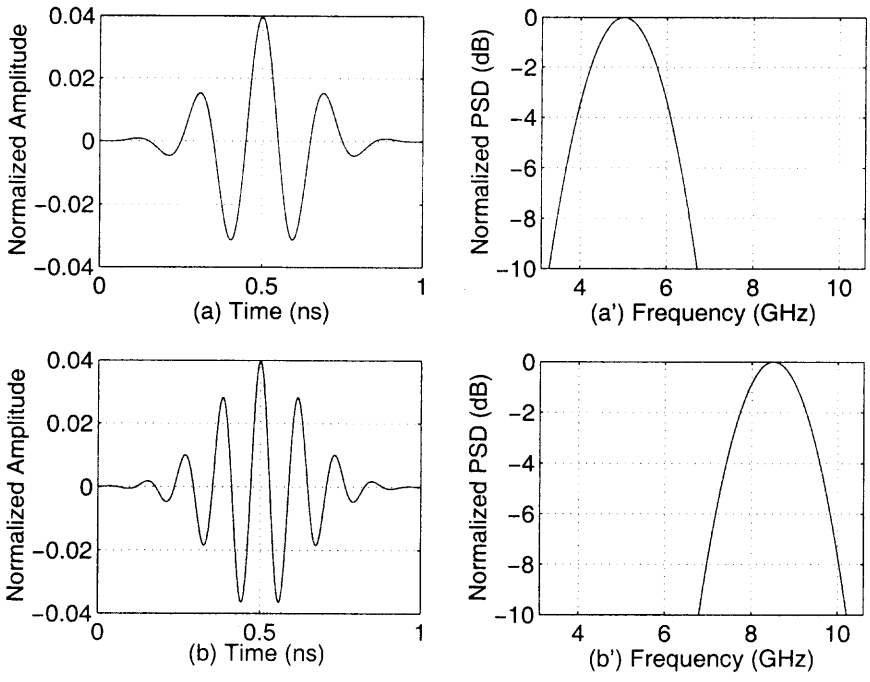

Figure 2.2 Two modulated Gaussian pulses and their power spectral densities. (a) The modulation center frequency is 5.2 GHz; (b) The modulation center frequency is 8.5 GHz.

2.3 New Pulse Shape Satisfying FCC Mask

The design of UWB pulse waveforms has been investigated extensively [34, 35]. In this dissertation, higher-order derivatives of the Gaussian pulse are proposed. In the time domain, the higher-order derivatives of the Gaussian pulse resemble sinusoids modulated by a Gaussian pulse-shaped envelope [36]. As the order of the derivative increases, the number of zero crossings in time also increases; more zero crossings in the same pulse width correspond to a higher "carrier" frequency sinusoid modulated by an equivalent Gaussian envelope. These observations lead to considering higher-order derivatives of the Gaussian pulse as candidates for UWB transmission. Specifically, by choosing the order of the derivative and a suitable pulse width, a pulse can be found which satisfies the FCC's mask. In this section, the spectrum of the higher-order derivatives of the Gaussian pulse is derived, and a pulse shape is chosen that meets the emission requirements.

2.3.1 Spectrum of Pulses Based on Higher-Order Derivatives

Using the general Gaussian pulse in (2.1), its n-th derivative can be determined recursively from

$$x^{(n)}(t) = -\frac{n-1}{\sigma^2}x^{(n-2)}(t) - \frac{t}{\sigma^2}x^{(n-1)}(t). \tag{2.6}$$

The Fourier transform of the n-th order derivative pulse is

$$X_n(f) = A(j2\pi f)^n \exp\{-\frac{(2\pi f\sigma)^2}{2}\}. \tag{2.7}$$

Consider the amplitude spectrum of the n-th derivative

$$|X_n(f)| = A(2\pi f)^n \exp\{-\frac{(2\pi f\sigma)^2}{2}\}. \tag{2.8}$$

The frequency at which the maximum value of (2.8) is attained, the *peak emission frequency*, f_M, can be found by differentiating (2.8) and setting it equal to zero. Differentiating (2.8) gives

$$\frac{d|X_n(f)|}{df} = A(2\pi f)^{n-1}2\pi \exp\{-\frac{(2\pi f\sigma)^2}{2}\}[n - (2\pi f\sigma)^2]. \tag{2.9}$$

The peak emission frequency then must satisfy $2\pi f_M\sigma = \sqrt{n}$, and the maximum value of the amplitude spectrum is

$$|X_n(f_M)| = A(\frac{\sqrt{n}}{\sigma})^n \exp(-\frac{n}{2}). \tag{2.10}$$

Define the normalized PSD of the transmitted pulse, $\left|\tilde{S}_t(f)\right|$, as

$$\left|\tilde{S}_t(f)\right| \triangleq \frac{|X_n(f)|^2}{|X_n(f_M)|^2} = \frac{(2\pi f\sigma)^{2n}\exp\{-(2\pi f\sigma)^2\}}{n^n\exp(-n)}, \tag{2.11}$$

which has a peak value of 1 (0 dB). If the n-th derivative of the Gaussian pulse is considered as the UWB transmitted pulse, then the PSD of the transmitted signal is given by

$$|S_t(f)| \triangleq A_{\max}\left|\tilde{S}_t(f)\right| = \frac{A_{\max}(2\pi f\sigma)^{2n}\exp\{-(2\pi f\sigma)^2\}}{n^n\exp(-n)}, \tag{2.12}$$

where $A_{\max}$ is the peak PSD that the FCC will permit. The parameters n and σ can now be chosen to satisfy the FCC mask. In the next subsection, an algorithm will be presented which provides the appropriate pulse shape.

2.3.2 New Pulse Shape Parameters

The objective here is to obtain a pulse that matches the FCC's PSD mask as closely as possible, but which also maximizes the bandwidth. Values of (n, σ) in (2.11) are chosen to achieve this goal. Note that the FCC spectral mask has several corner points and that any pulse spectrum must pass through or be below the mask at the corner frequencies (0.96, 1.61, 1.99, 3.1, and 10.6 GHz). The approach used to find (n, σ) is to first fix f equal to the frequency of one of the corner points. This enables us to rewrite (2.11) in the following form

$$20n \log_{10}(2\pi f\sigma) - \frac{10(2\pi f\sigma)^2}{\ln 10} - 10n \log_{10} n + \frac{10n}{\ln 10} - R_{\text{dB}} = 0, \tag{2.13}$$

where $R_{\text{dB}} \triangleq 10 \log_{10} \left|\tilde{S}_t(f)\right|$ is the backoff value in the spectral mask between the chosen corner point and -41.3 dB (for example, if $f = 10.6$ GHz, $R_{\text{dB}} = -10$ dB for indoor systems). Then start with $n = 1$ and solve (2.13) for σ. Notice that (2.13) has two roots for $f\sigma$ with respect to a fixed R_{dB} and n. Taking the peak emission frequency as one end point, the bisection method, or some other root-finding algorithm, can be used to find the roots of (2.13) numerically. Once σ is found, one simply checks to see if (2.11) using the above value of (n, σ) will meet the FCC mask at the other corner points. If not, n is increased and a new σ from (2.13) is found. In Figures 2.3 and 2.4, the normalized PSD's for the first-order through tenth-order derivatives of the Gaussian pulse are shown for indoor and outdoor systems respectively. Note that there are different optimum values of σ for indoor and outdoor systems. For indoor systems, at least the fifth-order derivative should be used, while for outdoor systems, the seventh or higher should be used. To keep the bandwidth

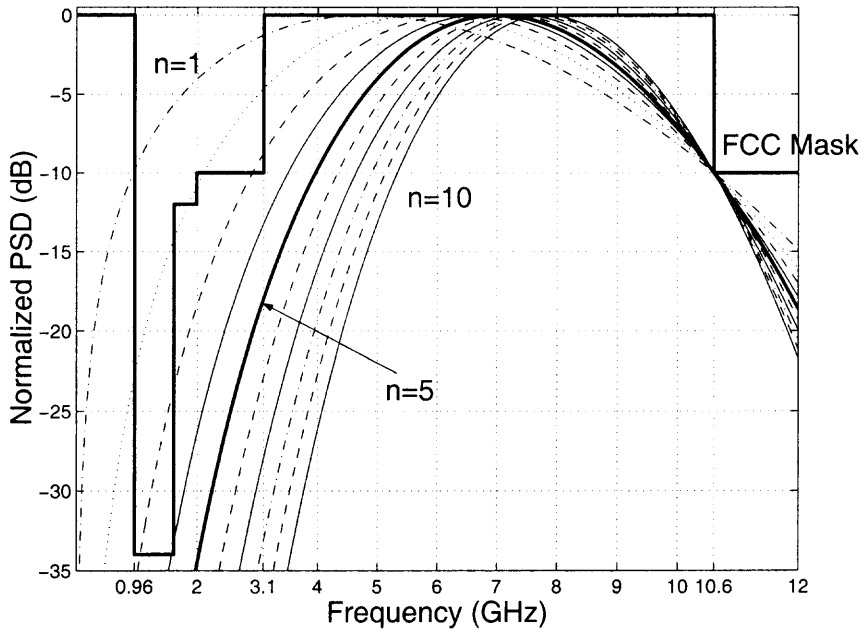

Figure 2.3 PSD of the higher-order derivatives of the Gaussian pulse for UWB indoor systems.

as wide as possible, the fifth-order derivative should be chosen for indoor systems and the seventh order for outdoor systems.

As before, the time duration of these pulses is infinite. Using the definition of pulse width previously given, for $n = 5$, there is $T_p \approx 8.5\sigma$. For convenience, $T_p = 10\sigma$ is chosen in this dissertation. The maximum PSD can be controlled by changing the value of the amplitude A of the pulse. In Tables 2.1 and 2.2, the pulse shapes are summarized with the parameter σ, the frequencies where the spectrum is 3 dB down from the peak, the peak emission frequency, and the 3-dB bandwidth, $W_{3\text{dB}}$, for indoor and outdoor systems, respectively, where the frequency is in GHz. These results show that the pulse width will be less than 1 nanosecond for all cases, and the 3-dB bandwidth is 2.5 GHz or greater. Note that to transmit the fifth derivative over the air, the Gaussian pulse must be filtered to the fourth-order derivative.

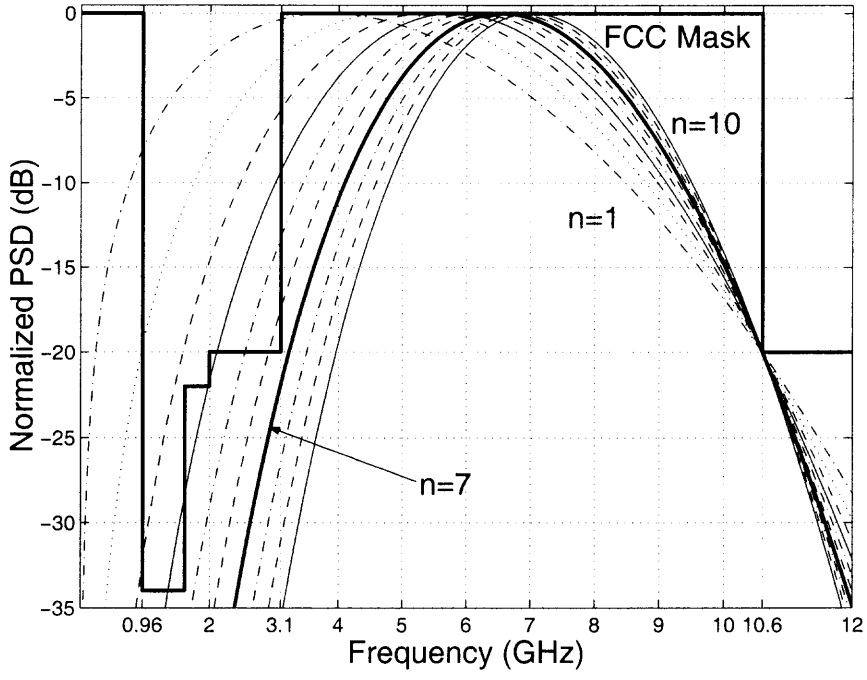

Figure 2.4 PSD of the higher-order derivatives of the Gaussian pulse for UWB outdoor systems.

Table 2.1 Summary of the Parameters for UWB Indoor Systems

n	σ(ps)	f_L	f_H	f_M	W_{3dB}(GHz)
1	33	2.31	7.84	4.79	5.53
2	39	3.57	8.33	5.78	4.76
3	44	4.33	8.60	6.34	4.28
4	47	4.85	8.79	6.72	3.93
5	51	5.25	8.92	7.01	3.67
6	53	5.57	9.03	7.23	3.46
7	57	5.83	9.12	7.42	3.29
8	60	6.05	9.19	7.57	3.14
9	62	6.24	9.26	7.70	3.01
10	64	6.41	9.30	7.81	2.90

Table 2.2 Summary of the Parameters for UWB Outdoor Systems

n	σ(ps)	f_L	f_H	f_M	W_{3dB}(GHz)
1	42	1.85	6.27	3.84	4.42
2	47	2.96	6.91	4.79	3.95
3	51	3.66	7.29	5.37	3.62
4	55	4.17	7.55	5.78	3.38
5	58	4.57	7.76	6.09	3.19
6	62	4.89	7.92	6.34	3.03
7	64	5.15	8.05	6.55	2.90
8	67	5.38	8.16	6.72	2.79
9	70	5.57	8.26	6.87	2.69
10	72	5.75	8.35	7.01	2.60

2.4 Link Budget and Data Rate

The bandwidth of the UWB signal is very large and should be able to transmit at a very high data rate; in particular, 100 Mbps should be possible over short distances. In this section, the permitted distances and data rates are determined using a simple link budget analysis. In [29], the distance as a function of throughput was analyzed for PAM UWB systems. However, the analysis was not performed using the more realistic monocycles presented here, and the path loss was considered constant over the bandwidth of the signal. In this section, the range and data rate relation are quantified for an M-PAM using the fifth derivative of the Gaussian pulse as the transmitted monocycle, and a realistic wideband path loss model.

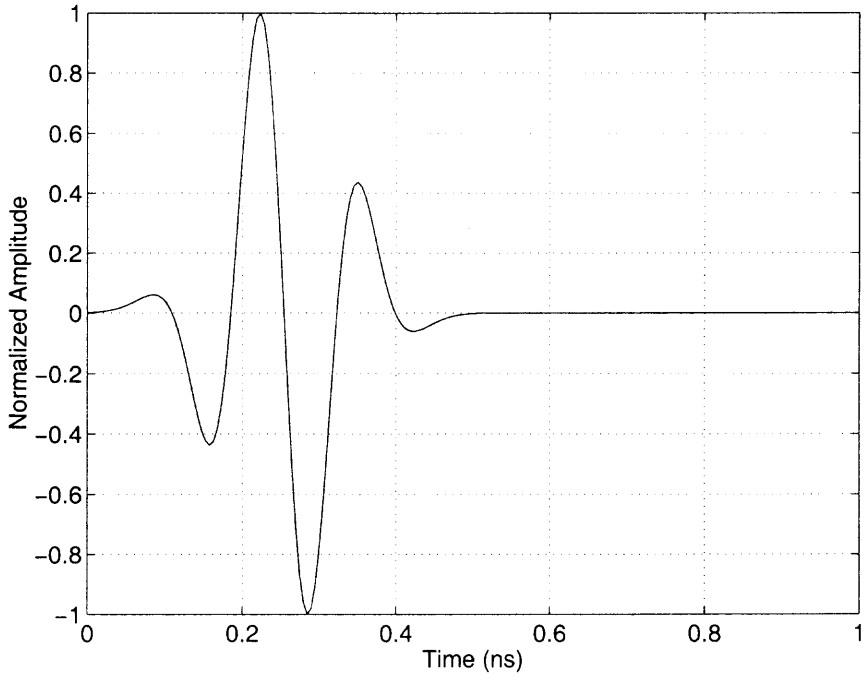

Figure 2.5 The pulse shape for the fifth derivative of the Gaussian pulse.

In the assumed indoor system, the transmitted monocycle over the air, $y_T(t)$, is the fifth-derivative of the Gaussian pulse,

$$y_T(t) = A(-\frac{t^5}{\sqrt{2\pi}\sigma^{11}} + \frac{10t^3}{\sqrt{2\pi}\sigma^9} - \frac{15t}{\sqrt{2\pi}\sigma^7})\exp(-\frac{t^2}{2\sigma^2}), \tag{2.14}$$

where A is a constant chosen to meet the limitations set by the FCC. The normalized pulse waveform is shown in Figure 2.5. For the outdoor system, the transmitted monocycle is the seventh-derivative of the Gaussian pulse,

$$y_T(t) = A(-\frac{t^7}{\sqrt{2\pi}\sigma^{15}} + \frac{21t^5}{\sqrt{2\pi}\sigma^{13}} - \frac{105t^3}{\sqrt{2\pi}\sigma^{11}} + \frac{105t}{\sqrt{2\pi}\sigma^9})\exp(-\frac{t^2}{2\sigma^2}). \tag{2.15}$$

In the following analysis, only indoor systems are considered, and additive white Gaussian noise is assumed at the receiver with a free-space propagation channel model. It is noted that the received pulse waveform at the output of the receiver antenna is the sixth derivative of the Gaussian pulse

$$y(t) = A(\frac{t^6}{\sqrt{2\pi}\sigma^{13}} - \frac{15t^4}{\sqrt{2\pi}\sigma^{11}} + \frac{45t^2}{\sqrt{2\pi}\sigma^9} - \frac{15}{\sqrt{2\pi}\sigma^7})\exp(-\frac{t^2}{2\sigma^2}), \tag{2.16}$$

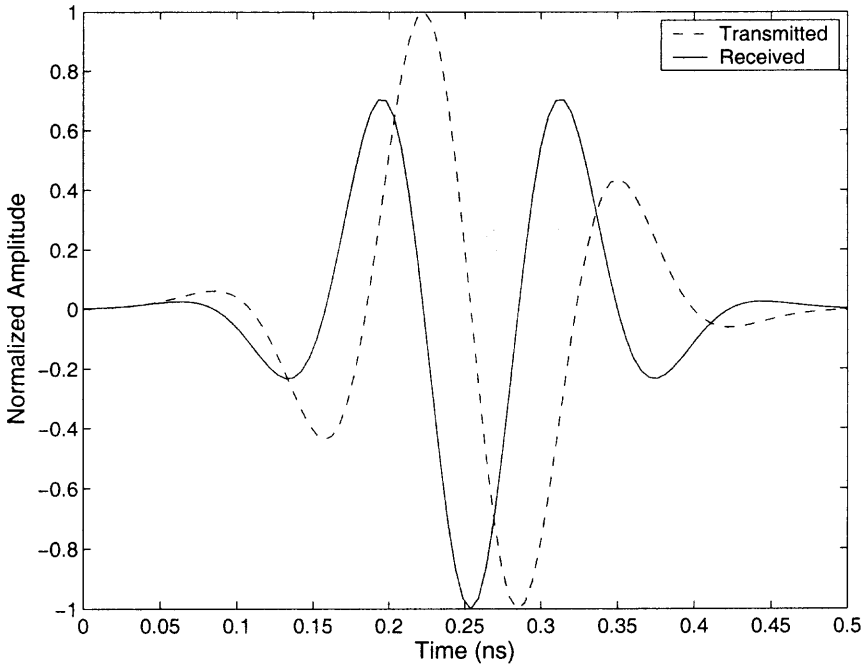

Figure 2.6 Comparison of the transmitted (the fifth derivative of the Gaussian pulse) and the received pulse (the sixth derivative of the Gaussian pulse).

and its amplitude spectrum is

$$|Y(f)| = A(2\pi f)^6 \exp\{-\frac{(2\pi f\sigma)^2}{2}\}. \tag{2.17}$$

Figure 2.6 shows a comparison between the transmitted and received pulses which are respectively, the fifth and sixth derivative of the Gaussian pulse.

For a narrowband signal, the received power at distance d is given by

$$P_s(\mathsf{d}) = \frac{P_t}{L_s(\mathsf{d})}, \tag{2.18}$$

and the free-space path loss $L_s(\mathsf{d})$, is given by [37]

$$L_s(\mathsf{d}) = \frac{(4\pi)^2 d^2 f_c^2}{G_t G_r c^2}, \tag{2.19}$$

where P_t is the transmitted power, G_t and G_r are the transmitted and received antenna gains respectively, f_c is the carrier frequency, and c is the speed of light.

The PSD is very wideband for a UWB transmission system. Therefore, equation (2.19) must be modified to account for variations across the bandwidth of the signal. In particular, the transmitted and received powers should be calculated using the integral of the PSD within a frequency region, and the total transmitted power should be based on the FCC restrictions. Note that G_t and G_r are also a function of the frequency. In this dissertation, it is assumed that an ideal antenna is used so that G_t and G_r are assumed constant over the frequency range. Therefore, the transmitted power is

$$P_t = \int_{-\infty}^{+\infty} |S_t(f)|\, df = \int_{-\infty}^{+\infty} A_{\max} \left|\tilde{S}_t(f)\right| df, \tag{2.20}$$

where $|S_t(f)|$ and $\left|\tilde{S}_t(f)\right|$ are defined in (2.12) and (2.11), respectively, and $A_{\max} = -41.3$ dBm/MHz is the maximum PSD permitted. Based on these parameters and $\sigma = 51$ ps and $n = 5$, the total transmitted power is $P_t = -5.1$ dBm. If the received signal is assumed to occupy a band from f_L to f_H, the received power at distance d becomes

$$P_s(\mathsf{d}) = \int_{f_L}^{f_H} \frac{A_{\max} \left|\tilde{S}(f)\right|}{L_s(\mathsf{d}, f)} df, \tag{2.21}$$

where $\tilde{S}(f)$ is the PSD of the received pulse, and $L_s(\mathsf{d}, f)$ is the frequency-dependent path loss for the free-space propagation model. The center frequency in (2.19) is replaced by the variable f. With this frequency-dependent path loss, the received power becomes

$$P_s(\mathsf{d}) = \frac{A_{\max} G_t G_r c^2}{(4\pi)^2 \mathsf{d}^2} \int_{f_L}^{f_H} \frac{\left|\tilde{S}(f)\right|}{f^2} df. \tag{2.22}$$

In the calculations that follow, the noise spectral density is $N_0 = kT_0F_0L_M = -102.83$ dBm/MHz, where k is Boltzmann's constant 1.38×10^{-23} Joules/K, T_0 is room temperature (300 K), the noise figure is $F_0 = 6$ dB, and a link margin, L_M, of 5 dB is assumed. Normalized by the maximum signal PSD, it follows $N_0/A_{\max} \approx -62$ dB. Then, if the receiver bandwidth is chosen corresponding to a 62-dB signal bandwidth, the maximum SNR can be achieved.

The received power (2.22) necessary at a distance, d to achieve a given average SNR can be computed from the relation

$$P_s(\mathsf{d}) = \mathsf{SNR} \cdot P_N, \tag{2.23}$$

where P_N is the received noise power and is equal to $N_0 W$, and where W is the noise equivalent bandwidth of the receiver. If the symbol rate is assumed to be equal to the pulse repetition rate, a single UWB pulse is transmitted for each data symbol, and the energy per information symbol equals the energy per pulse. Then, the average output SNR is given by

$$\mathsf{SNR} = \frac{E_s/T_s}{N_0 W} = \frac{E_s R_s}{N_0 W} = \frac{E_b}{N_0} \cdot \frac{R_b}{W}, \tag{2.24}$$

where E_s is the received symbol energy, T_s is the symbol duration, and R_s is the symbol rate. For uncoded systems, $E_s = E_b \log_2 M$ and $R_s = R_b / \log_2 M$, where E_b is the bit energy and R_b is the bit rate. The ratio $\beta \triangleq W/R_b$ is related to the duty cycle of the signal and can be thought of as the processing gain. By increasing the occupied bandwidth of the pulse or reducing the pulse repetition frequency, the overall data rate and the distance can be increased. This factor is what allows UWB systems to operate at a very low average transmit PSD while achieving useful data rates and transmission ranges [29]. For a target BER, the required E_b/N_0 for PPM and PAM can be obtained in [33, p. 262-268].

From (2.22), (2.23), and (2.24), the maximum distance d for a required E_b/N_0 is expressed as a function of the data rate R_b

$$\mathsf{d} = \frac{c}{4\pi} \sqrt{\frac{A_{\max} G_t G_r}{E_b/N_0 \cdot R_b N_0} \int_{f_L}^{f_H} \frac{\left|\tilde{S}(f)\right|}{f^2} df}. \tag{2.25}$$

From (2.25), it is observed that the transmission range can be increased for a given data rate by increasing the receiver antenna gain, using channel coding, and/or reducing the noise figure.

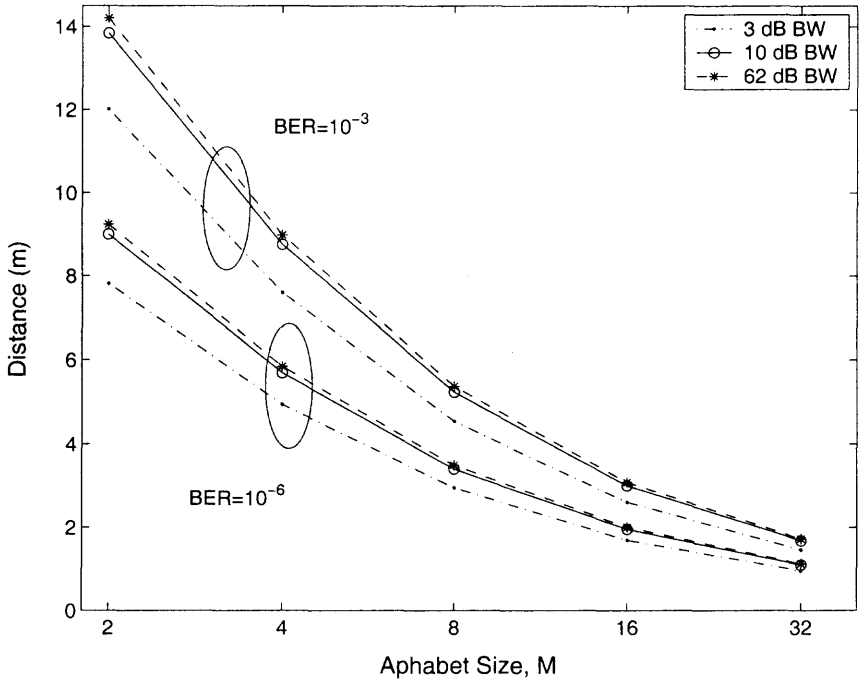

Figure 2.7 Transmission range for M-PAM for 100 Mbps data with different receiver bandwidth.

In Figure 2.7, the achievable distance in a free-space environment is presented for M-PAM at a 100-Mbps bit rate. Results are shown for two values of the target BER with G_t and G_r set to 0 dBi. For BER=10^{-6}, binary PAM can reach about 7 meters for a receiver with a bandwidth equal to the 3-dB bandwidth of the pulse. As indicated in Figure 2.7, the range can also be extended if the receiver bandwidth is increased. The improvement however is not significant.

In Figure 2.8, the achievable distance in a free-space environment is plotted as a function of bit rate for various values of M. For these results, the target BER is set at 10^{-6} with G_t and G_r set to 0 dBi, and the receiver bandwidth is set equal to the 62-dB bandwidth of the pulse. This achieves the maximum SNR. As expected, higher data rates can be achieved at shorter distances. For binary PAM, 100 Mbps can be reliably transmitted at a distance of approximately 8 meters; while 20 Mbps can be transmitted more than 18 meters. For 4-PAM, 100 Mbps can be reliably transmitted over a distance of only 5 meters. This occurs because, although PAM is a spectrally efficient modulation technique, it is not

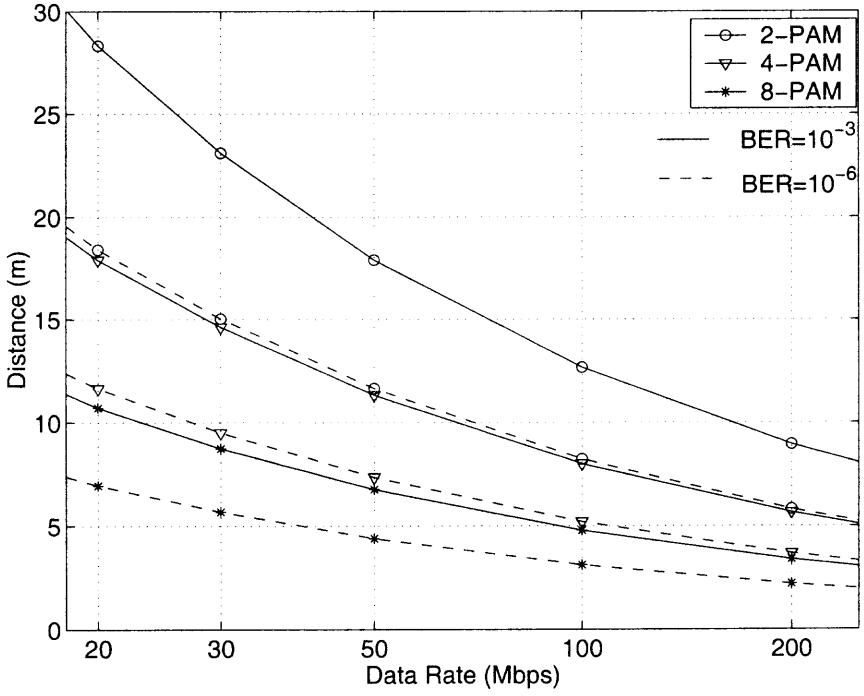

Figure 2.8 The achievable range versus data rates for M-PAM UWB systems.

power efficient. For an AWGN channel, the lower order PAM signal would result in the best performance for this power-limited system. In Figure 2.8, the allowed distance is also plotted as a function of bit rate for various values of M for BER=10^{-3}. This is the condition specified in [29]. From Figure 2.8, binary PAM can be reliably transmitted at 100 Mbps over about 13 meters. In [29], the permitted distance is about 20 meters. However, the results in [29] are optimistic because the actual pulse spectrum and frequency variation of the path loss were not considered. There is a 3 dB loss in received power by using the fifth-derivative Gaussian pulse as shown in Figure 2.9.

2.5 Implementation of Proposed Pulses

Note that the derivative operation could be implemented as highpass filtering. As an example, a 4th-order Chebyshev highpass filter with the stopband ripple 66 decibels down from 3 GHz is used. The output waveform is shown in Figure 2.10 with its spectrum shown in Figure 2.11.

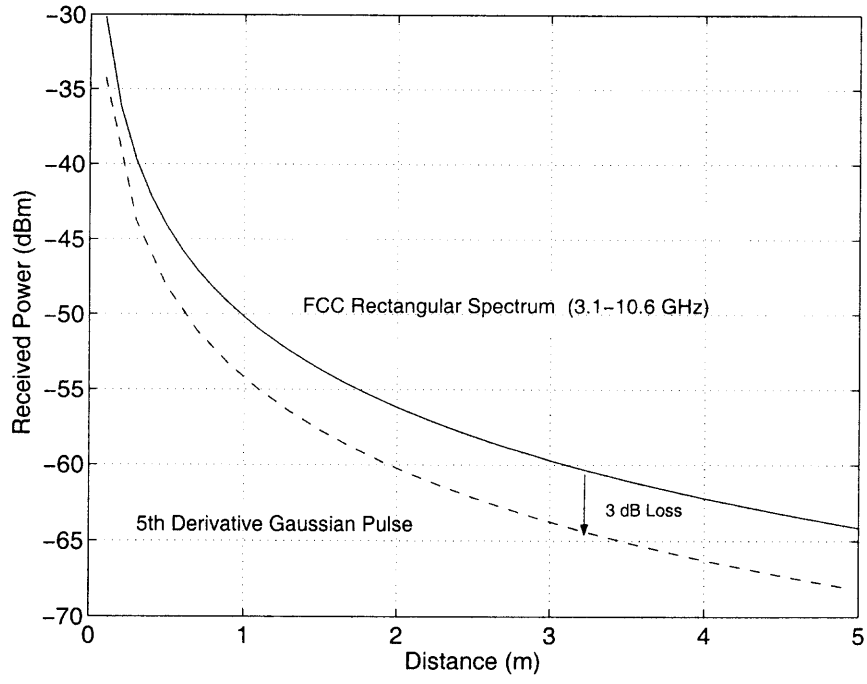

Figure 2.9 UWB received power as a function of distance by using the fifth-derivative of the Gaussian pulse and the rectangular PSD permitted by the FCC.

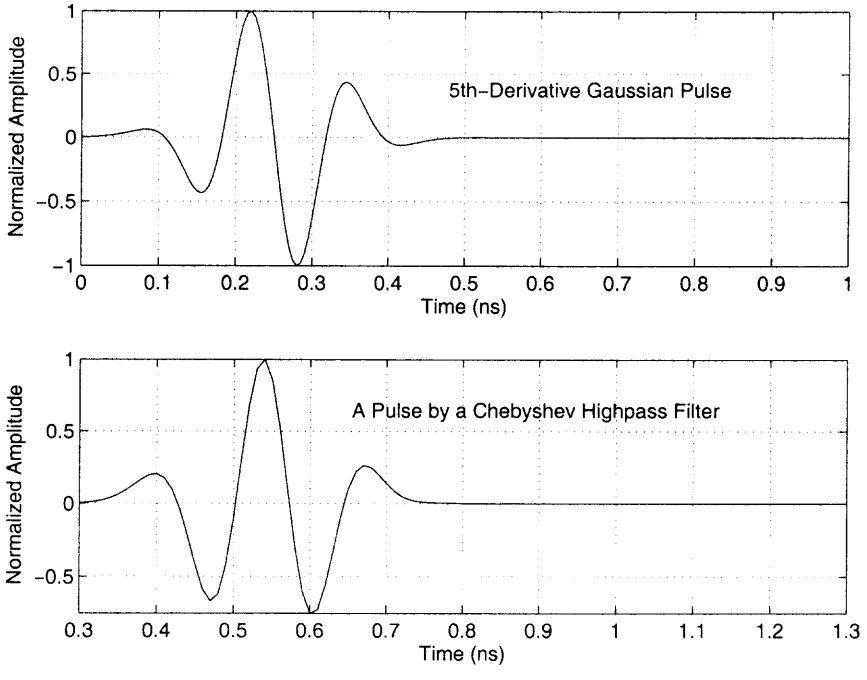

Figure 2.10 Comparison of the pulse waveform of the fifth-derivative of the Gaussian pulse (upper) and output waveform of a Chebyshev highpass filter (lower).

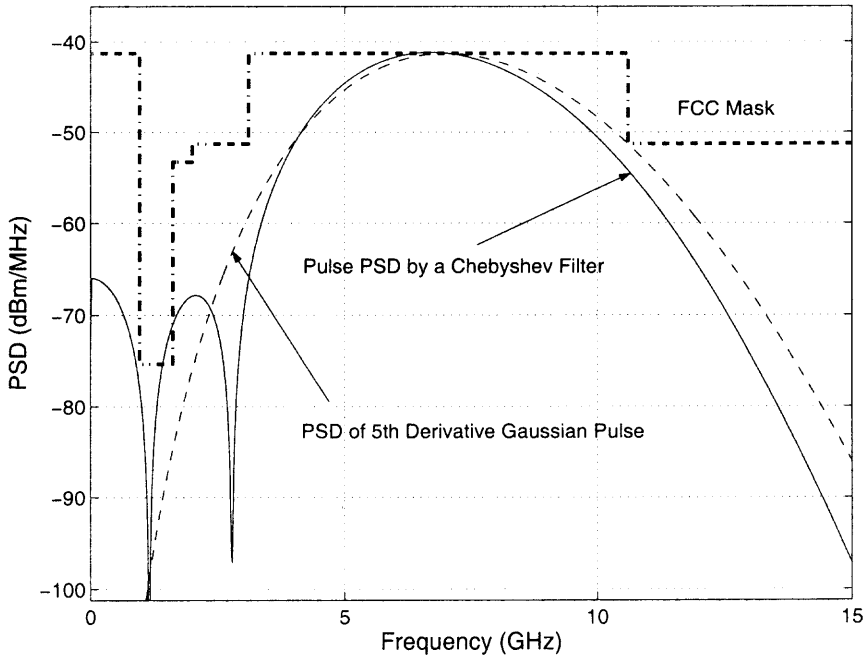

Figure 2.11 PSD of the fifth derivative of the Gaussian pulse and a Gaussian pulse with a 4th-order Chebyshev highpass filter.

It is noted that the PSD of the Chebyshev pulse can make use of the low frequency band. Therefore, the transmission range by the Chebyshev pulse is a little larger than that by the fifth-derivative pulse. This is plotted in Figure 2.12, where the achievable distance in a free-space environment is shown in terms of bit rate for 2-PAM and 4-PAM. The desired BER is at 10^{-6}. As observed, 100 Mbps can be reliably transmitted at a distance of approximately 8.5 meters.

2.6 Chapter Summary

In this chapter, a new monocycle based on the higher-order derivatives of the Gaussian pulse was proposed. This new pulse satisfies the FCC emission limits for UWB systems. In particular, it was demonstrated that the fifth-derivative of the Gaussian pulse meets the regulatory requirements. Possible implementation of this pulse was also presented. Based on this pulse and a more accurate frequency-dependent path loss calculation, the link budget was computed for an indoor UWB system, thus quantifying the relationship

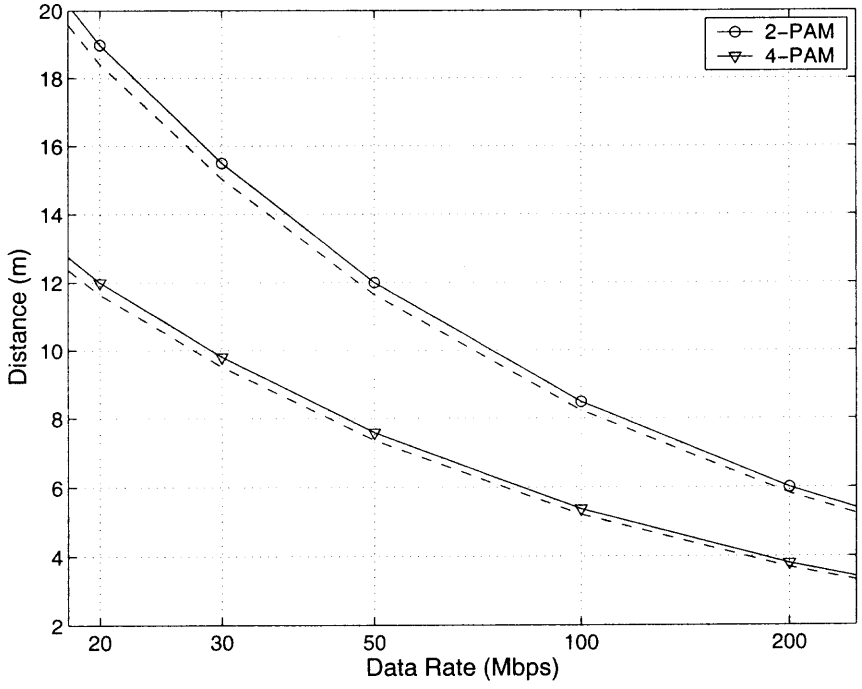

Figure 2.12 The achievable range for various data rates using the fifth-derivative of the Gaussian pulse (dash lines) and a Gaussian pulse filtered by a Chebyshev highpass filter (solid lines) at BER=10^{-6}.

between data rate and distance. It was shown that UWB can be a good candidate for high-rate transmission over short ranges with the capability for reliably transmitting 100 Mbps within large rooms.

If there is sufficiently large bandwidth, it can be shown that PPM provides significant performance improvements over PAM for power-limited applications [38,39]. It should be emphasized that the PSD of a PPM signal is not linearly related to the PSD of the individual pulse [40], and the spectral lines are not easily removed [41, p. 235].

The proposed pulse will be used in the subsequent chapters to evaluate the system performance.

CHAPTER 3

CODING, SPREADING, AND RATE SCALING IN UWB SYSTEMS

The achievable information rates of a single-user UWB communications are investigated under specific UWB constraints: limited power spectral density, specific modulation formats, and a highly dispersive channel. The work focuses on practical, low-duty cycle waveforms proposed for UWB applications such as the pulsed DS-UWB and impulse radio. The achievable rates of several modulation formats are evaluated as a function of the transmitter-receiver separation for the AWGN and the UWB multipath channel. Modulation formats are identified that have favorable performance over the multipath channel. Conditions are formulated for trading coding gain with spreading gain with only a small impact on performance. It is demonstrated that over the frequency-selective channel, the spreading gain may be beneficial in reducing the self and intersymbol interference resulting in higher information rates.

3.1 Introduction

Ultra-wideband technology is being considered as an alternative air interface for both high-rate [19] and low-rate [20] physical layers (PHYs). Two PHYs have been proposed for high-rate applications: one based on orthogonal frequency division multiplexing [17] and the other built on a pulsed direct sequence spread spectrum platform referred to as DS-UWB [14]. The latter is an evolution of the original concept of impulse radio [12] in the sense that its design includes the transmission of low duty-cycle waveforms. Impulse radio underlies the PHY recently proposed for low-rate applications. The discussion in this chapter comprises, in addition to DS-UWB, several other signaling formats proposed for UWB, such as M-ary pulse position modulation (M-PPM), biphase, and on-off keying (OOK) with time hopping (TH) [42].

Due to the regulatory constraints [11], UWB communication is inherently *power-limited* and generally takes place at the low SNR. This presents a different problem than other new technologies, such as multiple-input multiple-output (MIMO) [43], that operate over bandwidth-limited channels at spectral efficiencies larger than 1. This dissertation seeks to study the achievable information rates as a function of the transmitter-receiver separation and subject to the FCC PSD mask. Further, the rates are constrained by specific modulation formats that yield realistic performance evaluations of practical interest. The work presented here extends previous work that concerned itself mainly with the PPM modulation over the AWGN channel [44], multipath channel [45], and the presence of multiuser interference over the AWGN channel [46]. A realistic performance evaluation needs to take into account the highly dispersive nature of the UWB channel [21, 22]. Its effect is to degrade the capacity through fading as well as self interference (SI), inter-pulse interference (IPI), and intersymbol interference (ISI).

For a fixed bandwidth and due to the capping on the transmitted power, the main mechanism under the control of the transmitter is the *bandwidth expansion*, defined as the ratio of the Fourier bandwidth (see definition in the next section) to the information bit rate. The bandwidth expansion can be exploited to yield either coding or spreading gains. Coding gains are obtained by low-rate error correcting codes, whereas spreading gains are a result of spreading the spectrum with sequences independent of the data. The latter is a form of repetition coding. Spreading the spectrum might be more attractive to the design engineer than very low coding rates both as a practical matter (the complexity of codes with very low rates) as well as to accommodate other system requirements, such as multiple users. It is well known that in the AWGN channel, spreading the spectrum cannot increase capacity, but under certain conditions it ought not to significantly reduce it either [47]. Moreover, over the AWGN, spreading reduces capacity. This conclusion however, is not true for the multipath channel. It will be shown that, in some cases, spreading is actually beneficial in reducing the effect of SI and ISI and thus increases capacity. Understanding

the exact spread spectrum nature of UWB signals and the coding-spreading trade-off relation is of one the goals of this paper. By studying the performance of uncoded UWB communications, it can also be assessed over what distances UWB can perform adequately without coding.

Bandwidth scaling has been studied in the literature [48, 49]. The coding-spreading trade-off has been the topic of recent investigations that focused on multiuser cells over AWGN channels [50, 51, 52]. This dissertation is interested in this problem in a single user cell, but in a realistic setting of a large, but finite bandwidth, a limited maximum PSD, and a highly frequency-selective channel. Since practical systems are delay-limited, outage performance will be investigated.

The rest of this chapter is organized as follows. The next section introduces the system model. In Section 3.3, channel capacity is computed for various signaling inputs. Coding and bandwidth scaling are discussed in Section 3.4. Conclusions are drawn in Section 3.5.

3.2 UWB System Model

A UWB system diagram is shown in Figure 3.1. A UWB symbol consists of $N_p \geq 1$ pulses with an average inter-pulse interval of T_f. The pulse shape is denoted $q(t)$. The general model of the modulated UWB symbol is expressed

$$s_i(t) = d_i \sum_{j=0}^{N_p-1} a_j q\left(t - jT_f - c_j T_c - b_i T_{PPM}\right), \tag{3.1}$$

where $s_i(t)$ belongs to an M-ary signal set $\{s_1(t), s_2(t), \ldots, s_M(t)\}$. This expression is sufficiently general to comprise familiar formats of UWB transmission. With $a_j = d_i = 1$, a sequence of PPM signals is obtained with a time hopping signature determined by the coefficients c_j. With $c_j = b_i = 0$, equation (3.1) represents a DS-UWB transmission where the a_j's form the user signature and d_i is the data symbol.

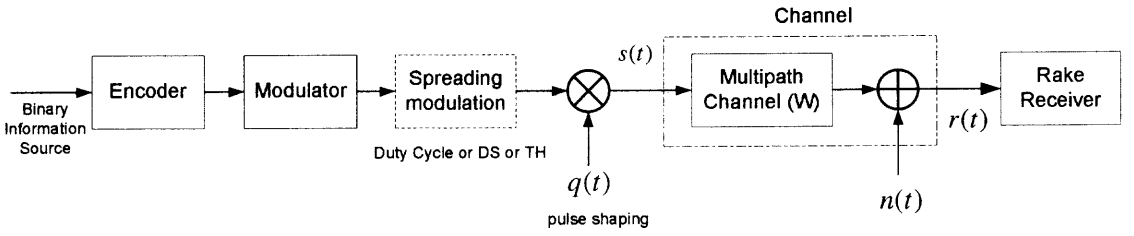

Figure 3.1 A single user UWB system diagram.

The *Fourier bandwidth* is identified as the range of frequencies that encompass the essential spectral bandwidth occupied by the pulse $q(t)$. According to the current DS-UWB proposal, the Fourier bandwidth of such signals is in either of the bands 3.1 to 4.85 GHz or 6.2 to 9.2 GHz [14]. With $T_f W \gg 1$, UWB pulses are transmitted at a low duty-cycle. The *Shannon bandwidth*, B, is defined as one-half the minimum number of dimensions (N) per second required to represent the signal in a signal space,

$$B = \frac{N}{2T_s}, \tag{3.2}$$

where T_s is the symbol duration. For M-PPM, $N = M$, and for biphase and OOK, $N = 1$. With these two quantities, Massey defines a spread spectrum signal as one for which the *spreading gain* [47]

$$\rho = \frac{W}{B} \gg 1. \tag{3.3}$$

The UWB multipath channel is modeled by the impulse response $h(t) = \sum_{\ell=0}^{L-1} \alpha_\ell \delta(t - \tau_\ell)$, where L is the number of multipath components, α_ℓ and τ_ℓ are the ℓ-th path amplitude and delay respectively, and $\tau_{\max} = \tau_{L-1} - \tau_0$ serves as the maximum delay spread. The channel gains α_ℓ are modeled as random variables with Nakagami-m statistics, whereas the path delay arrival times are assumed to be Poisson distributed [24]. The average received power of the ℓ-th path is expressed $\Omega_\ell = E[\alpha_\ell^2] = \bar{\Omega} \exp[-(\tau_\ell/\tau_{L-1})\delta_0]$, where $\bar{\Omega}$ is chosen such that the total average received power is unity, and δ_0 is a constant which determines the power decay factor.

The receiver implements a Rake receiver with L correlators (fingers) where each finger can extract the signal from one of the multipath components. The outputs of the correlators are combined coherently using MRC. The combiner requires knowledge of the paths' delays and amplitudes. In practice, it is obtained by channel estimation. Imperfect channel estimation leads to performance loss. The effect of imperfect CSI will be discussed in Chapters 5-6. In this chapter, it is assumed that the channel parameters are perfectly known. For a data symbol $d = 1$ or $b = 1$, the output of the MRC is given by

$$D = \sum_{\ell=0}^{L-1} \alpha_\ell^2 + \sum_{\ell=0}^{L-1} \alpha_\ell w_\ell + \sum_{\ell=0}^{L-1} \alpha_\ell z_\ell \tag{3.4}$$

where w_ℓ is the noise term in the corresponding branch of the Rake receiver, and z_ℓ represents the interference.

3.3 Achievable UWB Information Rates

One question answered in this section is, given the PSD constraint, bandwidth limitation, and the UWB channel characteristics, how fast and how far can the information data be transmitted reliably. The capacity of the AWGN channel is considered first, followed by the multipath channel. Gaussian inputs as well as specific UWB modulation formats are investigated.

3.3.1 Gaussian Signals

The capacity of the ideal linear Gaussian channel is achieved with a Gaussian distribution of the input signals. Using a notation that emphasizes the path loss effect on capacity at distance d from the transmitter, the Shannon capacity in bits/sec is

$$C(\mathsf{d}) = B \log_2 \left(1 + \mathsf{SNR}(\mathsf{d})\right), \tag{3.5}$$

where B is the Shannon bandwidth defined earlier and $\mathsf{SNR}(\mathsf{d})$ is the average SNR per dimension at distance d from the transmitter and given by

$$\mathsf{SNR}(\mathsf{d}) = \frac{P_s(\mathsf{d})}{N_0 B}. \tag{3.6}$$

In (3.6), $P_s(\mathsf{d})$ is the average received signal power per dimension and N_0 is the one-sided noise power spectral density. Due to the wide bandwidth, path loss variations across the bandwidth cannot be ignored, hence the signal power is expressed

$$P_s(\mathsf{d}) = \int_{f_L}^{f_H} \frac{S(f)}{L_s(\mathsf{d}, f)} df, \tag{3.7}$$

where f_L and f_H denote the two ends of the frequency range of interest (the Fourier bandwidth) and $S(f)$ is the PSD of the received UWB pulse. The numerical results in the sequel assume that f_L, f_H are measured at the -10 dB power spectrum points. In practice, the PSD depends on the specific waveform, which in turn, is designed to meet the regulatory restrictions [34, 35, 53]. As indicated earlier, numerical results in the sequel are generated using the ideal PSD of the FCC mask. The term $L_s(\mathsf{d}, f)$ is the frequency-dependent path loss

$$L_s(\mathsf{d}, f) = \frac{(4\pi)^2 f^2 \mathsf{d}_0^2}{G_t G_r c^2} \cdot \left(\frac{\mathsf{d}}{\mathsf{d}_0}\right)^n, \tag{3.8}$$

where c is the speed of light, and d_0 is a reference distance at which the received power is known. In the numerical calculations, this distance and the power are taken from the FCC mask that allows for -41.3 dBm/MHz at 3 meters from the transmitter. The term n is the path loss exponent. In generating numerical results, the path loss exponent is assumed to be $n = 2$ for LOS channels, and $n = 4$ for NLOS channels [22]. It is further assumed that the antennas are ideal and have no gain.

It is well known that over the AWGN channel, the Gaussian input achieves the capacity in (3.5). Different expressions are required to express the achievable information rates with specific digital modulations. These are discussed in the next subsection.

3.3.2 Modulated Signals

In this section, the information rate of UWB systems over AWGN channels is computed when specific modulation formats are employed. Define $\gamma(\mathsf{d})$ as the SNR per symbol at distance d

$$\gamma(\mathsf{d}) = \frac{2E_s}{N_0}(\mathsf{d}), \tag{3.9}$$

where E_s is the energy per symbol. Using (3.2) and (3.6), equation (3.9) becomes

$$\gamma(\mathsf{d}) = N \cdot \mathsf{SNR}(\mathsf{d}). \tag{3.10}$$

For M-PPM, the achievable information rate over the AWGN channel is given by the mutual information between the input and output to the channel when the input is discrete-valued M-PPM, with uniform distribution, and the output is continuous-valued. The mutual information in *bits/symbol* has been derived in [54] and given by

$$\mathcal{I}_{\text{M-PPM}}(\mathsf{d}) = E_{\mathbf{u}|\mathbf{s}_1} \log_2 \left\{ \frac{M}{1 + \sum_{m=2}^{M} \exp\left[-\sqrt{\gamma(\mathsf{d})}u_m\right]} \right\}, \text{bits/symbol} \tag{3.11}$$

where u_m is a Gaussian random variable with mean $\sqrt{\gamma(\mathsf{d})}$ and variance 2. Due to the symmetry of the PPM modulation and the assumption of uniform distribution of the inputs, the mutual information can be computed conditioned on symbol $s_1\,(t)$, represented here by the vector $\mathbf{s}_1$. The rate in *bits/sec* is obtained from the product of the mutual information per symbol in (3.11) and the number of symbols per second. Since this information rate represents the "capacity" of PPM, "$C_{\text{M-PPM}}$" is used to denote it:

$$C_{\text{M-PPM}}(\mathsf{d}) = \frac{2B}{N} E_{\mathbf{u}|\mathbf{s}_1} \log_2 \left\{ \frac{N}{1 + \sum_{m=2}^{N} \exp\left[-\sqrt{\gamma(\mathsf{d})}u_m\right]} \right\}. \tag{3.12}$$

The calculation of (3.12) has to be carried out numerically by Monte Carlo analysis. For the special case of 2-PPM, a closed-form expression of (3.12) is available [44]:

$$C_{\text{2-PPM}}(\mathsf{d}) = \frac{B}{\sqrt{\pi}} \int_{-\infty}^{\infty} e^{-x^2} \log_2 \left\{ \frac{2}{1 + \exp\left[-2\sqrt{\gamma(\mathsf{d})}\left(x + \frac{\sqrt{\gamma(\mathsf{d})}}{2}\right)\right]} \right\} dx. \quad (3.13)$$

Appendix A presents the derivation of the channel capacity for biphase modulation

$$C_{\text{biphase}}(\mathsf{d}) = \frac{2B}{\sqrt{\pi}} \int_{-\infty}^{\infty} e^{-x^2} \log_2 \left\{ \frac{2}{1 + \exp\left[-\sqrt{8\gamma(\mathsf{d})}\left(x + \sqrt{\frac{\gamma(\mathsf{d})}{2}}\right)\right]} \right\} dx, \quad (3.14)$$

and for OOK

$$C_{\text{OOK}}(\mathsf{d}) = \frac{2B}{\sqrt{\pi}} \int_{-\infty}^{\infty} e^{-x^2} \log_2 \left\{ \frac{2}{1 + \exp\left[-2\sqrt{\gamma(\mathsf{d})}\left(x + \frac{\sqrt{\gamma(\mathsf{d})}}{2}\right)\right]} \right\} dx, \quad (3.15)$$

respectively, both in bits/sec. Note that $C_{\text{OOK}}(\mathsf{d}) = 2C_{\text{2-PPM}}(\mathsf{d})$ for a fixed SNR per symbol. Expressions (3.13)-(3.15) have the general form of $y = \int_{-\infty}^{\infty} e^{-x^2} f(x) dx$. The numerical evaluation of this infinite integral can be simplified by the Hermite formula [55]

$$y = \frac{2}{\sqrt{\pi}} \sum_{k=1}^{\bar{N}} H_{x_k} f(x_k), \quad (3.16)$$

where x_k and H_{x_k} are, respectively, the zeros and weight factors of the k-th order Hermite polynomial tabulated in [55], and $\bar{N}$ is the highest order included in the calculation. Typically, $\bar{N} = 10$ terms are sufficient for good accuracy, resulting in considerable computational savings over the direct numerical evaluation of the infinite integral.

The benefit of coding UWB transmissions can be assessed by evaluating the performance of uncoded systems and comparing it to the information rates computed above. The uncoded bit rate can be expressed as a function of signal power to noise spectral

density ratio through the following relation

$$R_b(\mathsf{d}) = \frac{P_s(\mathsf{d})}{N_0 \cdot \left(\frac{E_b}{N_0}\right)_e}, \tag{3.17}$$

where $(E_b/N_0)_e$ is the SNR per bit required for a desired bit error probability performance. This information bit rate cannot be higher than what is allowed by the bandwidth. From (3.2), and denoting the symbol rate $R_s = 1/T_s$, it follows that for uncoded M-ary modulation in N-dimensional signal space, there is

$$R_b(\mathsf{d}) = R_s \log_2 M = \frac{2B}{N} \log_2 M \leq \frac{2W}{N} \log_2 M. \tag{3.18}$$

By letting the Shannon and Fourier bandwidths be equal, $B = W$, and substituting (3.17) in (3.18) leads to

$$\frac{P_s(\mathsf{d})}{N_0 \cdot \left(\frac{E_b}{N_0}\right)_e} = \frac{2W}{N} \log_2 M, \tag{3.19}$$

from which the maximum distance can be found for which the uncoded bit rate is given by (3.18).

Figure 3.2 compares the information rates versus distance for several modulation formats. The capacity (Gaussian signaling) is also shown for reference. The Shannon bandwidth is assumed to be equal to the Fourier bandwidth (no spreading). To be specific, the bandwidth is assumed to be equal to the *low-band* in the DS-UWB proposal [14] for which $W = 1.75$ GHz. For each of the modulations, the maximum distance (computed from (3.19)) at which the uncoded bit rate is still achieved is indicated by a marker on the curve corresponding to the modulation. Three regions are distinguished as a function of distance. In the high SNR region ($\mathsf{d} \approx 1$ m), the rate is limited by the spectral efficiency of the specific modulation. The biphase being the most spectrally efficient, has the highest rate, while 8-PPM is the least spectrally efficient and carries the lowest rate. At medium SNR ($\mathsf{d} \approx 10$ m), the rate relations are less intuitive, and the three orthogonal modulations (OOK, 2-PPM, and 8-PPM) have very similar performance. The rates with

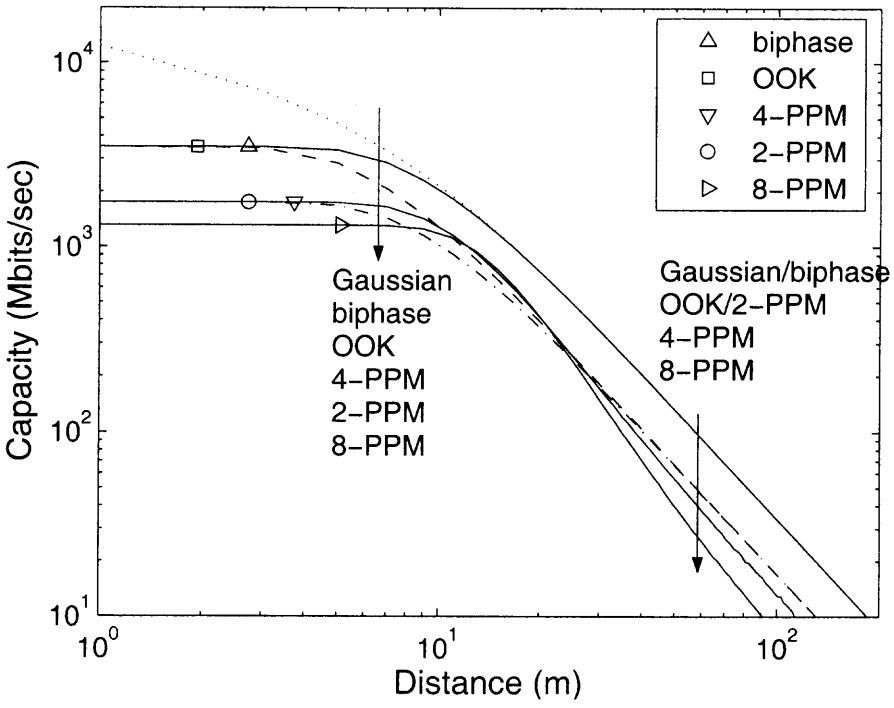

Figure 3.2 Capacity in AWGN for different modulation signals as a function of distance when the low-band is used with $\rho = 1$. The largest bit rates in uncoded cases with a given bit error rate 10^{-5} are also marked.

biphase modulation approach that of Gaussian signaling. Similarly, little loss compared to capacity is experienced if biphase is used at large distances (d $\approx$ 100 m). From (3.12) it is observed that the rates achievable with M-PPM decrease with M, which explains why 8-PPM has the lowest performance. The intuition to this effect is that with more dimensions, the chances of the noise popping up in *one* of the dimensions increases.

For the uncoded cases, $(E_b/N_0)_e$ was computed for a bit error rate of 10^{-5}. It is seen that for the same maximum bit rate, biphase achieves a larger distance than OOK, and 8-PPM has a larger distance than 2-PPM. For a BER of 10^{-5}, the largest distance for which the maximum bit rate is attained is less than 10 m.

Over multipath channels, interference due to delay spread will degrade the channel capacity. This is discussed in the next subsection.

3.3.3 Multipath Channels

In the previous discussion, equal Shannon and Fourier bandwidths were assumed since it is well understood that spreading reduces capacity over the AWGN channel [47]. The multipath channel, however, requires further consideration. It is assumed that the channel is known at the receiver, but not at the transmitter. The delay spread in the channel gives raise to self interference (among echoes of the same symbol), inter-pulse interference (among pulses representing the same symbol), and intersymbol interference. Irrespective of its source, this interference reduces capacity by violating the orthogonality among symbols. For example, delay spread may cause loss of orthogonality between PPM symbols.

As per Section 3.2, the multipath fading channel parameters $\{\alpha_\ell, \tau_\ell\}$ are modeled as random variables. It follows that the information rates are also modeled as random variables. For delay sensitive applications, it is of interest to characterize the complementary cumulative distribution function (CCDF) of the channel rates. To apply the results in (3.12)-(3.15) to the multipath channel, the Gaussian assumption is invoked, i.e., it is assumed that the interference (ISI+IPI+SI) is Gaussian distributed. With this assumption, the SNR in (3.9) can be replaced with the signal-to-interference plus noise ratio (SINR) at the output of the Rake combiner. In practice, Rake receivers often process and combines only a subset of the resolved multipath components (L_c paths out of the L resolved paths). Such a receiver is referred to as *selective*. With perfect knowledge of the channel parameters $\{\alpha_\ell, \tau_\ell\}$, it can be verified that the SINR at the output of the combiner is

$$\mathsf{SINR} = \frac{P_s(\mathsf{d}) \left[\sum_{\ell=0}^{L_c-1} \alpha_\ell^2\right]^2}{N_0 B \cdot \sum_{\ell=0}^{L_c-1} \alpha_\ell^2 + P_s(\mathsf{d}) \sum_{\ell=0}^{L_c-1} \alpha_\ell^2 z_\ell^2}, \tag{3.20}$$

where z_ℓ is assumed to be Gaussian random variable representing the interference at the ℓ-th path. Substituting in (3.12), (3.13), (3.14), and (3.15), one obtains the respective instantaneous rate conditioned on the channel realization.

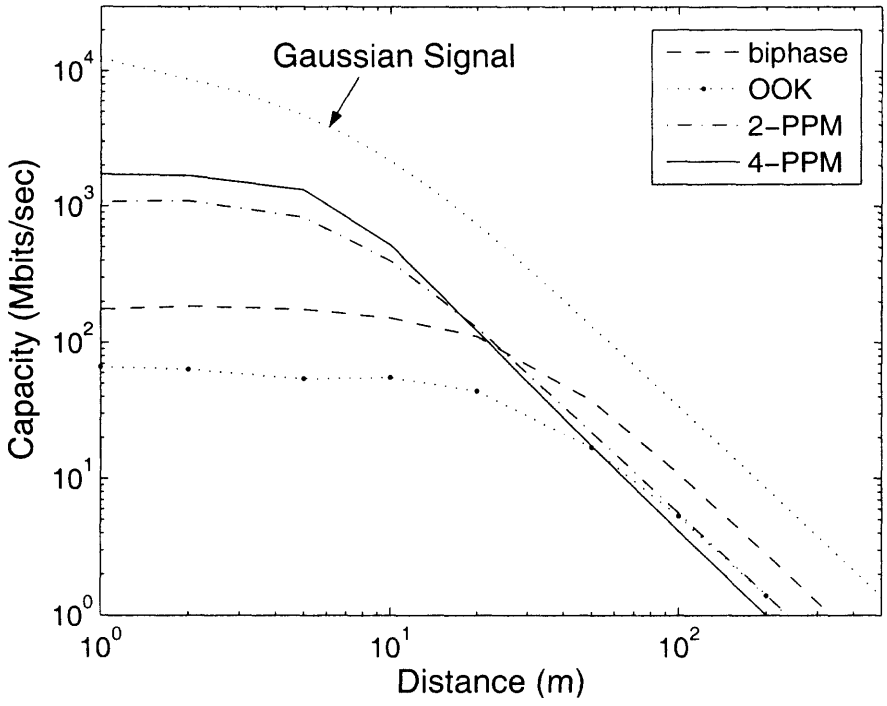

Figure 3.3 Capacity with 10% outage probability for different signalings as a function of distance over a UWB multipath channel. It is assumed $\tau_{\max} = 50$ ns, $\rho = 1$, and $L_c = 20$.

In Figure 3.3, the 10% outage capacity is plotted as a function of distance d for the various modulations. The channel is assumed with a maximum delay spread of $\tau_{\max} = 50$ ns. The Nakagami fading parameter is $m_l = 1$. Results are shown for the low-band (same as in the AWGN analysis) with a spreading ratio $\rho = 1$, and the number of selective-Rake fingers $L_c = 20$ (corresponding to approximately 60% of the total transmitted energy). At short distances, performance is dominated by the effect of the interference. As a result, the gap between the capacity (shown for the AWGN channel) and the rates for the various modulations is larger than the corresponding quantities in Figure 3.2. Interestingly, in this case, the rate for 4-PPM is the largest. This is due to the fact that for the same bandwidth, the symbol interval for 4-PPM is twice that of 2-PPM, and four times that of biphase and OOK, mitigating against the effects of ISI. At large distances, the performance is noise-limited and the order among the modulations reverts to that of the AWGN case.

3.3.4 Spectrum Spreading in UWB

So far, the Fourier and Shannon bandwidths were assumed equal. In this subsection, Massey's definition (3.3) is applied to evaluate the spreading ratio for various UWB signaling formats. For an unambiguous definition of the Fourier bandwidth, a sinc pulse is assumed, i.e., the pulse shape with bandwidth W is given by $q(t) = \text{sinc}(2Wt)$.

1) PPM with Time Hopping. It was shown by Massey that M-PPM does not meet the definition of spread spectrum [47]. Is a time hopping PPM signal spread spectrum? An M-PPM signal with N_p pulses per symbol and subject to time hopping with cardinality $N_h + M$ time slots is expressed in the time interval $0 \leq t \leq T_s$,

$$s(t) = \text{sinc}\left(\frac{M + N_h}{T_s/N_p}t - d_1 - c_j\right) \tag{3.21}$$

where $d_1 \in \{1, 2, \ldots, M\}$ are the data symbols, and $0 < c_j < N_h$ is the TH sequence. The Fourier bandwidth satisfies $W = (M + N_h) N_p/(2T_s)$. The signal space is minimally spanned by the orthonormal basis functions $\psi_i(t) = \sqrt{2W}\text{sinc}(2Wt - i)$, $i = 1, 2, \ldots, M$. Hence, the Shannon bandwidth is $B = M/(2T_s)$. It follows that the spreading gain is given by $\rho = (1 + N_h/M) N_p$. This signal is spread spectrum for a large cardinality of the TH sequence or a large number of pulses per symbol.

2) Biphase with Time Hopping. A biphase signal with time hopping is expressed for $0 \leq t \leq T_s$,

$$s(t) = d_1 \sum_{j=0}^{N_p-1} \text{sinc}\left(\frac{N_h}{T_s/N_p}t - c_j\right), \tag{3.22}$$

where d_1 is the data symbol and the other quantities were defined in connection with (3.21). From (3.22), the Fourier bandwidth is $W = N_h N_p/(2T_s)$, whereas the Shannon bandwidth is $B = 1/2T_s$. It follows that the spreading gain $\rho = N_h N_p$.

3) DS-UWB. The DS-UWB waveform consists of a sequence of coded pulses. A parameter N_f is introduced to denote the duty-cycle of the waveform. Using quantities already defined, the duty-cycle can be expressed $N_f = T_f W$. Then the DS-UWB signal is

expressed as

$$s(t) = d_1 \sum_{j=0}^{N_p-1} c_j \text{sinc}\left(\frac{N_f}{T_s/N_p}t - j\right), \tag{3.23}$$

where d_1 is the data symbol and $c_j \in \{-1, 0, 1\}$. This signal is characterized by the same Fourier and Shannon bandwidths as the signal in (3.22), and hence it has the same spreading gain.

The large bandwidth in UWB systems enables not only large spreading ratios, but also low coding rates. In the next section, the coding-spreading trade-off is investigated.

3.4 Coding-Spreading Tradeoff

In this section, the coding-spreading trade-off is studied for UWB communications. The goal is to determine how to allocate the bandwidth expansion inherent in low duty-cycle between coding and spreading. This problem is form the single user point of view for both the AWGN and multipath channels. The required E_b/N_0 is derived as a function of the coding rates for the various modulation schemes. For a single user scenario, it is optimal to allocate all the bandwidth expansion to coding and none to spreading. A "threshold" is determined in terms of coding rate beyond which the bandwidth expansion can be allocated to spreading without much loss in information rate.

3.4.1 Coding Gain

The amount of *information bits per dimension* transmitted over the channel can be interpreted as either coding rate (for an infinite length block code) or spectral efficiency. The interpretation of coding rate is more insightful in the context of the discussion here. The coding rate is defined as

$$r = \frac{R_b}{NR_s}, \text{ bits/dim}, \tag{3.24}$$

where R_b is the information bit rate in bits/sec, and $R_s = 1/T_s$ is the symbol rate in symbols/sec. Substituting (3.2) in (3.24), the coding rate is expressed in terms of the Shannon bandwidth $r = R_b/(2B)$. At capacity, $R_b = C$, hence the spectral efficiency C/B is related to the coding rate, $C/B = 2r$. Applying (3.2) and (3.24) in (3.6), the following expression is obtained which links between the SNR, the coding rate and the SNR per bit:

$$\mathsf{SNR} = 2r\frac{E_b}{N_0}, \tag{3.25}$$

where E_b is the energy per bit. With the help of these relations, the Gaussian channel capacity (3.5) can be expressed as

$$2r = \log_2\left(1 + 2r\frac{E_b}{N_0}\right). \tag{3.26}$$

The SNR per bit required for reliable transmission is then related to the coding rate [56]

$$\frac{E_b}{N_0}(r) = \frac{2^{2r}-1}{2r}. \tag{3.27}$$

It is seen that the required E_b/N_0 increases monotonically with r. Note that both E_b/N_0 and r are implicit functions of the distance d (both decrease when d increases, see (3.25)). In the limit, for $r \to 0$, E_b/N_0 converges to the familiar Shannon limit $\ln 2 = -1.6$ dB.

Using an argument similar to the one leading to (3.27), i.e., substituting $C/B = 2r$ and expressing (3.13)-(3.15) as a function of E_b/N_0, the required E_b/N_0 as a function of r is obtained for various modulation signaling formats. In particular, the relations are for 2-PPM,

$$\int_{-\infty}^{\infty} e^{-x^2} \log_2\left\{2^{2r-1}\left[1 + \exp\left(-4\sqrt{r\frac{E_b}{N_0}}\left(x + \sqrt{r\frac{E_b}{N_0}}\right)\right)\right]\right\} dx = 0, \tag{3.28}$$

for biphase,

$$\int_{-\infty}^{\infty} e^{-x^2} \log_2\left\{2^{r-1}\left[1 + \exp\left(-4\sqrt{r\frac{E_b}{N_0}}\left(x + \sqrt{r\frac{E_b}{N_0}}\right)\right)\right]\right\} dx = 0, \tag{3.29}$$

and for OOK,

$$\int_{-\infty}^{\infty} e^{-x^2} \log_2 \left\{ 2^{r-1} \left[1 + \exp\left(-2\sqrt{2r\frac{E_b}{N_0}} \left(x + \sqrt{\frac{r}{2}\frac{E_b}{N_0}} \right) \right) \right] \right\} dx = 0. \tag{3.30}$$

Since no simple closed expression appears to be available to express $\frac{E_b}{N_0}(r)$, numerical computations are used based on the Hermite formula.

The results are plotted in Figure 3.4. For a meaningful comparison between the modulations, the abscissa in the figure is the normalized coding rate defined

$$r_{\text{norm}} = r\frac{N}{\log_2 M}. \tag{3.31}$$

The normalized coding rate in (3.31) is confined to the range $0 \leq r_{\text{norm}} \leq 1$. At one end of this range is the Shannon limit, at the other is the uncoded case (SNR per bit values shown in the figure are for BER $= 10^{-5}$). For a given modulation, $\frac{E_b}{N_0}(1) - \frac{E_b}{N_0}(r_{\text{norm}})$ is the coding gain at coding rate r_{norm}. As the coding rate decreases from 1, the increase in coding gain is initially rapid, but it slows down at lower coding rates. It is observed that little incremental coding gain can be achieved by lowering the coding rate below, say, $r = 1/4$ ($r_{\text{norm}} = N/(4\log_2 M)$). In other words, not much capacity is lost by limiting the coding rate to $1/4$ and applying the rest of the bandwidth expansion to spreading. It is also noted that in this low SNR regime, biphase performs almost as well as Gaussian signaling, consistent with the detailed discussion in [49].

3.4.2 Information Rate with Fixed Coding Rates

In this section, the achievable information rates are estimated in the presence of a fixed coding rate. The coding rate r and the SNR per bit E_b/N_0 are interdependent through one of the relations (3.27)-(3.30). As the distance from the transmitter increases, the received power and the SNR decrease. The optimal pair of values of coding rate and SNR per bit to meet the SNR at some distance d is given by the capacity and rate relations. These relations indicate that as the power decreases, the bandwidth expansion is set to meet the coding rate

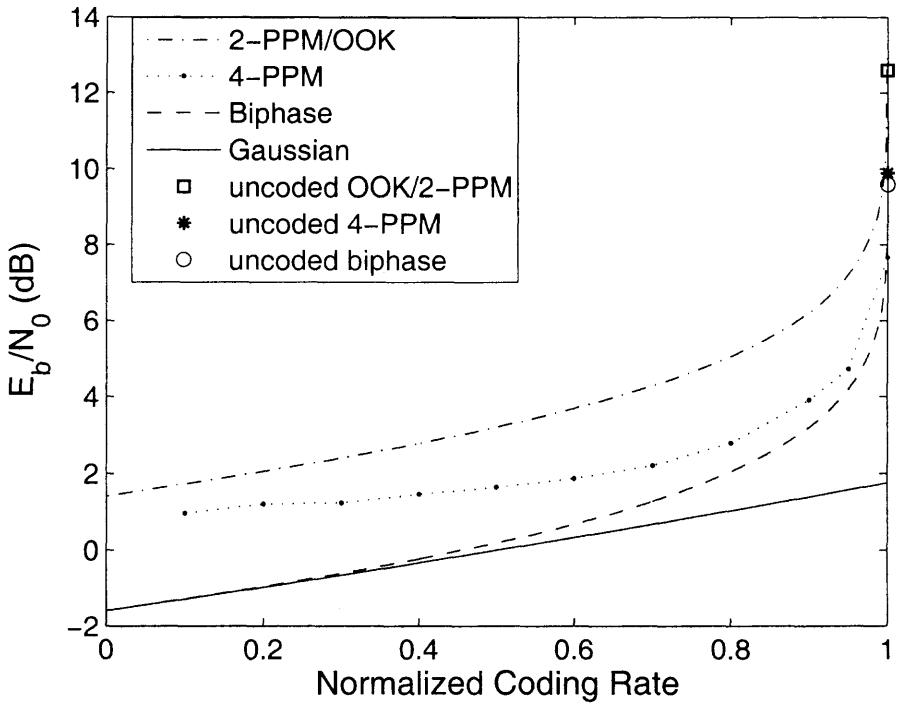

Figure 3.4 Required E_b/N_0 to obtain a reliable transmission as a function of the normalized coding rate for various signalings.

requirement. Initially, this decrease in coding rate (and the accompanying decrease in capacity) is greatly mitigated by the decrease in required E_b/N_0. As the SNR continues to decrease, there are diminishing returns in the gain of SNR per bit. Finally, as discussed earlier, at low coding rates, any additional reduction in power is accommodated mainly by the bandwidth expansion (coding rate). Let the spreading ratio be ρ. The SNR relation (3.25) can be rewritten for the case of a spreading gain as

$$\text{SNR} = 2r\beta \frac{E_b}{N_0}(r) \tag{3.32}$$

with $\beta = 1/\rho$. In (3.32), both terms r and β represent the reciprocal of a bandwidth expansion. With r, the bandwidth expansion is applied to coding, whereas with β, the bandwidth expansion is applied to spreading. The difference between coding and spreading is in their effect on $\frac{E_b}{N_0}(r)$. While lowering r (lower coding rate) decreases the required $\frac{E_b}{N_0}(r)$, lowering β (increasing spreading ratio) has no impact on the SNR per bit. That

is why applying the bandwidth expansion to coding gain is preferred, particularly at the high SNR per bit. However, at the low SNR (for a given coding rate) when the gain in $\frac{E_b}{N_0}$ is almost bottomed out, applying any *additional* bandwidth expansion to spreading rather than coding, may carry only a small loss in capacity. In other words, under these conditions, the spreading gain and coding gain will be roughly equal.

This is demonstrated numerically as follows: Let r_0 be the selected coding rate and d_{r_0} be the corresponding distance at which (3.32) is met. For $\mathsf{d} > \mathsf{d}_{r_0}$, the bandwidth expansion is applied to spreading to compensate for the SNR attenuation with the distance. Let $\left(\frac{E_b}{N_0}\right)_{r_0}$ be the SNR per bit required at capacity at this coding rate. The spreading gain needs to ensure that this SNR per bit is met. For $\mathsf{d} > \mathsf{d}_{r_0}$, it is required

$$\frac{P_s(\mathsf{d})}{N_0} = R_b(\mathsf{d}) \left(\frac{E_b}{N_0}\right)_{r_0}. \tag{3.33}$$

From (3.24) and (3.2), the following relation is obtained between the Shannon bandwidth, coding rate and information rate

$$B(\mathsf{d}) = \frac{R_b(\mathsf{d})}{2r_0} = \frac{1}{2r_0} \cdot \frac{P_s(\mathsf{d})}{N_0 \cdot \left(\frac{E_b}{N_0}\right)_{r_0}}. \tag{3.34}$$

From this expression it follows that for $\mathsf{d} > \mathsf{d}_{r_0}$, the spreading gain needs to be distance-dependent, viz., $\rho(\mathsf{d}) = W/B(\mathsf{d})$.

To express the channel capacity for a specified spreading gain, it is needed to substitute W/ρ for B in the capacity expression. For the AWGN channel, the channel capacity in (3.5) can be expressed as a function of spreading ratio

$$C(\mathsf{d}) = \frac{W}{\rho} \log_2 \left(1 + \rho \frac{P_s(\mathsf{d})}{N_0 W}\right), \text{ bits/sec.} \tag{3.35}$$

The last expression and the rate expression obtained by substituting $B = W/\rho$ in (3.14) are used to generate Figure 3.5. A spreading gain of $\rho = 100$ was assumed for the calculations. For clarity, only Gaussian and biphase signaling are shown. The signals were assumed to

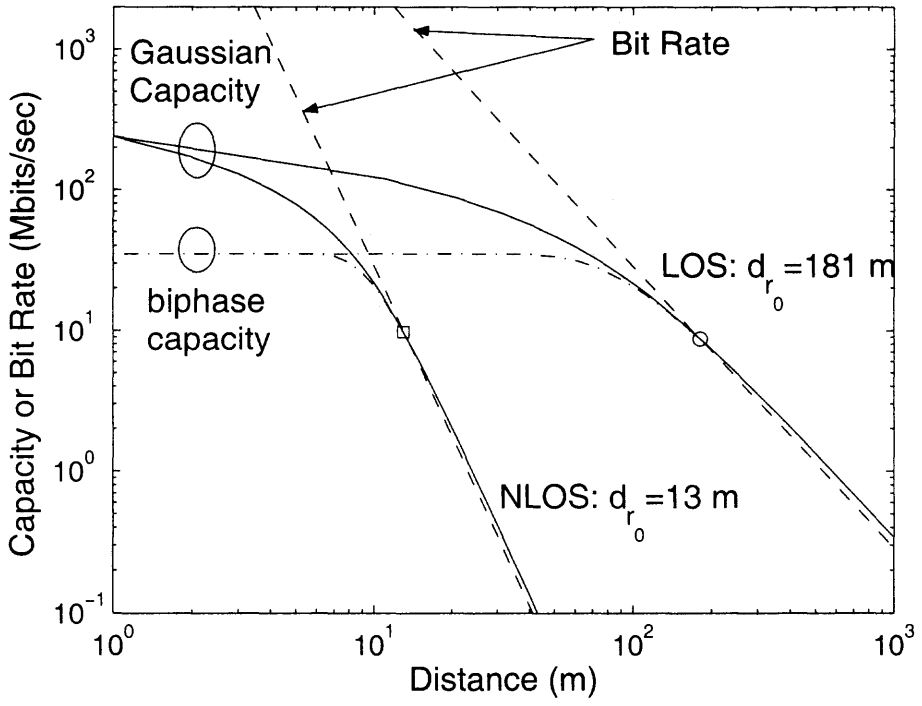

Figure 3.5 Bit rate and capacity versus distance for Gaussian and biphase inputs at a fixed coding rate $r_0 = 1/4$. The spreading ratio is $\rho = 100$.

conform to the FCC mask over the band 3.1-4.85 GHz. Marked on the capacity curves in the figure are distances at which the coding rate is $r_0 = 1/4$, for two types of path loss (LOS and NLOS, respectively). Also shown in the figure are the information rates obtained from (3.33). By design, where the latter curves intersect the capacity curves, the spreading gain is $\rho = 100$. However, for points $\mathsf{d} > \mathsf{d}_{r_0}$, there is $\rho > 100$. The main lesson drawn from the figure is that the loss in capacity is negligible if the coding rate is fixed and the SNR attenuation is compensated for with spreading gain.

Figure 3.6 depicts the needed spreading ratio versus distance for a fixed coding rate $r_0 = 1/4$. Only the result for the LOS case is plotted. The SNR attenuation with the distance is compensated by the buildup of the spreading ratio.

Figures 3.7-3.8 displays a metric referred to as *capacity loss* and defined

$$\eta(\mathsf{d}, \rho) = 1 - \frac{C(\mathsf{d}, \rho)}{\max C(\mathsf{d})}. \tag{3.36}$$

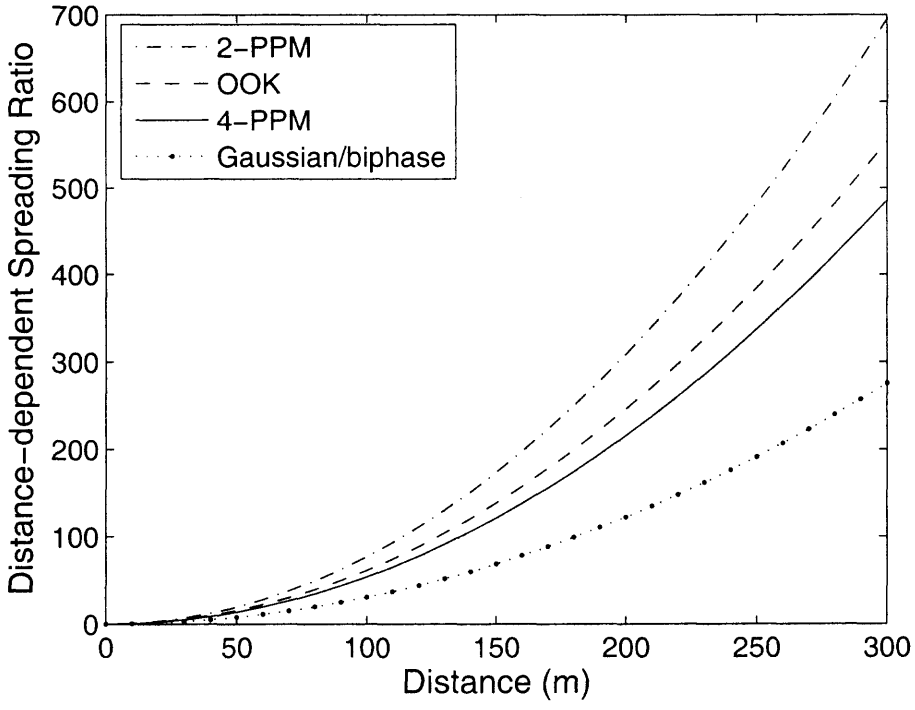

Figure 3.6 Distance-dependent spreading ratio to maintain a desired E_b/N_0 at a fixed coding rate $r_0 = 1/4$.

The capacity loss is a function of the spreading gain, but is distance dependent. For no spreading gain $\rho = 1$, $\eta(\mathsf{d}, \rho) = 0$, for all d, but the rate of change of η versus ρ depends on d, with η becoming less sensitive to ρ at larger distances (low SNR).

Figure 3.7 demonstrates capacity loss in terms of spreading ratio. It clearly shows that spreading degrades channel capacity. However, in the low SNR regime, for example, when $\mathsf{d} = 100$ at NLOS, little capacity loss occurs. It is also indicated that biphase and 2-PPM have the same capacity loss. Using various signaling inputs result in little difference of capacity loss. Figure 3.8 presents the loss in information rate as a function of distance for three signaling formats, two types of channel, and for a specified value of spreading gain. Due to the lower SNR, the rate loss is less noticeable for the NLOS channel. Conversely, at the high SNR, the rate decreases fast with the increase in spreading. When $\mathsf{d} > 13$ m for NLOS, and $\mathsf{d} > 200$ m for LOS, the rate loss is less than 10%. The actual modulation

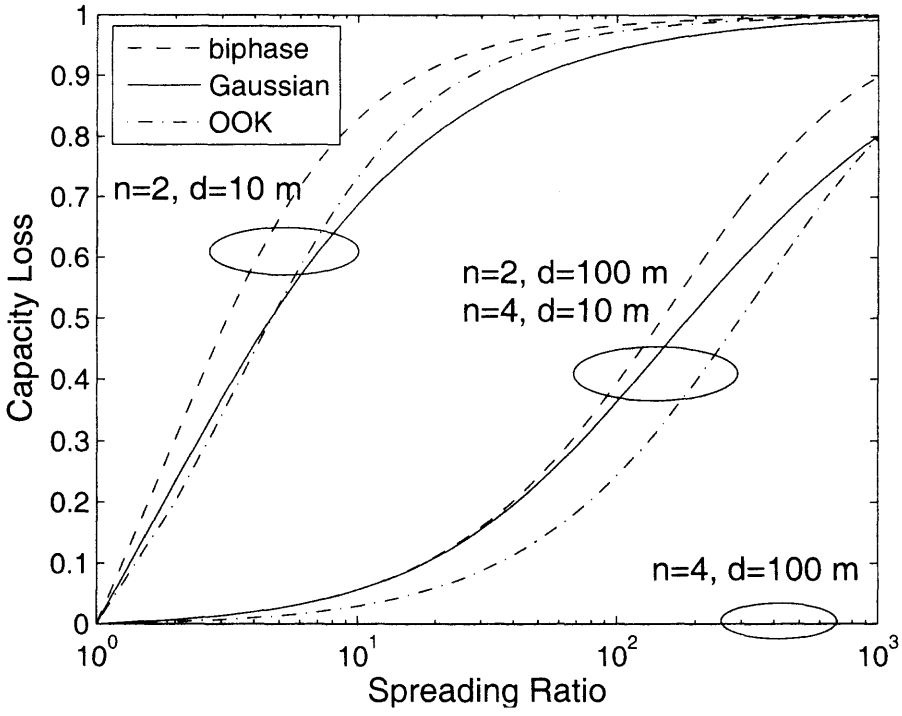

Figure 3.7 Capacity loss as a function of spreading ratio for different signaling inputs with LOS ($n = 2$) and NLOS ($n = 4$).

format seems to have little impact on the results. It is clearly demonstrated that at the low SNR (corresponding to a large distance), the capacity loss due to spreading is small.

3.4.3 Information Rates in Multipath Channels

Throughout this section, it was argued that when the SNR is sufficiently low, substituting spreading gain for coding gain carries only a small loss in performance over the AWGN channel. Now turn the attention to the multipath channel. For the AWGN channel, it is clear from inspecting (3.35) or any of the expressions for specific modulations that the capacity (information rates for the modulations) is monotonically non-increasing with the spreading gain ρ. The effect of the spreading gain on the capacity over multipath channels is demonstrated in Figure 3.9. The figure plots the 10% outage probability of the information rate versus spreading ratio for four different UWB modulation formats and two frequency selective channels. The maximum delay spread is $\tau_{\max} = 50$ ns, or 88 resolved multipaths

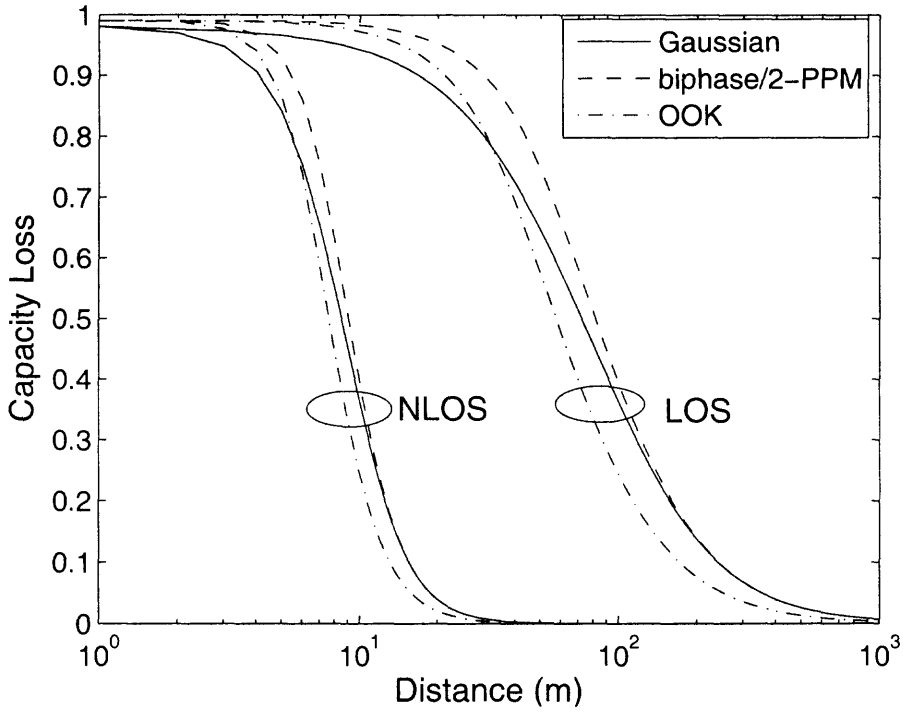

Figure 3.8 Capacity loss as a function of transmission distance for a given spreading ratio $\rho = 100$.

over 1.75 GHz signal bandwidth. The distance from the transmitter is assumed d $= 100$ m (for the purpose of computing the SNR), and the number of paths processed is $L_c = 20$.

The channel C1 features a Rayleigh channel, while the channel C2 is assumed to be a log-normal fading with standard deviation 3.3941 dB [21]. In an interesting contrast with the AWGN channel, it is observed for all the curves in the figure that there are regions for which the rate *rises* with the spreading gain. An intuitive explanation to this is that for the signals of interest, the spreading gain is realized by reducing the duty-cycle, which in turn mitigates against the SI and ISI. The capacity increases when a higher spreading gain improves the SINR.

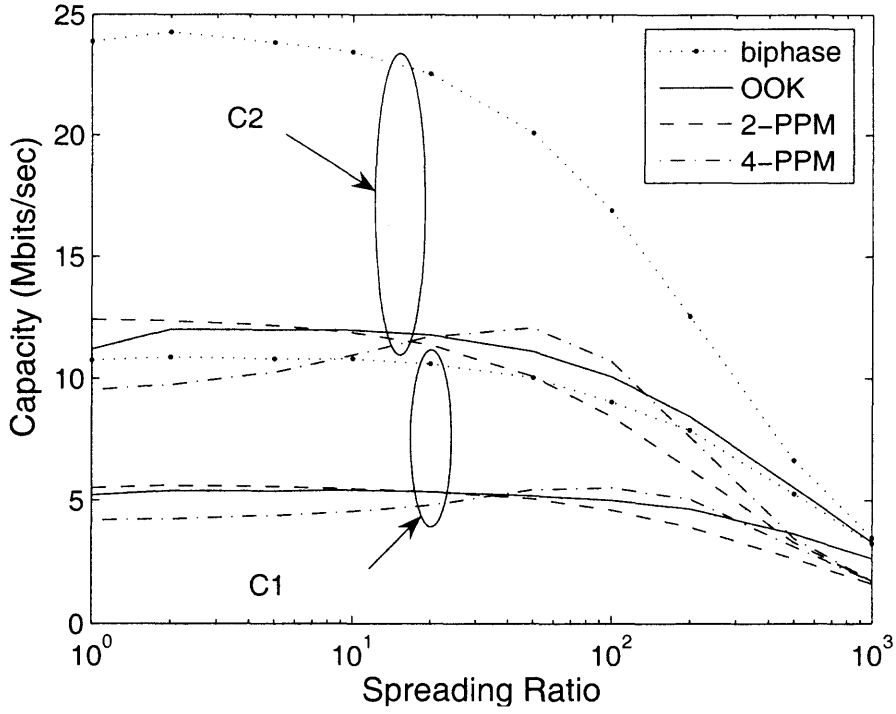

Figure 3.9 Capacity with 10% outage probability over multipath fading channels as a function of spreading ratio for different signaling inputs. The C2 (IEEE 802.15.3a LOS channel) is also plotted as a comparison. It is assumed $\tau_{\max} = 50$ ns, d $= 100$ m, and $L_c = 20$.

3.5 Chapter Summary

The achievable rates for UWB systems was investigated for different signaling formats and under specific conditions: constrained power spectral density and a highly frequency-selective channel. Under these conditions, the achievable rates were evaluated as a function of the transmitter-receiver separation. For the multipath channel, the effect of interference (SI, IPI, and ISI) was quantified, and modulation formats that mitigate against the interference were identified. It was shown that modulations with larger separation between signals are more favorable for use over the frequency-selective channel. Thus, at high and medium SNR, where the performance is interference-limited, 4-PPM outperforms 2-PPM, and the latter outperforms biphase and OOK. At low SNR, where the performance

is noise-limited, and over the AWGN channel, biphase provides the best performance among conventional modulation formats.

The spreading gain was evaluated for several modulations. The relations between the SNR per bit and coding rate at capacity were formulated for these modulations. It was shown that limiting the coding to a low rate such as 1/4 and applying the rest of the bandwidth expansion to spreading incurs only a small loss compared to exploiting the full bandwidth for coding. Finally, it was demonstrated that over the multipath channel, spreading is actually beneficial in reducing the effect of SI and ISI and thus, rather surprisingly, leads to higher capacity in some cases.

CHAPTER 4

OPTIMUM COMBINING FOR UWB RAKE RECEIVERS

In this chapter, the application of reduced-rank adaptive filtering techniques is applied to solve the problem of interference suppression in UWB communications. The performance of the proposed reduced-rank combining methods, in particular the eigencanceler (EC), is compared with the MMSE Rake receiver. It is shown that the EC is effective in suppressing interference modeled as WLAN 802.11a signals. Simulation results are presented to show that the EC requires a shorter data record than MMSE Rake receivers.

4.1 Introduction

Ultra-wideband technologies are proposed as an alternative physical layer for emerging WPAN's. The ability to resolve multipath is one of the most attractive features of UWB. Numerous investigations have confirmed that the UWB channel can be resolved into a significant number of multipath components (for example, [57]). A Rake receiver can be employed to exploit multipath diversity [42, 58]. The Rake receiver using MRC, is optimum only when the disturbance to the desired signal is sourced by AWGN. The WPAN's, including those with a UWB physical layer typically will be required to operate in proximity to other wireless networks, for example, the proliferating WLAN's [59]. In the presence of narrowband interference emitted by WLAN's, a UWB receiver with a conventional Rake combiner will exhibit an error floor dependent on the SINR. A more suitable diversity scheme to employ in this case is *optimum combining* (OC), whereby the received signals are weighted and combined to maximize the output SINR [60].

The MMSE Rake is a possible implementation of OC [61, 62]. The MMSE scheme is optimal (in the sense that it achieves the maximum likelihood solution for Gaussian interference plus noise) if the correlation of the received signal (aggregate of transmitted

signals, interference, and noise) is known. When this correlation matrix has to be estimated, the MMSE solution is affected by measurement noise and is no longer optimal. An eigenanalysis based OC scheme, referred to as the *eigencanceler* (EC), has been suggested for various applications, among them suppression of narrowband interference in direct-sequence spread spectrum [63]. The EC exploits the inherent low-rank property of the narrowband interference correlation matrix. It is designed as a weight vector orthogonal to the *interference subspace*. The interference subspace is defined as the signal space spanned by the eigenvectors associated with the dominant eigenvalues. For the method to be effective, the dominant eigenvalues need to be contributed mainly by the interference. This is the case for low SINR. The EC is motivated by the observation that the correlation matrix of the received signal consists of a limited number of large eigenvalues contributed by the narrowband interference, and a large number of small and almost equal eigenvalues contributed by the desired signal and AWGN. A tap-weight vector orthogonal to the interference eigenvectors effectively cancels the interference, leaving most of the data untouched. The EC is computed from relatively few stable eigenvectors spanning the interference subspace. Thus, even with a short data record, it can obtain a high degree of interference cancellation. In this chapter, the application of the EC is applied to UWB systems over time dispersive channels.

This chapter is organized as follows. In Section 4.2, the UWB system model is described. Section 4.3 presents the two approaches, MMSE and EC, for optimum combining at the UWB Rake receiver. Simulation results are provided in Section 4.4 to compare the performance of the MMSE and EC according to bit error rate, output power of the interference-plus-noise, SINR improvement, and normalized weight variance. In Section 4.5, conclusions are drawn and further investigations are proposed.

4.2 System Model

A received signal diagram is plotted in Figure 4.1. Consider a binary bit stream $\{d_k\} \in \{\pm 1\}$ transmitted over a multipath channel. For an impulse radio UWB, each data bit is represented by a sequence of N_p time-delayed pulses. The basic pulse is chosen to meet the limits imposed by the FCC emissions mask [11]. An example of such a pulse is proposed in Chapter 2 and in [53]. Denote $p(t)$ the basic pulse as seen at the receiver. Then the basic waveform representing a data bit as seen at the receiver is given by

$$q(t) = \sum_{j=1}^{N_p} p(t - jT_f - c_j T_c), \tag{4.1}$$

where without loss of generality $p(t)$ is scaled such that $\int_{-\infty}^{+\infty} q^2(t)dt = 1$. The average pulse interval is T_f, and T_c provides an additional time shift to the jth pulse due to the time-hopping sequence c_j. Polarity reversals can eliminate the spectral lines and reduce the peak-to-average ratio [38, 39]. Two types of modulation, biphase and binary PPM, are considered. Hence, the following model is used for the received signal at time epoch k,

$$r_k(t) = \begin{cases} d_k\sqrt{E_b}q(t - kT_s) * h(t) + i(t) + n(t), & \text{biphase} \\ \sqrt{E_b}q(t - kT_s - d_k\tau_p) * h(t) + i(t) + n(t), & \text{binary PPM} \end{cases} \tag{4.2}$$

where the subscript k represents the bit index, E_b is the energy per bit, $T_s = T_f N_p$ is the symbol duration, and τ_p is a PPM shift that ensures orthogonality between the two symbols of the modulation. The dispersive channel response, $h(t)$, is modeled by a tapped-delay-

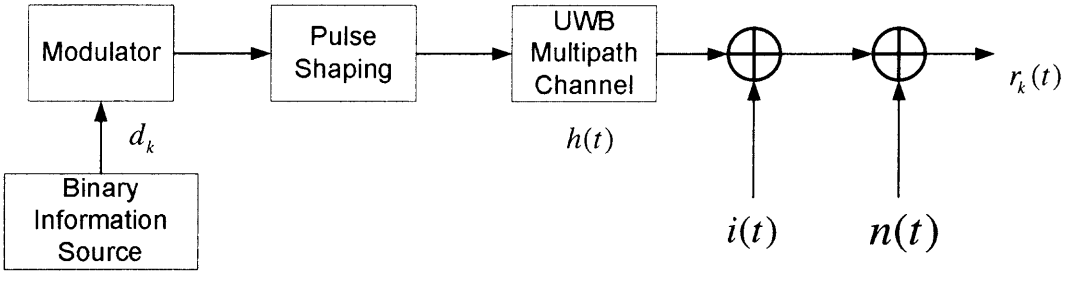

Figure 4.1 A simple UWB received signal model with narrowband interference.

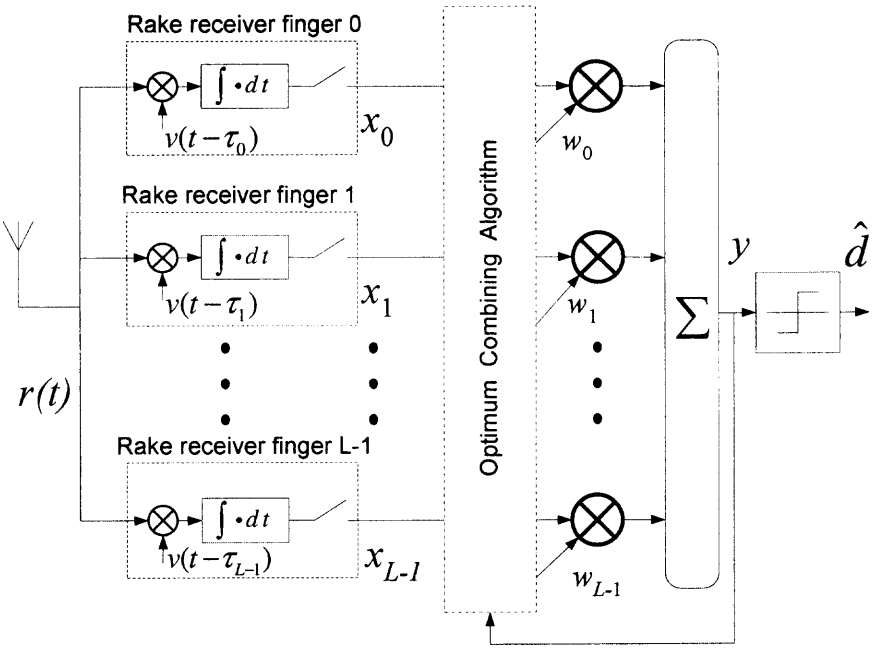

Figure 4.2 A Rake receiver with optimum combining to cancel narrowband interference for impulse radio UWB systems.

line

$$h(t) = \sum_{\ell=0}^{\widetilde{L}-1} \alpha_\ell \delta(t - \tau_\ell), \tag{4.3}$$

where $\widetilde{L}$ is the number of resolvable delay bins in the multipath channel, and α_ℓ and τ_ℓ are the channel path amplitude and delay, respectively. Denote $i(t)$ the narrowband interference and residual ISI. The noise $n(t)$ is white, Gaussian with zero-mean and two-sided power spectral density of $N_0/2$. Consistent with the baseband model assumed, all quantities are real-valued.

An OC Rake receiver is composed of L correlators followed by a linear combiner as shown in Figure 4.2. The Rake receiver samples the received signals at the symbol rate and correlates them with suitably delayed references [64]. The correlator is operated with perfect knowledge of the channel amplitudes and delays. The reference $v(t)$, is given

by [62]

$$v(t) = \begin{cases} q(t), & \text{biphase} \\ q(t-\tau_p) - q(t+\tau_p), & \text{binary PPM.} \end{cases} \tag{4.4}$$

The received signal at the output of the correlator corresponding to the ℓ th finger of the Rake receiver and the reference delayed by τ_ℓ, is

$$\begin{aligned} x_{\ell,k} &= \int_{-\infty}^{+\infty} r_k(t) v(t - kT_s - \tau_\ell) dt \\ &= d_k \sqrt{E_b} \alpha_\ell + i_{\ell,k} + n_{\ell,k},\ 0 \leq \ell \leq L-1 \end{aligned} \tag{4.5}$$

where $i_{\ell,k}$ and $n_{\ell,k}$ are the interference and noise at the output of the correlators, respectively. The signal model in vector notation is

$$\mathbf{x}_k = d_k \sqrt{E_b} \mathbf{h} + \mathbf{i}_k + \mathbf{n}_k, \tag{4.6}$$

where $\mathbf{x}_k = [x_{0,k}, \ldots, x_{L-1,k}]^T$, $\mathbf{h} = [\alpha_0, \ldots, \alpha_{L-1}]^T$, $\mathbf{i}_k = [i_{0,k}, \ldots, i_{L-1,k}]^T$, $\mathbf{n}_k = [n_{0,k}, \ldots, n_{L-1,k}]^T$, and the superscript ^{T} denotes vector transposition. A bit decision is made at the output of the combiner, $\widehat{d}_k = \text{sgn}(\mathbf{w}^T \mathbf{x}_k)$, where $\mathbf{w} = [w_0, \ldots, w_{L-1}]^T$ is the combiner weight vector.

4.3 Optimum Combining for Rake Receivers

4.3.1 MMSE Rake Receiver

The MMSE filter parameters are varied such that the mean square error between the desired and the actual output is minimized. The SINR is maximized when the optimal weight vector of the MMSE combiner is adopted [65]. The optimal weight vector satisfies

$$\widetilde{\mathbf{w}}_0 = \arg\min_{\mathbf{w}} E\left[\left\| d_k - \mathbf{w}^T \mathbf{x}_k \right\|^2\right]. \tag{4.7}$$

The solution to the MMSE combiner is

$$\widetilde{\mathbf{w}}_0 = \kappa_1 \mathbf{R}^{-1} \mathbf{r}_{dx}, \tag{4.8}$$

or alternatively is [66, p. 74]

$$\widetilde{\mathbf{w}}_0 = \kappa_2 \mathbf{M}^{-1} \mathbf{r}_{dx}, \tag{4.9}$$

where κ_1 and κ_2 are scaling constants, $\mathbf{R} = E\left[\mathbf{x}_k \mathbf{x}_k^T\right]$ and $\mathbf{M} = E\left[\mathbf{i}_k \mathbf{i}_k^T + \mathbf{n}_k \mathbf{n}_k^T\right]$ are the correlation matrix of the received signal and the interference-plus-noise, respectively. The vector $\mathbf{r}_{dx}$ is the correlation output of d_k and $\mathbf{x}_k$. In practice, the matrix $\mathbf{M}$ has to be estimated from a block of training symbols. In this case, MMSE is no longer optimal. It depends on how good is the estimate of $\mathbf{M}$. The maximum likelihood estimate is given by the sample covariance matrix $\widehat{\mathbf{M}} = (1/K) \sum_{k=0}^{K-1} \mathbf{x}_k \mathbf{x}_k^T$, where K is the block size. Since training is an overhead function that consumes resources, it is of interest to develop techniques that can work with short training sets. It is well known that the number of vector samples required to estimate an $L \times L$ correlation matrix within 3 dB of its true value is $2L$ [67]. For a dispersive channel resulting in a large number of non-zero paths L, the number of samples required to train MMSE might be prohibitive. In the next subsection, a reduced-rank optimum combiner is proposed based on an eigenanalysis approach which is more robust to errors caused by short training sets.

4.3.2 EC Rake Receiver

By eigen-decomposition, the correlation matrix of the interference-plus-noise is expressed as

$$\mathbf{M} = \mathbf{Q}_I \mathbf{\Lambda}_I \mathbf{Q}_I^T + \mathbf{Q}_v \mathbf{\Lambda}_v \mathbf{Q}_v^T, \tag{4.10}$$

where the columns of $\mathbf{Q}_I$ and $\mathbf{Q}_v$ consist of, respectively, the interference eigenvectors and the noise eigenvectors. The matrices $\mathbf{\Lambda}_I$ and $\mathbf{\Lambda}_v$ are diagonal and contain the interference and noise eigenvalues, respectively. For an interference with bandwidth considerably smaller than the signal bandwidth, the eigenanalysis of the interference-plus-noise matrix reveals a few large eigenvalues and a large number of small eigenvalues. The eigenvectors associated with large eigenvalues span the interference subspace. Since the interference

subspace is orthogonal to the noise subspace, a tap-weight vector residing in the noise subspace will effectively cancel the interference, leaving most of the information data untouched. The tap-weight of the EC is designed to minimize the norm of the weight vector while maintaining linear and eigenvector constraints given by

$$\min \mathbf{w}^T\mathbf{w} \text{ subject to } \mathbf{w}^T\mathbf{r}_{dx} = g \text{ and } \mathbf{Q}_I^T\mathbf{w} = \mathbf{0}, \tag{4.11}$$

where g is a constant. The solution then follows [68, 69]

$$\widetilde{\mathbf{w}}_e = \kappa_2 \left(\mathbf{I} - \mathbf{Q}_I\mathbf{Q}_I^T\right) \mathbf{r}_{dx}, \tag{4.12}$$

where κ_2 is a fixed scalar. It shows that the weight vector of the EC is constructed from the stable eigenvectors of the largest eigenvalues of the received signal. It is unaffected by fluctuations in the noise eigenvalues. This leads to a high degree of interference cancellation shown next.

4.4 Performance Evaluation

In this section, the performance of MMSE and EC-Rake receivers is evaluated with respect to bit error rate, residual interference-plus-noise power, SINR improvement, and normalized variance of the weight vectors.

The channel is simulated using the IEEE 802.15.3a channel model [21], a modified model from [25]. This channel is passed through a bandpass filter at the center frequency of 5 GHz with the bandwidth corresponding to a 1 GHz UWB system. Biphase modulation is used with the data rate of 40 Mbps over the dispersive 802.15.3a CM1 (LOS) channel. With this data rate, the ISI can be ignored and about 98% of the energy can be collected within one bit duration.

The transmitted UWB signal power is restricted by the FCC allowing emissions with a power spectral density of -41.3 dBm/MHz. Due to the very low transmission power, even the large processing gain of the UWB system is not sufficient to suppress high levels

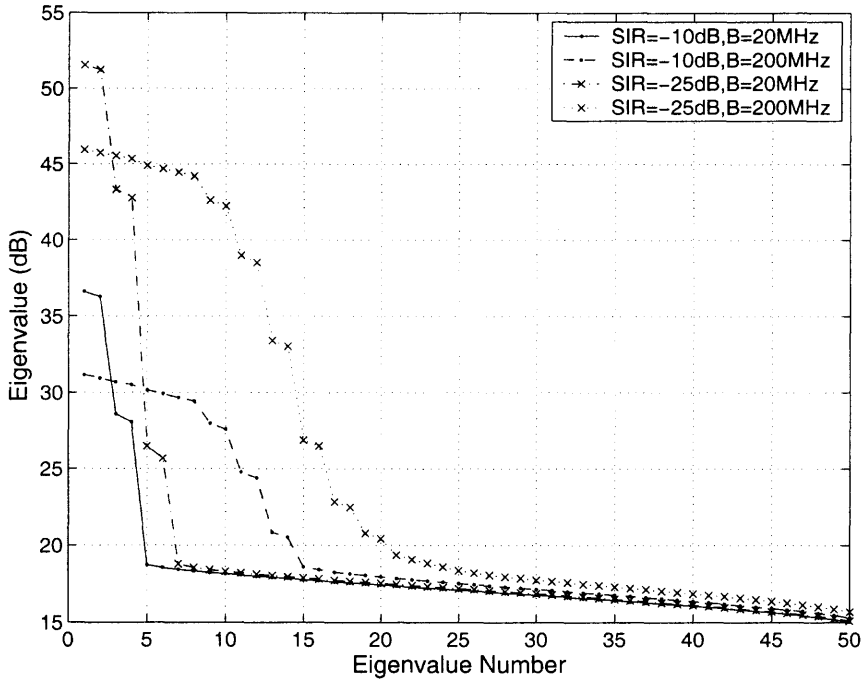

Figure 4.3 Eigenvalues of the correlation matrix over the IEEE 802.15.3a LOS channel in the presence of narrowband interference.

of interference [30]. The narrowband interference is modeled as a bandpass Gaussian signal representing the IEEE 802.11a interference with bandwidth $B = 20$ MHz [61]. The transmitted power of the interference is assumed to be 15 dBm. Assume a scenario where the UWB receiver is placed 1 meter from the UWB transmitter, and 2 meters from the interfering transmitter. A simple link budget calculation shows that the average SIR is approximately -10 dB in free-space. In the simulation, the SIR is assumed to be -10 dB, and the signal-to-noise ratio per bit (E_b/N_0) is 10 dB.

Figure 4.3 plots the eigenvalues of the interference-plus-noise correlation matrix for a 50-tap receiver. It is noted that for a 1 GHz system, and an interference with SIR = -10 dB and bandwidth 20 MHz, the number of dominant eigenvalues is 4 out of a total of 50. The interference subspace used to determine the tap weights of the EC is constructed from the 4 eigenvectors associated with these eigenvalues.

Figure 4.4 shows the BER performance of selective-combining (SC) Rake parameterized by the number of the best branches combined, L, for a biphase system.

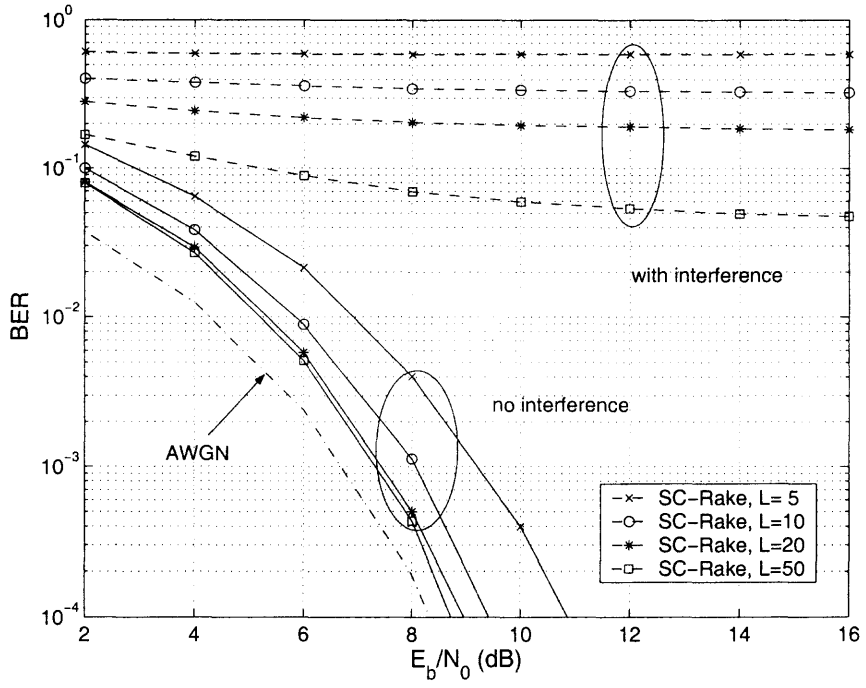

Figure 4.4 BER performance of biphase UWB systems by MRC with SC-Rake over IEEE 802.15.3a LOS channel in the presence of 802.11a interference with SIR=-10 dB.

The combining is carried out utilizing MRC. It is observed that the interference causes a high error floor. This motivates seeking optimum combining techniques.

The performance of SC-Rake with MMSE and EC receivers is compared in Figure 4.5. The $L = 40$ largest energy paths of the channel are selected for processing. At BER of 10^{-4}, the EC with $K = 30$ bit training has a 2.5 dB advantage over MMSE with 80 bit training, and about a 5 dB gain compared with MMSE with 60 bit training.

Further insight into the effect of the training data set can be gained by measuring the residual interference power $P_J = \widetilde{\mathbf{w}}^T \mathbf{M} \widetilde{\mathbf{w}}$. Figure 4.6 plots the interference-plus-noise power at the output of the EC, MMSE combiners versus the size of the training data. The $L = 50$ paths are combined. The figure indicates that with limited data, the output interference-plus-noise power from the EC is much lower than of the MMSE combiner.

The advantage of the EC can be also gleaned from the SINR improvement defined as the ratio of SINR's at the combiner output and input. From (4.6), the SINR per bit at the

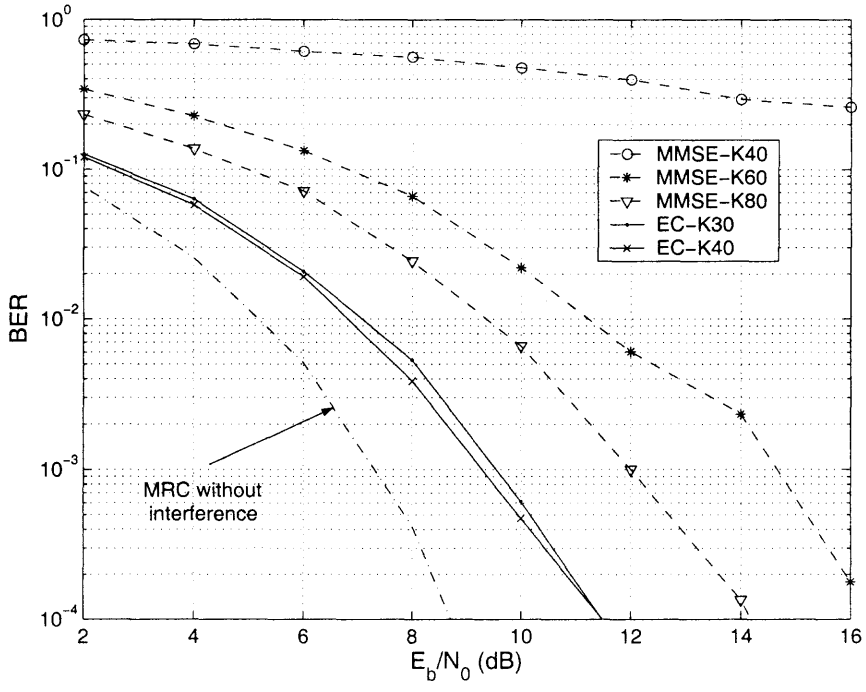

Figure 4.5 BER for biphase UWB systems by MMSE and EC combiner with selected $L = 40$ largest fingers over the 802.15.3a LOS channel in the presence of 802.11a interference.

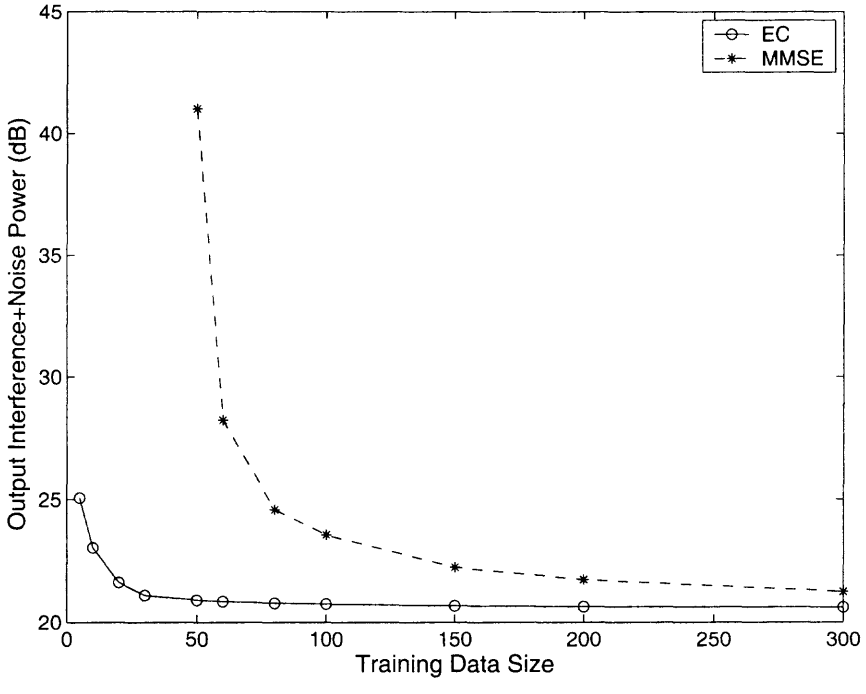

Figure 4.6 Comparison of the output power of the interference-plus-noise as a function of training data size between the MMSE and EC Rake receiver. The L=50 taps are used.

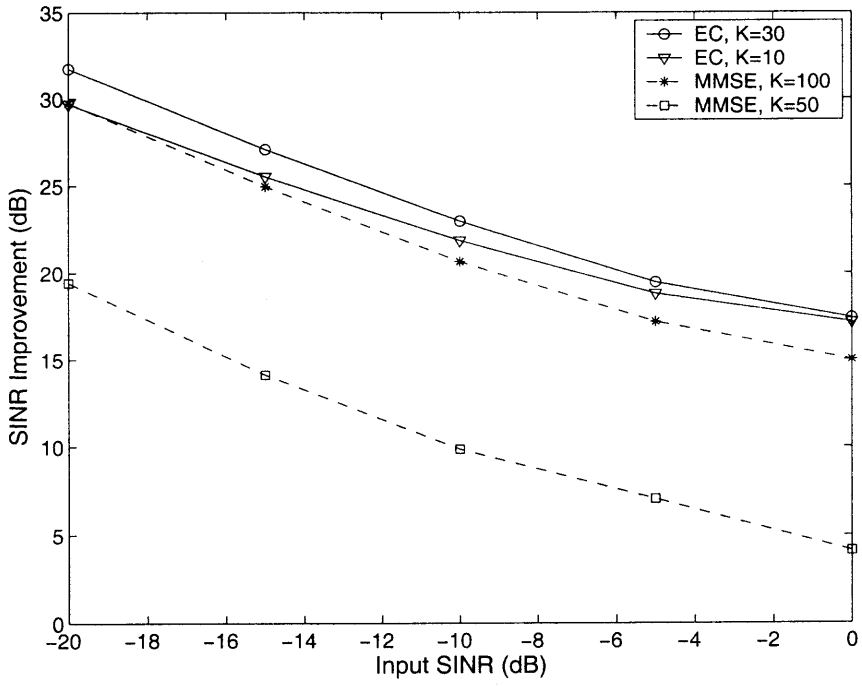

Figure 4.7 SINR improvement as a function of input SINR in the presence of the 802.11a OFDM interference over the 802.15.3a LOS channel. L=50 taps are employed. SNR per bit is 10 dB.

input to the combiner is

$$\text{SINR}_i = \frac{E_b}{I_0 + N_0}, \tag{4.13}$$

where I_0 is the power spectral density of the interference. The output SINR is given by

$$\text{SINR}_o = \frac{E_b \left\| \mathbf{w}^T \mathbf{r}_{dx} \right\|^2}{\mathbf{w}^T \mathbf{M} \mathbf{w}}. \tag{4.14}$$

The SINR improvement as a function of input SINR is plotted in Figure 4.7 in the presence of an IEEE 802.11a interference at SNR per bit of 10 dB. The $L = 50$ paths are combined. With a small data size K, the EC achieves larger SINR improvement than the MMSE. For example, the SINR improvement of the EC with 30 bit training is 2 dB larger than that of MMSE with 100 bit training, and 13 dB larger than MMSE with 50 bit training. Even with very short training of 10 bits, the EC still provides a larger SINR improvement than the MMSE with a training of 50.

The normalized variance of the weight vectors is a measure of the robustness of the combiners of the effects of noise. When the correlation matrix is estimated from a finite number of samples, the receiver noise causes perturbations in the values of the weight vectors. The normalized weight variance is defined as [68]

$$E\left[\frac{\|\Delta\mathbf{w}\|^2}{\|\mathbf{w}\|^2}\right] = \frac{E\left[\|\widehat{\mathbf{w}}-\mathbf{w}\|^2\right]}{\mathbf{w}^T\mathbf{w}}, \tag{4.15}$$

where $\widehat{\mathbf{w}} = \mathbf{w}+\Delta\mathbf{w}$ is the estimated weight vector, $\mathbf{w}$ is the optimal weight vector computed with known signal statistics, and $\Delta\mathbf{w}$ is the perturbation of the weight vector. Table 4.1 lists the normalized weight variances for the MMSE and EC combiners as a function of the training data size K. It is observed that the EC has a much lower normalized weight variance than the MMSE.

Table 4.1 Normalized Variance of the Weight Vector for the Combiner

K	50	60	80	100	150	200
MMSE	3.9037	1.4250	1.1237	0.9749	0.8167	0.7485
EC	0.0092	0.0074	0.0055	0.0043	0.0029	0.0023

In this chapter, ideal channel information was assumed. In practice, the channel also has to be estimated from the training data. Estimation error will lead to performance loss. This is shown in Figure 4.8. It is assumed that only 10 pilot symbols are allocated for channel estimation. It is shown that EC is still superior to MMSE with a short data record. However, more than 4 dB loss occurs due to imperfect channel estimation. In the next two chapters, the work will assess the effect of Rake combiners when channel estimation is taken into account.

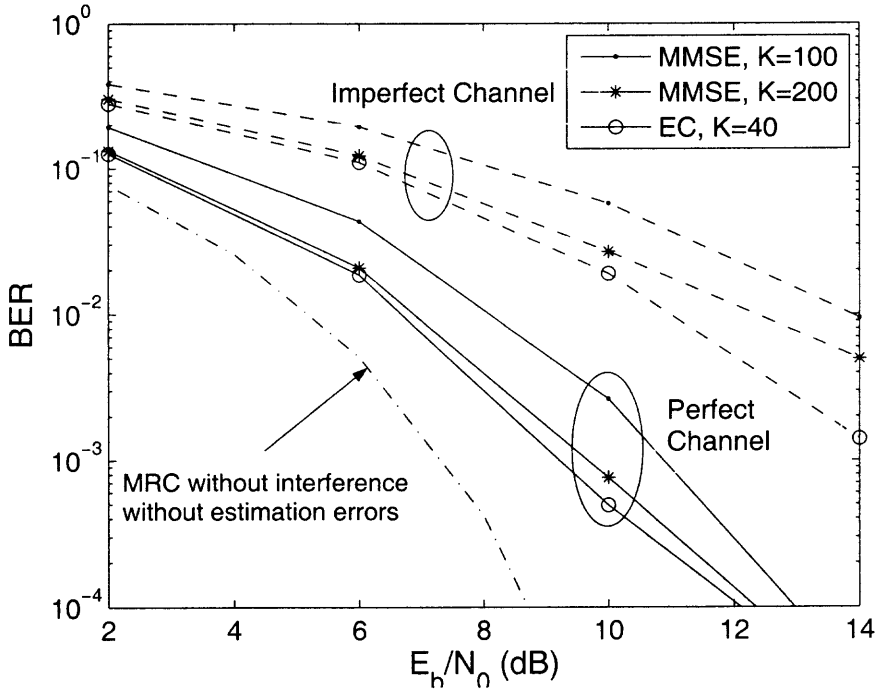

Figure 4.8 Imperfect channel estimation degrades the performance for OC. The number of selected Rake fingers is $L = 40$. Pilot symbols are used for channel estimation with 10 number of pilot symbols. It is assumed that SIR is -10 dB.

4.5 Chapter Summary

In this chapter, an eigenanalysis based optimum combining scheme was applied for impulse radio UWB Rake receivers in the presence of narrowband interference. The performance was evaluated in WPAN scenarios with respect to BER, residual interference-plus-noise power, SINR improvement, and normalized variance of the weight vectors. Simulation results were presented by comparing the performance of eigencanceler and MMSE. It was demonstrated that the performance of the proposed method is superior to the MMSE when the correlation matrix is estimated from limited data.

In this chapter, perfect channel information was assumed. In practice, channel state information is not known *a priori* and has to be estimated. Estimation errors will lead to performance loss and affect the criterion of transceiver design. In the next two chapters,

the impact of imperfect channel estimation will be discussed on performance of the UWB system and the design of optimum transceiver parameters.

CHAPTER 5

BER OF UWB RAKE RECEIVERS WITH IMPERFECT CSI

In the following two chapters, the impact of imperfect channel estimation is investigated on performance of the UWB system and the design of optimum transceiver parameters. This chapter analyzes the effect of non-idea estimates on system performance when path delays and path amplitudes are jointly estimated. The CRB of the path delay estimates is derived as a function of the SNR and signal bandwidth. The performance of a UWB system employing a Rake receiver with MRC is analyzed taking into account estimation errors as predicted by the CRB. Expressions of the BER are obtained displaying the effect of the number of pilot symbols and the number of multipath components on the overall system performance.

Using the derived BER, Chapter 6 will evaluate the impact on information rates. It will determine the optimal transceiver parameter design, such as the fraction of a transmitted packet constituted by the pilot symbols, signal bandwidth, and the number of diversity paths used at the receiver.

5.1 Introduction

The UWB channel can be resolved into a significant number of distinct multipath components [21, 22, 24, 70, 71]. A Rake receiver with MRC can be employed in UWB systems to exploit multipath diversity [57]. However, Rake receivers require knowledge of multipath delays and amplitudes. In practice, that is obtained through pilot aided channel estimation [72], producing imperfect CSI which leads to degraded performance.

The effect of errors in the estimation of path amplitudes in diversity combining systems has been investigated extensively in the literature [73, 74, 75, 76, 77]. In some of these works, the estimation error of each path amplitude was characterized by a correlation

coefficient between the true path amplitude and its estimate. This correlation coefficient was assumed independent of the SNR. This model does not reflect the fact that as the SNR increases, the quality of the estimator improves. The problem of channel estimation and diversity combining is particularly relevant to UWB communications. Application of pilot aided channel estimation to UWB systems was discussed in [78]. The performance of diversity combining as a function of the signal bandwidth was reported in [79] in the presence of path amplitude estimation errors. In these studies, perfect path delay information was assumed. In [72], the effects of estimation errors of path delays and amplitudes on performance were evaluated numerically. No analytical results are available on the performance of IR-UWB with joint estimation of path delays and amplitudes.

In this chapter, the impact of non-ideal estimates of both path delays and path amplitudes is analyzed on UWB system performance. An analytical expression of the BER is derived with imperfect channel estimates. To obtain the CSI, pilot symbols are transmitted over a multipath channel with a diversity of paths. The maximum likelihood (ML) estimation is used. In Section 5.3, the CRB of the variance of path parameters' estimates is derived. Using the errors predicted by the CRB, in Section 5.4, the average SNR and BER are analyzed for a Rake receiver employing MRC. The SNR and BER are expressed in terms of the number of pilot symbols and the number of diversity paths. This BER will be used in the next chapter for the design of transceiver parameters.

5.2 System Model

A single user IR-UWB system model is shown in Figure 5.1. A binary bit stream is transmitted over a multipath channel. Each data bit is represented by a short duration pulse, denoted $q(t)$, with energy $E_p = \int_{-\infty}^{\infty} q^2(t)dt$. Examples of such pulses are the general Gaussian pulse,

$$q(t) = \frac{c_1}{\sqrt{2\pi}\sigma_p} \exp\left(-\frac{t^2}{2\sigma_p^2}\right), \tag{5.1}$$

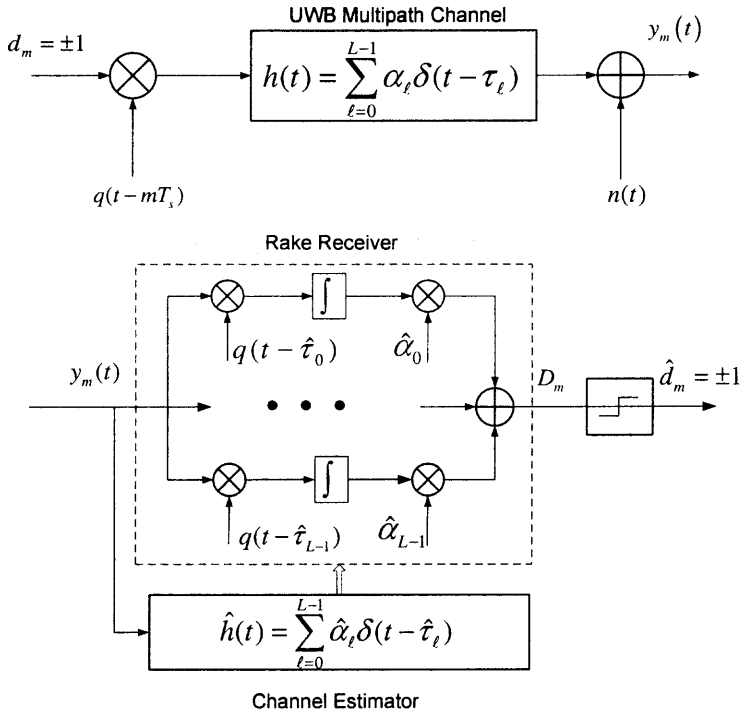

Figure 5.1 A complete impulse radio UWB transmission model over a dispersive multipath channel.

and its higher derivatives [57, 53], where c_1 is a constant, and σ_p controls the pulse width and pulse bandwidth. By the definition of the duration of the Gaussian pulse in Chapter 2, the pulse width, $T_p \approx 10\sigma_p$.

The UWB multipath channel can be modelled by the impulse response $h(t) = \sum_{\ell=0}^{L-1} \alpha_\ell \delta(t - \tau_\ell)$, where L is the number of multipath components, and α_ℓ and τ_ℓ are the ℓ-th path amplitude and delay, respectively. The delays τ_ℓ take values in the continuum of time. Measurements show that the UWB channel has an inherently sparse structure [21, 22, 26, 71]. This means that not each resolvable delay bin contains significant energy. Mathematically, this is expressed as $L \ll \widetilde{L} = \lceil \tau_{\max}/T_p \rceil$, where "$\lceil\ \rceil$" denotes the next integer larger than the listed value, and $\tau_{\max} = \tau_{L-1} - \tau_0$ serves as the maximum delay spread. A sparse UWB channel is illustrated in Figure 5.2. In the sparse channel model, the inter-path interference is negligible [80].

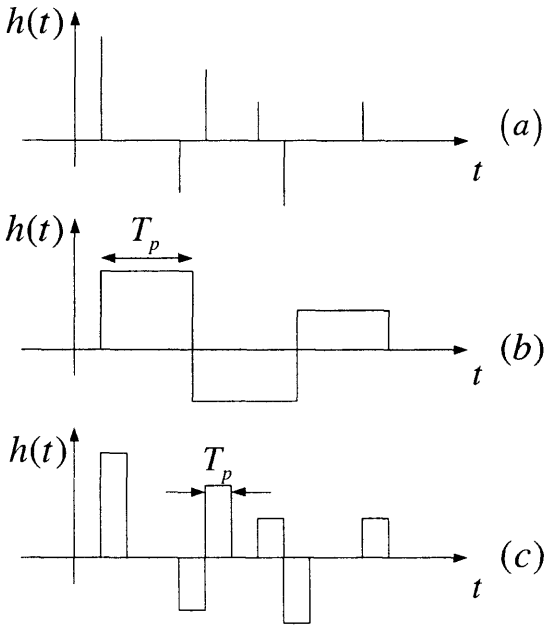

Figure 5.2 Sparse and dense channels: (a) true channel impulse response (b) effective response for small bandwidth systems (dense) (c) effective response for large bandwidth systems (sparse). It is assumed that the multipath resolution achieved by the receiver is equal to the pulse width T_p.

The channel statistics are Nakagami-*m* fading for the distribution of the paths' envelopes [24]. The average power over different channel realizations at the output of the ℓ-th path is expressed $\Omega_\ell = E[\alpha_\ell^2] = \bar{\Omega} \exp[-(\tau_\ell/\tau_{L-1})\,\delta_0]$, where $\bar{\Omega}$ is chosen such that the total average received power is unity, and δ_0 is a constant which determines the power decay factor. In order to reasonably compare channels with different numbers of paths L, δ_0 is determined by the procedure suggested in [81] and reviewed below for the convenience of the reader. The constant δ_0 is chosen such that channel observations have a prescribed dynamic range, say $x = 30$ dB, independent of L. Thus, δ_0 can be found from $\exp[\delta_0(1 - \tau_0/\tau_{L-1})] = 10^3$. It follows that $\delta_0 = \frac{\tau_{L-1}}{\tau_{\max}}(3 \ln 10)$. Implicitly, this formulation neglects paths outside a prescribed dynamic range.

It is of interest to note the relation between the number of paths L and the signal bandwidth. In all of these studies, the signal power is assumed constant. The number of

resolvable delay bins in the channel is $\widetilde{L} \approx \lceil \tau_{\max}/T_p \rceil \approx \lceil \tau_{\max} W \rceil$, where W is the signal bandwidth (according to an arbitrary definition of bandwidth). Even though the actual number of paths $L \ll \widetilde{L}$, increasing the bandwidth will entail an increase in the number of paths L. Similarly, since the averaged received power is assumed constant, increasing the bandwidth will lead to a reduction of the path amplitude.

Let the transmitted pulses be biphase modulated with a pulse representing a UWB symbol. The symbol interval is denoted T_s. The signal received during the interval $0 \leq t \leq T_s$ can be expressed as

$$\begin{aligned} y(t) &= dq(t) * h(t) + n(t) \\ &= d\sum_{\ell=0}^{L-1} \alpha_\ell q(t - \tau_\ell) + n(t), \ 0 \leq t \leq T_s, \end{aligned} \tag{5.2}$$

where $d \in \{\pm 1\}$ denotes a binary symbol, '$*$' represents the convolution operation, and $n(t)$ is additive white Gaussian noise with zero-mean and two-sided power spectral density $N_0/2$. The symbol duration is assumed to be much longer than the maximum delay spread, i.e., $T_s \gg \tau_{\max}$, such that inter-symbol interference can be neglected.

The receiver, shown in Figure 5.1, implements a Rake receiver with L correlators (fingers), where each finger can extract the signal from one of the multipath components. The outputs of the correlators are combined using MRC. The combiner requires knowledge of the paths' delays and amplitudes. In practice, the parameters $\{\alpha_\ell\}$ and $\{\tau_\ell\}$ are not known *a priori* and must be estimated. In this work, it is assumed that the estimation is aided by a preamble of M pilot symbols. The full data packet consists of Q symbols. If the total energy available for transmitting $(Q - M)$ data symbols is $(Q - M) E_b$, then the energy per pulse is $E_p = (1 - M/Q) E_b$.

The channel estimates computed from the pilot symbols are used to detect the subsequent data symbols. Block fading is assumed, where α_ℓ and τ_ℓ are invariant over the duration of one packet and change independently from packet to packet.

5.3 Estimation Errors of Channel Parameters

In this section, the ML estimate and the CRB of the path delay and amplitude estimation errors are calculated as functions of the parameters of the pilot symbols. The ML estimate is used in the numerical simulations discussed in Section 5.4. The closed-form expression of the CRB of the path is used in the theoretical analysis. The ML path amplitude estimate is biased by the delay errors. In this case, the conditional estimate and its error are computed. Throughout, the number of paths L is assumed known.

Without loss of generality, all M pilot symbols in a packet are assumed to be $d = 1$. Then, the received signal associated with the pilot symbols and the ℓ-th path is

$$y_\ell(t) = \sum_{m=0}^{M-1} \alpha_\ell q(t - mT_s - \tau_\ell) + n(t), \quad 0 \le t \le MT_s. \tag{5.3}$$

The likelihood function for the ℓ-th path, conditioned on the path parameters α_ℓ and τ_ℓ, is given by

$$p(y_\ell|\alpha_\ell, \tau_\ell) = c_2 \exp\left\{-\frac{1}{N_0}\int_0^{MT_s}\left[y_\ell(t) - \sum_{m=0}^{M-1}\alpha_\ell q(t - mT_s - \tau_\ell)\right]^2 dt\right\}, \tag{5.4}$$

where c_2 is a normalization factor for the distribution. The ML estimates of the path delay and path amplitude are the values that maximize (5.4). Due to the monotonicity of the exponential function, the ML changes to maximizing

$$J(\alpha_\ell, \tau_\ell) = 2\alpha_\ell \sum_{m=0}^{M-1}\int_0^{MT_s} y_\ell(t) q(t - mT_s - \tau_\ell) dt - ME_p\alpha_\ell^2. \tag{5.5}$$

In deriving (5.5), the assumption is made that the sparse IR-UWB channel is devoid of inter-path interference. Next, the CRBs of the estimation errors of the path delays and amplitudes are evaluated.

5.3.1 Estimation Errors of Path Delays

The ML estimate of the ℓ-th path delay, using (5.5), reduces to maximizing [72]

$$\left[\sum_{m=0}^{M-1}\int_{0}^{MT_s} y_\ell(t)q\left(t-mT_s-\tau_\ell\right)dt\right]^2, \tag{5.6}$$

which amounts to correlating the received signal with a delayed pulse waveform and adjusting the delay to find the locations of the extrema at the output of the correlator.

The CRB of the variance of $\hat{\tau}_\ell$ is given by [82], $\text{var}\left(\hat{\tau}_\ell\right) \geq \left(E\left[\left(\frac{\partial \ln p(y_\ell|\alpha_\ell,\tau_\ell)}{\partial \tau_\ell}\right)^2\right]\right)^{-1}$. From (5.4), it follows that

$$E\left[\left(\frac{\partial \ln p\left(y_\ell|\alpha_\ell,\tau_\ell\right)}{\partial \tau_\ell}\right)^2\right] = E\left[\left(\frac{2}{N_0}\int_{0}^{MT_s} n(t)\sum_{m=0}^{M-1}\frac{\alpha_\ell \partial q(t-mT_s-\tau_\ell)}{\partial \tau_\ell}dt\right)^2\right]. \tag{5.7}$$

After some algebraic manipulations, it can be shown that

$$E\left[\left(\frac{\partial \ln p\left(y_\ell|\alpha_\ell,\tau_\ell\right)}{\partial \tau_\ell}\right)^2\right] = \frac{2}{N_0}\Omega_\ell M\int_{0}^{T_p}\left[\frac{dq(t)}{dt}\right]^2 dt. \tag{5.8}$$

Finally, applying Parseval's theorem with $S(f)$ as the Fourier transform of $q(t)$,

$$E\left[\left(\frac{\partial \ln p\left(y_\ell|\alpha_\ell,\tau_\ell\right)}{\partial \tau_\ell}\right)^2\right] = \frac{2}{N_0}\Omega_\ell M\int_{-\infty}^{\infty}\left[2\pi f S(f)\right]^2 df. \tag{5.9}$$

It follows that the variance of the estimate error is bounded by

$$\text{var}\left(\hat{\tau}_\ell\right) \geq \frac{1}{\frac{2}{N_0}\Omega_\ell M\int_{-\infty}^{\infty}\left[2\pi f S(f)\right]^2 df}. \tag{5.10}$$

The last expression can be rewritten in terms of the root-mean-square bandwidth of the UWB pulse, ν,

$$\text{var}\left(\hat{\tau}_\ell\right) \geq \frac{1}{\frac{2E_p}{N_0}\Omega_\ell M\nu^2}, \tag{5.11}$$

where

$$\nu^2 \triangleq \frac{\int_{-\infty}^{\infty}(2\pi f)^2\left|S\left(f\right)\right|^2 df}{\int_{-\infty}^{\infty}\left|S\left(f\right)\right|^2 df}. \tag{5.12}$$

For example, for the Gaussian pulse in (5.1), it can be shown that

$$\nu = \frac{2\pi}{\sqrt{2\ln 10}} W, \tag{5.13}$$

where W is the -10 dB bandwidth of the pulse [53].

Equation (5.11) indicates that the CRB of the path delay estimate is inversely proportional not only to the path SNR $(2E_p/N_0)\,\Omega_\ell M$, but also to the mean-square bandwidth of the pulse (ν^2). As the signal bandwidth increases, the estimate of the delays becomes more accurate for a given path gain. However, as discussed in the previous section, an increase in bandwidth also reduces the average power per path Ω_ℓ. That will increase the variance of the estimate. In conclusion, the value of the error variance is controlled by the bandwidth.

Now express the estimate of the ℓ-th path delay as a sum of two terms

$$\hat{\tau}_\ell = \tau_\ell + \epsilon_\ell T_p, \tag{5.14}$$

where ϵ_ℓ is the delay estimate error normalized by the pulse width. From (5.11), the CRB of the variance of ϵ_ℓ is

$$\sigma^2_{\epsilon_\ell} \geq \frac{1}{\frac{2E_p}{N_0}\Omega_\ell M \nu^2 T_p^2}. \tag{5.15}$$

Figure 5.3 plots the variance (mean square error) of the path delay estimates versus E_p/N_0 parameterized by a different number of pilot symbols. The ML estimate and variance are found via Monte Carlo simulation. A path gain $\alpha_\ell = 0.7$ is assumed. It is shown that the variance of the path delay asymptotically approaches the CRB for a large number of pilot symbols and/or high SNR. For example, see the result for $M = 10$ and $E_p/N_0 = 6$ dB.

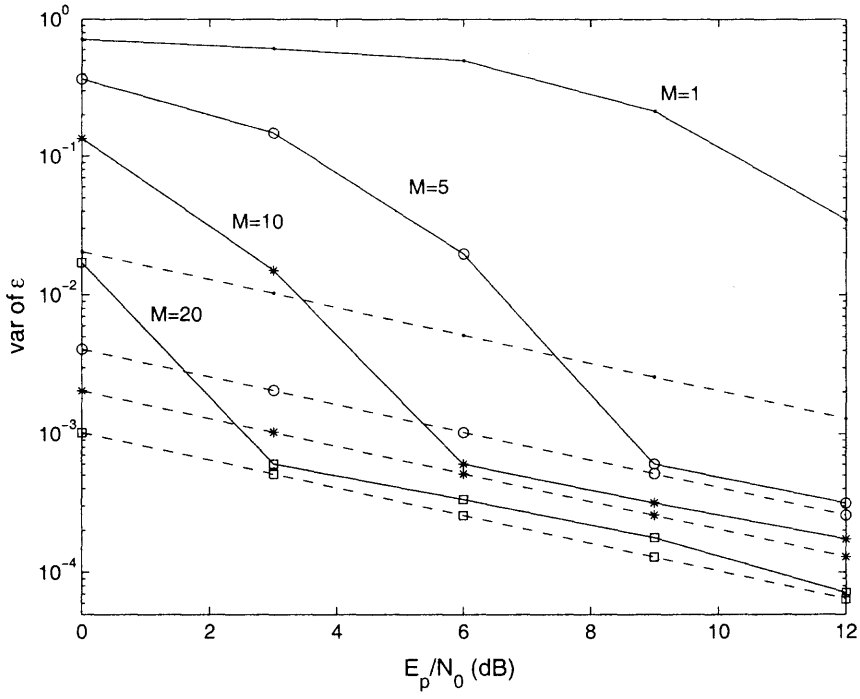

Figure 5.3 Variance comparison of path delays between CRB (dash lines) and Monte Carlo simulation (solid lines) with respect to different number of pilot symbols.

5.3.2 Estimation Errors of Path Amplitudes

The ML estimate of the path amplitude conditioned on the path delay estimate, is the value of α_ℓ that maximizes (5.5) with $\tau_\ell = \hat{\tau}_\ell$. It is not difficult to verify that the conditional estimate of the path amplitudes is given by

$$\begin{aligned} \hat{\alpha}_\ell &= \frac{1}{ME_p} \sum_{m=0}^{M-1} \int_0^{MT_s} y_\ell(t) q(t - mT_s - \hat{\tau}_\ell) dt \\ &= \alpha_\ell \mu_\ell + e_\ell, \end{aligned} \tag{5.16}$$

where μ_ℓ is the normalized correlation function for the ℓ-th path, defined as

$$\mu_\ell \triangleq \frac{1}{E_p} \int_{-\infty}^{\infty} q\left(t - \tau_\ell\right) q(t - \hat{\tau}_\ell) dt, \tag{5.17}$$

and e_ℓ is the estimation error due to noise,

$$e_\ell \triangleq \frac{1}{ME_p} \sum_{m=0}^{M-1} \int_0^{MT_s} n(t) q(t - mT_s - \hat{\tau}_\ell) dt. \tag{5.18}$$

When the path delays τ_ℓ are perfectly known, it can be proved that the amplitude estimates are both unbiased and efficient [82, p. 32]. However, since $\mu_\ell \leq 1$, the estimate $\hat{\alpha}_\ell$ becomes biased. From (5.18), note that the estimation errors e_ℓ can be modeled as real Gaussian random variables with mean $E[e_\ell] = 0$ and variance

$$\sigma_e^2 = \frac{1}{\frac{2E_p}{N_0} M}. \tag{5.19}$$

Figure 5.4, Part (a) depicts the CRB of path delay estimation errors for respectively, the strongest ($\ell = 0$) and the weakest ($\ell = L - 1$) paths, versus the SNR per pulse E_p/N_0. Results are shown for signal bandwidths of $W = 0.5$ GHz and $W = 7.5$ GHz with a maximum delay spread $\tau_{\max} = 50$ ns. The curves are generated using (5.15). Part (b) of the same figure depicts the amplitude estimation error from (5.19) normalized by the path power Ω_ℓ, versus the SNR per pulse for the same signal bandwidths as (a). The number of pilot symbols M is assumed to be 10. It is seen that the weaker the path power, the larger the normalized variance of the estimation error for both path amplitudes and path delays. Similarly, the errors increase with the signal bandwidth due to reduced power per path. This characterization affects the system performance and the system design as discussed in the sequel.

5.4 SNR and BER with Imperfect Channel Estimates

In this section, the average SNR and BER for a Rake receiver employing MRC are derived when the estimate errors for path delays and amplitudes are taken into account. The expressions are able to directly exhibit the effect of the number of pilot symbols and the number of multipath components on the overall system performance.

Given the model (5.2), and the estimated channel parameters (delay and amplitude), the output of the MRC for received signal $y(t)$ is given by

$$D = \frac{1}{E_p} \int_0^{T_s} y(t) \sum_{\ell=0}^{L-1} \hat{\alpha}_\ell q(t - \hat{\tau}_\ell)\, dt. \tag{5.20}$$

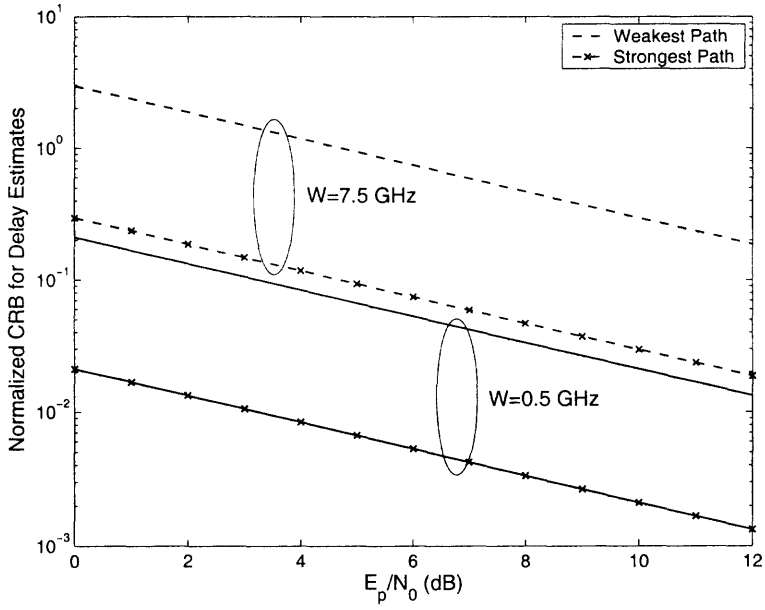

(a)

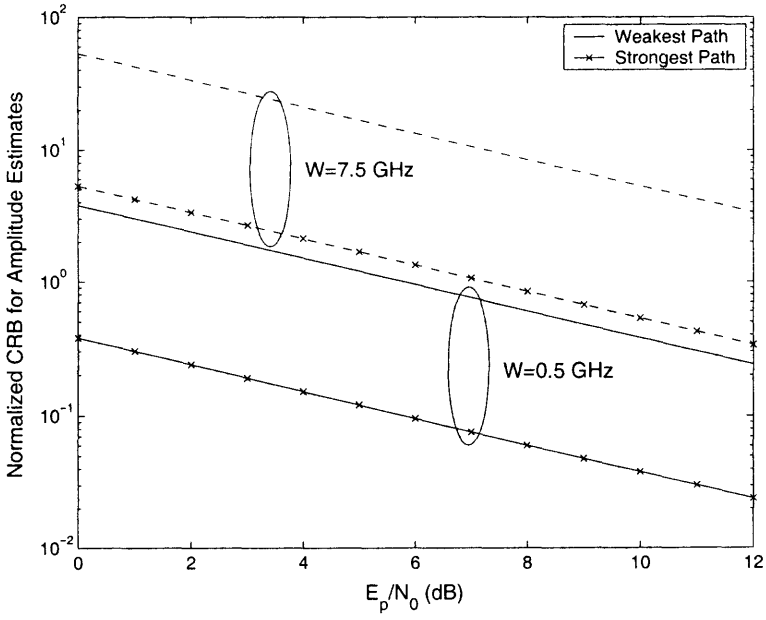

(b)

Figure 5.4 CRB of the variance of (a) the estimate of path delays normalized by the square of the pulse width, and (b) the estimate of path amplitudes normalized to the power of each path. The number of pilot symbols M is assumed to be 10. The total power is fixed for bandwidth W of 0.5 GHz (solid lines) and 7.5 GHz (dash lines).

Applying the definition of μ_ℓ in (5.17), the decision statistic D can be expressed,

$$D = d\sum_{\ell=0}^{L-1} \hat{\alpha}_\ell \alpha_\ell \mu_\ell + \sum_{\ell=0}^{L-1} \hat{\alpha}_\ell w_\ell, \tag{5.21}$$

where

$$w_\ell = \frac{1}{E_p} \int_{-\infty}^{\infty} n(t) q\left(t - \hat{\tau}_\ell\right) dt \tag{5.22}$$

is the noise term in the corresponding branch of the Rake receiver. Its mean is zero, and variance

$$\sigma_w^2 = \frac{1}{2E_p/N_0}. \tag{5.23}$$

The significance of (5.21) is that the channel estimation errors impact the decision statistic in two ways: 1) an effective loss in the signal gain due to the timing error, as manifested by $\mu_\ell \leq 1$, and 2) a mismatch of the path gains used with the MRC, $\hat{\alpha}_\ell \alpha_\ell$.

5.4.1 SNR Analysis

Without loss of generality, let the data symbol, $d = +1$, then an error will occur if $D < 0$. It is necessary to evaluate the BER, $P_e = \Pr(D < 0)$. Substituting the path amplitude estimate (5.16) in (5.21), after some manipulations, the decision statistic becomes

$$D = \sum_{\ell=0}^{L-1} \alpha_\ell^2 \mu_\ell^2 + \eta_1 + \eta_2 + \eta_3, \tag{5.24}$$

where it is defined as $\eta_1 \triangleq \sum_{\ell=0}^{L-1} \alpha_\ell \mu_\ell e_\ell$, $\eta_2 \triangleq \sum_{\ell=0}^{L-1} \alpha_\ell \mu_\ell w_\ell$, and $\eta_3 \triangleq \sum_{\ell=0}^{L-1} e_\ell w_\ell$. Conditioned on the set of values $\{\alpha_\ell \mu_\ell\}_{\ell=0}^{L-1}$, η_1 and η_2 are Gaussian with zero means, and variances $E\left[\eta_1^2\right] = \frac{N_0}{2ME_p} \sum_{\ell=0}^{L-1} \alpha_\ell^2 \mu_\ell^2$ and $E\left[\eta_2^2\right] = \frac{N_0}{2E_p} \sum_{\ell=0}^{L-1} \alpha_\ell^2 \mu_\ell^2$, respectively. By the central limit theorem, when L is large, η_3, which contains the product of two uncorrelated Gaussian noise components, is also approximately Gaussian with zero mean and variance

$$E\left[\eta_3^2\right] = \sum_{\ell=0}^{L-1} E\left[e_\ell^2\right] E\left[w_\ell^2\right] = L \times \frac{N_0}{2ME_p} \times \frac{N_0}{2E_p}. \tag{5.25}$$

Expression (5.24) affords the following interpretation. The effect of timing errors on the decision statistic is a multiplicative noise term, while amplitude errors are manifested as additive noise. Hence the performance analysis bears similarities to the analysis over fading channels. For a given channel realization, the communication can be viewed as taking place over a "fading" channel, where the "fading" is due to the timing errors. In the analysis below, the effective SNR conditioned on the timing errors is first determined. The average SNR for a given channel realization is obtained by averaging over the timing errors.

To continue the analysis, note that the noise terms η_1, η_2, η_3 are mutually uncorrelated. The *effective* SNR, conditioned on the channel realization and the time delay estimation errors $\{\alpha_\ell \mu_\ell\}$, is given by

$$\begin{aligned} \gamma_{\text{eff}} &= \frac{\left(\sum_{\ell=0}^{L-1} \alpha_\ell^2 \mu_\ell^2\right)^2}{E\left[\eta_1^2\right] + E\left[\eta_2^2\right] + E\left[\eta_3^2\right]} \\ &= \frac{2E_p}{N_0} \sum_{\ell=0}^{L-1} \alpha_\ell^2 \mu_\ell^2 \cdot \frac{1}{1 + \frac{1}{M}\left(1 + \frac{L}{\frac{2E_p}{N_0}\sum_{\ell=0}^{L-1} \alpha_\ell^2 \mu_\ell^2}\right)}. \end{aligned} \tag{5.26}$$

Define

$$\gamma_t \triangleq \frac{2E_p}{N_0} \sum_{\ell=0}^{L-1} \alpha_\ell^2 \mu_\ell^2, \tag{5.27}$$

then, (5.26) becomes

$$\gamma_{\text{eff}} = \frac{\gamma_t}{1 + \frac{1}{M}\left(1 + \frac{L}{\gamma_t}\right)}. \tag{5.28}$$

The effective SNR for a given channel realization, in (5.26), is a function of the path delay estimation errors as embodied in the terms μ_ℓ within γ_t. It can be verified that γ_{eff} is a convex function of γ_t. Then, averaging over the path delay errors and by Jensen's inequality, it follows for $\overline{\gamma}_{\text{eff}} \triangleq E\left[\gamma_{\text{eff}}\right]$,

$$\overline{\gamma}_{\text{eff}} \leq \frac{\overline{\gamma}_t}{1 + \frac{1}{M}\left(1 + \frac{L}{\overline{\gamma}_t}\right)} \leq \frac{\gamma_0}{1 + \frac{1}{M}\left(1 + \frac{L}{\gamma_0}\right)}, \tag{5.29}$$

where

$$\overline{\gamma}_t \triangleq E\left[\gamma_t\right] = \frac{2E_p}{N_0}\sum_{\ell=0}^{L-1}\alpha_\ell^2 E\left[\mu_\ell^2\right], \tag{5.30}$$

and

$$\gamma_0 \triangleq \frac{2E_p}{N_0}\sum_{\ell=0}^{L-1}\alpha_\ell^2. \tag{5.31}$$

The fact that γ_{eff} is a monotonically increasing function of γ_t was used to obtain (5.29).

A few comments are in order with respect to (5.28). Under the assumption stated in Section 5.2 that the average power gain of the channel is 1, $\overline{\gamma}_{\text{eff}}$ is a decreasing function of the number of paths L. Nevertheless, as an effect of diversity combining, var $[\gamma_{\text{eff}}]$ is also decreasing with increasing L. For a fixed L, the effect of the number of pilot symbols is seen through a reduction of the error term in the denominator of (5.28). An opposite effect is observed recalling that γ_t is a function of E_p/N_0 (see (5.27)), and that the total energy for transmitting $(Q-M)$ data symbols is $(Q-M)E_b$. Then the SNR per pulse is

$$\frac{E_p}{N_0} = \left(1-\frac{M}{Q}\right)\frac{E_b}{N_0}. \tag{5.32}$$

This relation indicates that for a fixed energy per bit E_b, the SNR per pulse, E_p/N_0, is lower than the SNR per data bit, E_b/N_0. As a consequence, through (5.27), the effective SNR in (5.28) tends to decrease with M. The effects of these parameters are better captured through the ensuing BER and capacity analysis.

5.4.2 BER Analysis

From (5.28), the average BER is given by

$$P_e = E\left[\Pr(e|\gamma_t)\right] = E\left\{\frac{1}{2}\text{erfc}\left(\sqrt{\frac{\gamma_t}{2\left[1+\frac{1}{M}\left(1+\frac{L}{\gamma_t}\right)\right]}}\right)\right\}, \tag{5.33}$$

where $\text{erfc}\,(z) \triangleq \frac{2}{\sqrt{\pi}}\int_z^\infty \exp\left(-t^2\right)dt$ is the complementary error function, and the expectation is taken with respect to γ_t (i.e., average over path delay and amplitude errors).

Since a closed form of (5.33) is unknown, an alternative method is used in deriving the BER.

The decision statistic in (5.24) can be alternatively expressed as

$$D = \sum_{\ell=0}^{L-1} (\alpha_\ell \mu_\ell + e_\ell)(\alpha_\ell \mu_\ell + w_\ell). \tag{5.34}$$

Now, denote $X_\ell \triangleq \alpha_\ell \mu_\ell + e_\ell$ and $Y_\ell \triangleq \alpha_\ell \mu_\ell + w_\ell$. Substituting back in (5.34),

$$D = \sum_{\ell=0}^{L-1} X_\ell Y_\ell. \tag{5.35}$$

Conditioned on α_ℓ and μ_ℓ, X_ℓ and Y_ℓ are independent and Gaussian since the noise terms e_ℓ and w_ℓ are measured at different times (training and data transmission, respectively). The L pairs $\{X_\ell, Y_\ell\}$ are real-valued, independent Gaussian random variables with respective means $E[X_\ell] = E[Y_\ell] = \alpha_\ell \mu_\ell$, and variances (see (5.19) and (5.23))

$$\text{var}(X_\ell) = E\left[(X_\ell - E[X_\ell])^2\right] = \sigma_e^2 = \frac{1}{\frac{2E_p}{N_0} M}, \tag{5.36}$$

$$\text{var}(Y_\ell) = E\left[(Y_\ell - E[Y_\ell])^2\right] = \sigma_w^2 = \frac{1}{\frac{2E_p}{N_0}}. \tag{5.37}$$

Therefore, D is a quadratic form of Gaussian random variables. With the help of [83], the BER conditioned on $\{\alpha_\ell \mu_\ell\}$ is expressed as

$$\begin{aligned} \Pr(e|\gamma_t) &= Q_1(a,b) - \frac{1}{2} I_0(ab) \exp\left(-\frac{a^2+b^2}{2}\right) \\ &\quad + \frac{1}{2} \sum_{n=1}^{L-1} I_n(ab) \left[\left(\frac{b}{a}\right)^n - \left(\frac{a}{b}\right)^n\right] C_n \exp\left(-\frac{a^2+b^2}{2}\right) \end{aligned} \tag{5.38}$$

for $L \geq 2$, and

$$\Pr(e|\{\alpha_\ell \mu_\ell\}) = Q_1(a,b) - \frac{1}{2} I_0(ab) \exp\left(-\frac{a^2+b^2}{2}\right) \tag{5.39}$$

for $L = 1$, where $Q_1(a,b)$ is the first-order Marcum function, $I_n(z)$ is the n-th order modified Bessel function of the first kind,

$$a = \frac{1}{2}\sqrt{\gamma_t}\left|\sqrt{M}-1\right|, \tag{5.40}$$

$$b = \frac{1}{2}\sqrt{\gamma_t}\left|\sqrt{M}+1\right|, \tag{5.41}$$

and

$$C_n = \frac{1}{2^{2L-2}}\sum_{k=0}^{L-1-n}\binom{2L-1}{k}. \tag{5.42}$$

In (5.42), $\binom{2L-1}{k} = \frac{(2L-1)!}{(2L-1-k)!k!}$ denotes the binomial coefficient.

Now, define $\zeta \triangleq \frac{a}{b} = \left|\frac{\sqrt{M}-1}{\sqrt{M}+1}\right|$, and use the alternative form of $Q_1(a,b)$ with finite limits [84, p. 79, (4.28)], to obtain

$$\begin{aligned} & Q_1(a,b) = Q_1(\zeta b, b) \\ = & \frac{1}{2\pi}\int_0^{\pi}\left\{\exp\left[-\frac{b^2}{2}\left(1-2\zeta\cos\theta+\zeta^2\right)\right]+\exp\left[-\frac{b^2}{2}\left(\frac{(1-\zeta^2)^2}{1-2\zeta\cos\theta+\zeta^2}\right)\right]\right\}d\theta, \end{aligned}$$

as well as the alternative form of $I_n(z)$ [55, p. 376]

$$I_n(z) = \frac{1}{\pi}\int_0^{\pi}\cos(n\theta)\exp(z\cos\theta)d\theta.$$

After some manipulations, the BER conditioned on γ_t can be shown to be equal to

$$\begin{aligned} \Pr(e|\gamma_t) = & \frac{1}{2\pi}\int_0^{\pi}\left\{\exp\left[-\gamma_t\frac{\left(\sqrt{M}+1\right)^2}{8}\frac{(1-\zeta^2)^2}{g(\theta,\zeta)}\right]\right. \\ & \left.+f(\theta,\zeta)\exp\left[-\gamma_t\frac{\left(\sqrt{M}+1\right)^2}{8}g(\theta,\zeta)\right]\right\}d\theta, \end{aligned} \tag{5.43}$$

where

$$f(\theta,\zeta) = \sum_{n=1}^{L-1}\left(\zeta^{-n}-\zeta^n\right)C_n\cos(n\theta),$$

and

$$g(\theta,\zeta) = 1 - 2\zeta\cos\theta + \zeta^2.$$

To obtain the unconditional BER, note that (5.43) consists of exponential functions, and

$$E\left[\exp\left(s\gamma_t\right)\right] = \mathcal{M}_{\gamma_t}(s), \tag{5.44}$$

where the expectation is taken with respect to γ_t, and $M_{\gamma_t}(s)$ is the moment generating function (MGF) of the random variable γ_t [84]. It follows that

$$\begin{aligned} P_e &= E\left[\Pr\left(e|\gamma_t\right)\right] \\ &= \frac{1}{2\pi}\int_0^{\pi}\left\{\mathcal{M}_{\gamma_t}\left(-\frac{\left(\sqrt{M}+1\right)^2}{8}\frac{\left(1-\zeta^2\right)^2}{g(\theta,\zeta)}\right)\right. \\ &\quad \left. + f(\theta,\zeta)\,\mathcal{M}_{\gamma_t}\left(-\frac{\left(\sqrt{M}+1\right)^2}{8}g(\theta,\zeta)\right)\right\}d\theta. \end{aligned} \tag{5.45}$$

Using (5.27) in (5.44), one has

$$\mathcal{M}_{\gamma_t}(s) = \prod_{\ell=0}^{L-1}\mathcal{M}_{\ell}(s), \tag{5.46}$$

where

$$\mathcal{M}_{\ell}(s) = E\left[\exp\left(s\frac{2E_p}{N_0}\alpha_{\ell}^2\mu_{\ell}^2\right)\right], \tag{5.47}$$

and the expectation is taken with respect to both α_ℓ and μ_ℓ. Assuming that the path amplitude α_ℓ has a Nakagami-m distribution with parameters Ω_ℓ and m_ℓ, where Ω_ℓ has been defined earlier, it follows that α_ℓ^2 has a Gamma distribution. Turning now to the random variable μ_ℓ, for the Gaussian pulse in (5.1), it can be shown that

$$\mu_{\ell}^2 = \exp\left(-\frac{T_p^2}{2\sigma_p^2}\epsilon_{\ell}^2\right), \tag{5.48}$$

where ϵ_ℓ was defined in (5.14). Taking the expectation, equation (5.47) becomes

$$\mathcal{M}_\ell(s) = \int_{-\infty}^{+\infty} \left[1 - s\frac{2E_p}{N_0}\frac{\Omega_\ell}{m_\ell}\exp\left(-\frac{T_p^2}{2\sigma_p^2}\epsilon_\ell^2\right)\right]^{-m_\ell} p(\epsilon_\ell)\, d\epsilon_\ell. \tag{5.49}$$

In Figure 5.3, it is shown that the ML estimate of the channel path delay τ_ℓ has an error ϵ_ℓ, which, asymptotically, has a Gaussian distribution with zero mean and variance equal to the CRB (5.15). Using this information in (5.49), and after some algebraic manipulations, (5.49) can be computed by the Hermite formula [55]

$$\mathcal{M}_\ell(s) = \frac{2}{\sqrt{\pi}}\sum_{i=1}^{\bar{N}} H_{x_i} f_s(x_i), \tag{5.50}$$

where $\bar{N}$ is the order of the Hermite polynomial, x_i and H_{x_i} are respectively, the zeros and weight factors of the i-th order Hermite polynomial tabulated in [55, Table 25.10], and

$$f_s(x_i) = \left[1 - s\frac{2E_p}{N_0}\frac{\Omega_\ell}{m_\ell}\exp\left(-\frac{x_i^2}{\frac{E_p}{N_0}\Omega_\ell M}\right)\right]^{-m_\ell}. \tag{5.51}$$

Upon completing the evaluation of (5.49), the results are substituted in (5.46), and finally in (5.45).

As a check, when the SNR allocated to the pilot is very large, i.e., $M \to \infty$, while E_p/N_0 is constant, then $f(\theta,\zeta) \to 0$, $g(\theta,\zeta) = 2(1-\cos\theta)$, and $\gamma_t = \frac{2E_p}{N_0}\sum_{\ell=0}^{L-1}\alpha_\ell^2$. After some manipulations, it follows that

$$\Pr(e|\gamma_t) = \frac{1}{\pi}\int_0^{\pi/2} \exp\left(-\frac{\gamma_t}{2\sin^2\theta}\right) d\theta, \tag{5.52}$$

and the unconditional BER is given by

$$P_e = \frac{1}{\pi}\int_0^{\pi/2} \mathcal{M}_{\gamma_t}\left(-\frac{1}{2\sin^2\theta}\right) dx. \tag{5.53}$$

As expected, this is the BER expression with perfect channel estimation [84, p. 268].

It is noted that if $M = 1$, then $a = 0$ and $b = \sqrt{\gamma_t}$. In such a case, (5.38) becomes indeterminate. Thus the expression (5.45) is suitable only for cases $M \geq 2$. For $M = 1$,

the BER conditioned on γ_t has been derived in [85] and is given by

$$\Pr(e|\gamma_t) = \frac{1}{2}\sum_{n=0}^{L-1} C_n \frac{1}{n!}\left(\frac{\gamma_t}{2}\right)^n \exp\left(-\frac{\gamma_t}{2}\right). \tag{5.54}$$

It can be verified that the unconditional BER in this case is

$$P_e = E_{\gamma_t}\{\Pr(e|\gamma_t)\} = \frac{1}{2}\sum_{n=0}^{L-1} C_n \frac{1}{n!}\frac{\partial^n}{\partial s^n}\mathcal{M}_{\gamma_t}(\frac{s}{2})|_{s=-1}. \tag{5.55}$$

Figure 5.5 compares the BER in (5.45) with the Monte Carlo numerical simulation when path parameters are estimated by ML. The number of multipath components is assumed as $L = 35$, and the curves are parameterized by the number of pilot symbols M out of $Q = 800$ symbols in a packet. Monte Carlo results are shown for $M = 10$ and $M = 5$, respectively. The Nakagami parameter m_ℓ is assumed to be 1. The analytical expression of the BER closely matches the Monte Carlo simulation for the larger M value. This result clearly demonstrates that with a large number of pilot symbols, the ML path delay estimates asymptotically achieve the CRB. By observing the E_b/N_0 gap between delay+amplitude errors and amplitude errors only, it is concluded that path delay estimation errors are an important factor, particularly at the low SNR.

5.5 Chapter Summary

The effect of imperfect estimates on UWB system performance was investigated when path delays and path amplitudes were jointly estimated. Pilot symbols were transmitted over a UWB multipath channel to estimate path parameters. It was shown that due to delay estimation errors, the estimate of path amplitudes is biased. The CRB's were derived for the variance of the path delay and amplitude estimates. It was observed from the CRB of path delay estimates that the value of the error variance is a function of the bandwidth. As the signal bandwidth increases, the estimate of the delay becomes more accurate for a given path gain. At the same time, an increase in bandwidth reduces the average power per path, increasing the variance of the estimate. It is needed to indicate that less fading occurs when

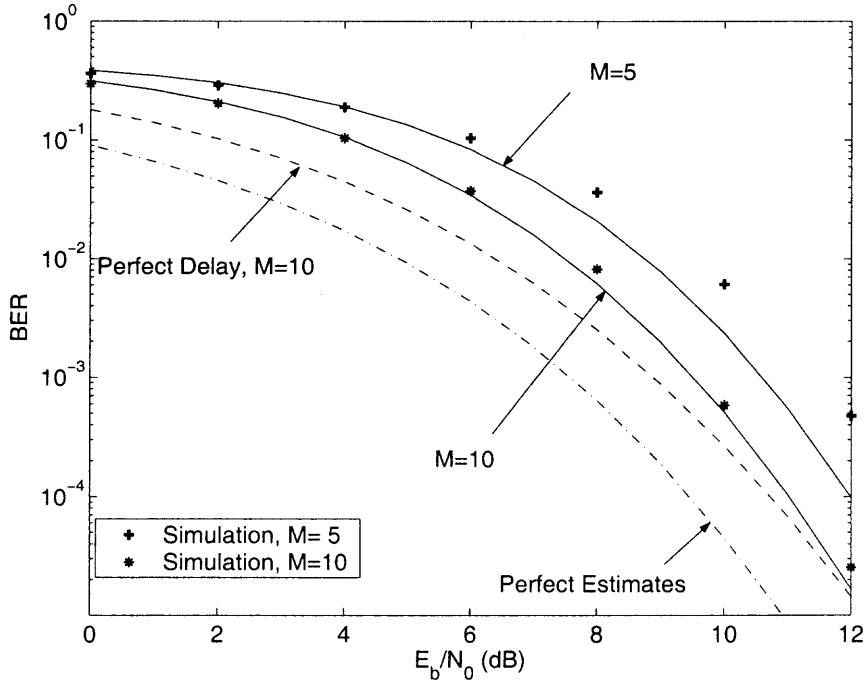

Figure 5.5 BER as a function of E_b/N_0 parameterized by the number of pilot symbols M.

increasing bandwidth (higher m_ℓ). Future work can investigate the evolution of the fading statistics and the effect of imperfect channel estimation as a function of signal bandwidth.

Furthermore, using the errors obtained from the CRB's, the system performance was analyzed for a Rake receiver employing MRC when estimation errors of both path delays and path amplitudes were taken into account. An effective SNR and an exact BER expression were derived. The SNR and BER were expressed in terms of the number of pilot symbols and the number of paths.

In the next chapter, the BER is used to characterize a BSC and the achievable communications rates are evaluated. The impact of imperfect CSI on two transceiver design parameters, the signal bandwidth and the number of fingers of Rake receivers, will be exploited.

CHAPTER 6

IMPACT OF CHANNEL ESTIMATION ON UWB SYSTEMS

In this chapter, the BER analysis in Chapter 5 is applied to transceiver design issues such as the fraction of a transmitted packet constituted by the pilot symbols, signal bandwidth, and which paths are to be combined at the receiver. Allocations of power resources to pilot symbols are determined to optimize the channel capacity. Results indicate that the impact of path delay estimation errors has to be taken into account, particularly at the low SNR. With a limited number of pilot symbols (< 10), the optimal bandwidth is smaller than 1 GHz. For a given bandwidth of 2 GHz, the optimal number of paths to be processed by Rake receivers is approximately 20.

6.1 Introduction

The derived BER in the previous chapter is used to characterize a BSC and its capacity is evaluated. Allocations of power resources to pilot symbols are determined to optimize the channel capacity. One expects the accuracy of channel estimators to improve as the fractions of power and number of symbols allocated to the pilot increase. A higher level of estimator accuracy increases the information rate of the system for both path delays and path amplitudes. However, when given a total power and a total number of transmitted symbols, the resources available for data transmission decrease as the fractions devoted to pilot symbols increase. The objective is to determine the optimum fraction of a transmitted packet constituted by the pilot symbols. In Section 6.2, the impact of pilot aided channel estimation on the information rate is analyzed, and the optimum fraction of symbols allocated to the the pilot signal is determined.

Subsequently, in Section 6.3, the estimation errors are taken into account in order to optimize the signal bandwidth and the number of fingers used at the Rake receiver.

The goal is to provide insights on signal bandwidth design, and on how many paths one should combine in a Rake receiver. The selection of the signal bandwidth represents a significant design choice due to its impact on the multipath resolution achieved by the receiver. As the signal bandwidth increases, so does the number of resolved multipath components. Moreover, due to the ability of UWB signals to resolve multipath down to individual scatterers, effects of fading become less pronounced [86]. At the same time, an increase in the number of resolved multipaths also means a reduction in the average power per path for a fixed total signal power [87, 88]. This in turn leads to higher channel estimation errors. Thus, there is a trade-off leading to an optimal choice of the signal bandwidth that should be used in the UWB communication link. In principle, given the signal bandwidth, a Rake receiver can resolve and combine all paths. However, due to both practical limitations as well as channel estimation error considerations, only a subset of available diversity branches should be combined at the receiver. In particular, the trade-off between the number of diversity paths used and performance will be demonstrated.

6.2 Impact of Channel Estimation on Capacity

Assuming that pilot and data symbols have the same energy, and that the total energy for transmitting a packet is constrained, there is an obvious tension between power allocated to pilot and data symbols, since the power allocated to the pilot is subtracted from the data symbols. In this section, the optimal power strategy for optimizing the channel capacity is determined. The BSC provides a convenient framework for incorporating the channel estimation effects since the BER is explicitly contained in its characterization.

The overall system in Figure 5.1 can be viewed as a BSC with transition probability

$$p_0 \triangleq \Pr\left(e|\gamma_t\right) = \frac{1}{2}\mathrm{erfc}\left(\sqrt{\frac{1}{2}\gamma_{\mathrm{eff}}}\right), \tag{6.1}$$

where γ_{eff} is given in (5.28). The capacity of the BSC channel is achieved when the input is symmetrically distributed, $\Pr\left(d = \pm 1\right) = 1/2$, independently of the channel transition

probabilities. Unlike the Shannon capacity, the BSC capacity depends on the transceiver structure (the channel estimator and Rake combiner). Recall that for each packet, only $(Q - M)$ out of Q symbols are data conveying. The capacity expressed in bits per channel use, and conditioned on the channel realization and specific estimation errors, is given by

$$\mathsf{C}(\gamma_t) = \left(1 - \frac{M}{Q}\right)\left[1 + p_0 \log_2 p_0 + (1 - p_0)\log_2(1 - p_0)\right]. \tag{6.2}$$

The effective SNR γ_{eff} is for a given channel realization and path delay estimation error. Averaged over delay errors and over channel realizations, the ergodic capacity in bits per channel use is expressed as

$$\mathsf{C} = \left(1 - \frac{M}{Q}\right) E\left[1 + p_0 \log_2 p_0 + (1 - p_0)\log_2(1 - p_0)\right]. \tag{6.3}$$

Given Q, if a larger percentage of symbols is assigned to the pilot, then M is larger and $(1 - M/Q)$ is smaller. Therefore, on one hand, the effective SNR γ_{eff} in (5.28) increases, the BER conditioned on channel realizations p_0 in (6.1) decreases, and the capacity increases. On the other hand, the capacity is reduced due to fewer symbols available for data transmission. This is shown in Figure 6.1 where the capacity C in (6.3) is plotted versus the percent of symbols allocated to the pilot, M/Q, and parameterized by values of E_b/N_0. It is assumed that an average pedestrian walking speed of 5 km/hour is taken into account. This corresponds to a coherence time of 7.7 ms [37, (4.40b)] at a center frequency of 5 GHz. If it is further assumed that the packet size is equal to the coherence time, then the number of symbols per packet Q, equals the normalized coherence time, T_c/T_s, where T_c is the coherence time, and T_s is the symbol duration. For comparison, the capacity without path delay estimation errors is also plotted by substituting the upper bound (5.29) into (5.28), then in (6.1), and finally in (6.3). It is assumed that the number of multipath components is $L = 100$. It is observed that the optimal fraction of symbols allocated to the pilot at high E_b/N_0 is smaller than that for low E_b/N_0. This reflects the fact that the accuracy of the channel estimator is proportional to E_b/N_0. It is also observed that

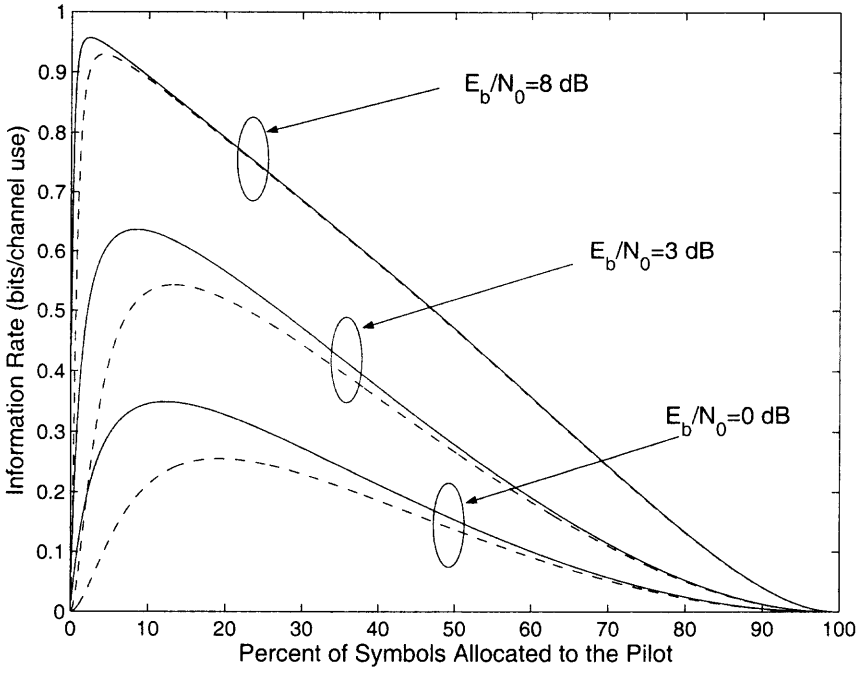

Figure 6.1 Capacity of the BSC as a function of the fraction of symbols allocated to the pilot parameterized by E_b/N_0, for $Q = 800$ symbols in a packet. Solid lines are without delay estimation errors; dash lines are in the presence of both path delay and amplitude estimation errors.

the optimal percentage of symbols allocated to the pilot in the presence of both path delay and amplitude estimation errors is larger than that with only amplitude estimation errors. This means that extra pilot symbols are required to compensate for the penalty of delay estimation errors. Further insight into the effect of channel estimation can be obtained from the gap between the capacity curves with and without path delay estimation errors. The gap narrows with the increase in E_b/N_0. This further strengthen the conclusion that the impact of delay estimation errors has to be taken into account, especially at low SNR.

In Figure 6.2, the effect of various Q on C is demonstrated for a given E_b/N_0. For a large Q, say 800, the optimum percentage of symbols assigned to the pilot is smaller. Therefore, the transmission efficiency increases, and the information rate improves. For a small Q, say 80, the gap between the information rates with/without path delay estimation errors is evident. This is because, here, the number of pilot symbols is not large enough and the impact of delay errors is large. Also note that the optimal percentage of symbols

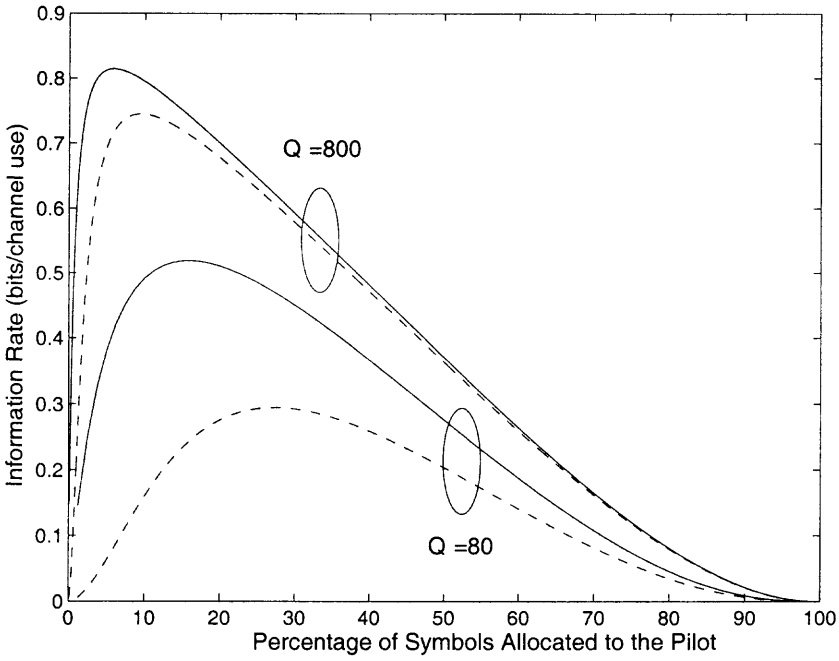

Figure 6.2 Achievable information rates as a function of percentage of symbols allocated to the pilot with respect to normalized coherence time Q, at E_b/N_0 of 5 dB. Solid lines are the cases without delay estimation errors, and dash lines are in the presence of both path delay and amplitude estimation errors.

allocated to the pilot in the presence of path delay and amplitude estimation errors is larger than the percentage that does not consider delay estimation errors. This means more pilot symbols are required to compensate for the penalty of delay estimation errors. Note that $Q = 80$ and 800 are approximately corresponding to symbol rates of $R_s = 10$ kbps and 100 kbps, respectively. This is based on the assumption that an average pedestrian walking speed is taken into account.

The optimum percentage of symbols allocated to the pilot as a function of the normalized coherence time is plotted in Figure 6.3 for various E_b/N_0 values. It shows in a low SNR regime ($E_b/N_0 = 0$ dB), when the normalized coherence time is small ($Q < 100$), the optimum fraction of the number of symbols assigned to the pilot is more than 35% of the total symbols available.

Choosing the number of pilot symbols M to use in the channel estimation is an important aspect of system design. Clearly, M cannot be arbitrarily large. With limited M,

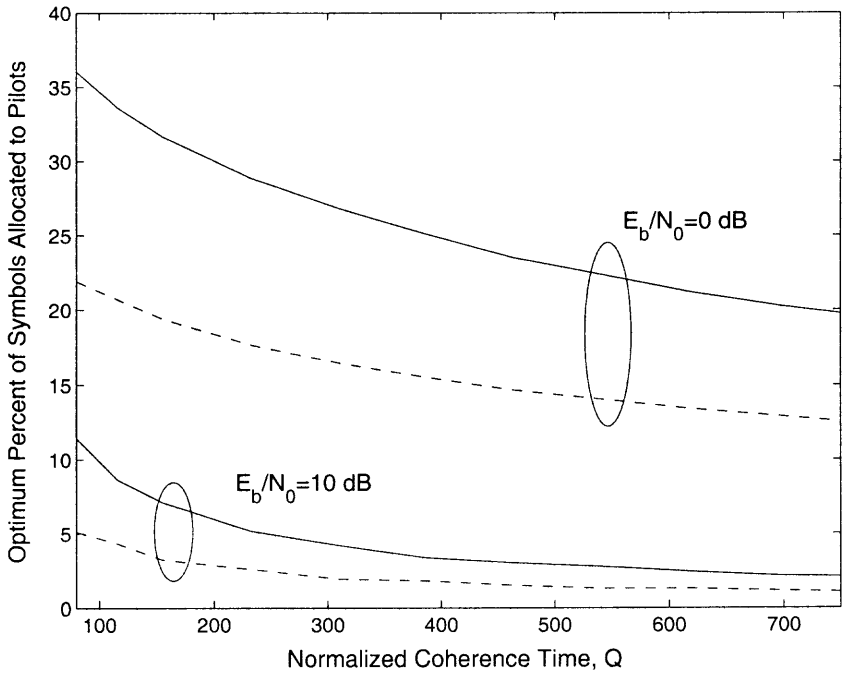

Figure 6.3 Optimum percent of the number of symbols allocated to the pilots versus the normalized coherence time for various E_b/N_0. Solid lines are the cases without delay estimation errors, and dash lines are in the presence of both path delay and amplitude estimation errors.

it is of interest to investigate the impact on the design of UWB transceivers, in particular, the signal bandwidth and the number of Rake receiver fingers.

6.3 Impact of Channel Estimation on System Design

The goal in this section is to optimize performance by controlling the signal bandwidth and the number of Rake receiver fingers.

6.3.1 Signal Bandwidth

The impact of channel estimation errors is first investigated on the performance as a function of the signal bandwidth. According to FCC regulations, IR-UWB may operate over a maximum bandwidth of 7.5 GHz. Finding how much bandwidth one should use for optimum performance is therefore of interest. As pointed out in [86,88,89,90], the number

of multipath components, L, increases linearly with the signal bandwidth. Within the limit, when the channel has been resolved into non-fading paths, an increase in bandwidth will not add any more paths. It is assumed that the latter regime has not been reached yet, and that the linear relation, number of paths - bandwidth, holds. More specifically,

$$L = \lceil \kappa \tau_{\max} W \rceil , \tag{6.4}$$

where the operator $\lceil \ \rceil$ is used to ensure that L is the closest larger integer, and κ is a scalar depending on the scattering in the channel and the pulse waveform. In particular, for the general Gaussian pulse in (5.1), and $L/\widetilde{L} = 0.5$, it can be verified that $\kappa \approx 0.7$. Substituting (6.4) into the BER expressions such as (5.45), links the performance to the signal bandwidth, W.

In the system model, it is assumed that the sum of the channel gains is fixed, independent of L. Hence, for perfect CSI, and if the Rake receiver uses all available paths, increasing the signal bandwidth will initially lead to better performance due to higher diversity. This advantage will quickly level off since diversity has diminishing returns as the number of paths increases. As the bandwidth increases, the resolution advances towards single paths with no fading. Based on this scenario, one may be tempted to conclude that the signal bandwidth should be as large as possible. This conclusion, however, does not hold when the effects of channel estimation are thrown into the mix. In the latter case, as W increases, L increases, while the average SNR per path decreases. This, in turn, leads to higher estimation errors and to degraded performance. Therefore, a tradeoff exists where there is an optimum selection of the signal bandwidth.

Since no simple analytic expression for the optimum W appears to be available, its value is determined through numerical computations. In Figure 6.4, the E_b/N_0 required to achieve specified error rates is plotted as a function of the -10 dB signal bandwidth W. The delay spread is assumed to be 50 ns and the curves are parameterized by the number of pilot symbols M. The approach used is to substitute (6.4) into (5.45), and compare the

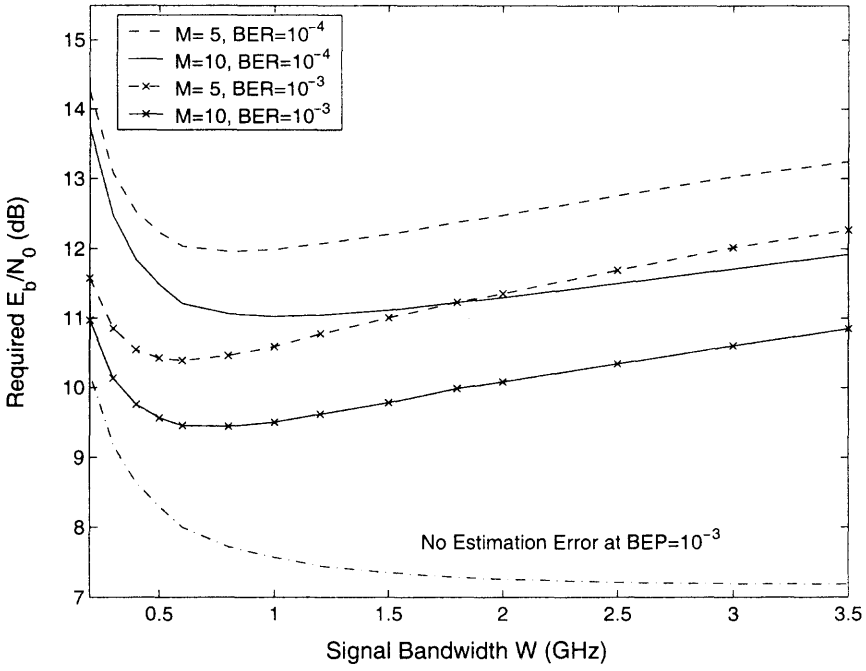

Figure 6.4 Required E_b/N_0 to achieve a specified BER as a function of the signal bandwidth W for a fixed number of pilot symbols M.

performance of systems using different bandwidths by determining the required E_p/N_0 to achieve a specified BER. The required E_b/N_0 is then obtained from (5.32) with the number of symbols per packet $Q = 800$. Estimation errors of both path delays and amplitudes are taken into account. Optimal values of the signal bandwidth can be evaluated from the curves. Using a very large bandwidth leads to higher error rates due to imperfect CSI. For the set of parameters used, the optimal bandwidth is less than 1 GHz. As the number of pilot symbols M increases, the quality of channel estimators improves, hence the optimal W increases. The case of ideal channel CSI is also plotted for reference. When channel estimation errors are not a factor, it is apparent that better performance can be achieved by increasing the signal bandwidth.

In Figure 6.4, it is assumed that the Nakagami fading parameter $m_\ell = 1$. To observe the effect of m_ℓ, in Figure 6.5, the BER is shown as a function of the signal bandwidth for several values of m_ℓ. Here, $E_b/N_0 = 10$ dB and $M = 5$. In general, a large m_ℓ value is associated with less fading and a strong LOS path. It is seen that as m_ℓ increases, the BER

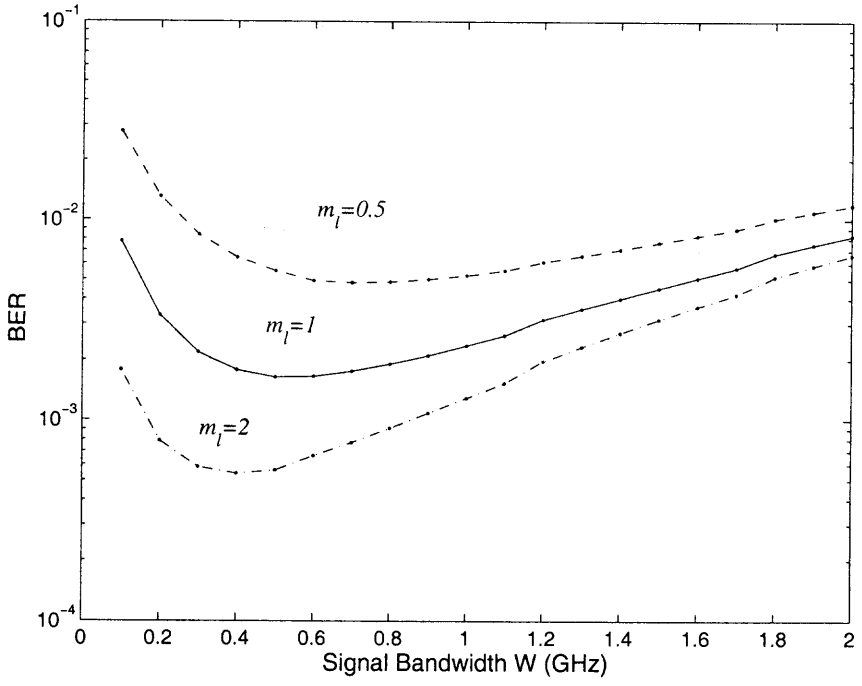

Figure 6.5 BER versus the signal bandwidth as a function of Nakagami fading parameters m_ℓ with $E_b/N_0 = 10$ dB and the number of pilot symbols $M = 5$.

decreases and the optimal signal bandwidth is smaller. It is indicated that m_ℓ is a function of delay ℓ and bandwidth W. This topic is left for future work.

6.3.2 Design of Rake Receivers

The foregoing analysis of the performance for a given bandwidth assumes the capture of all available multipath components. In practice, Rake receivers often process only a subset of the resolved multipath components. Such Rake receivers are referred to as *selective*. One possibility is to process the first L_c arriving paths out of the L available multipath components, and then combine them using MRC. This is usually motivated by a reduction in the receiver complexity. It is argued here that selective-Rake makes sense also from the point of view of performance in the presence of imperfect CSI. On one hand, as L_c increases, more signal energy is captured. In reality, however, the weaker paths contribute less energy to the combiner and are more susceptible to estimation errors. Thus, it is anticipated that an optimal number of paths exists dependent on the specific delay spread.

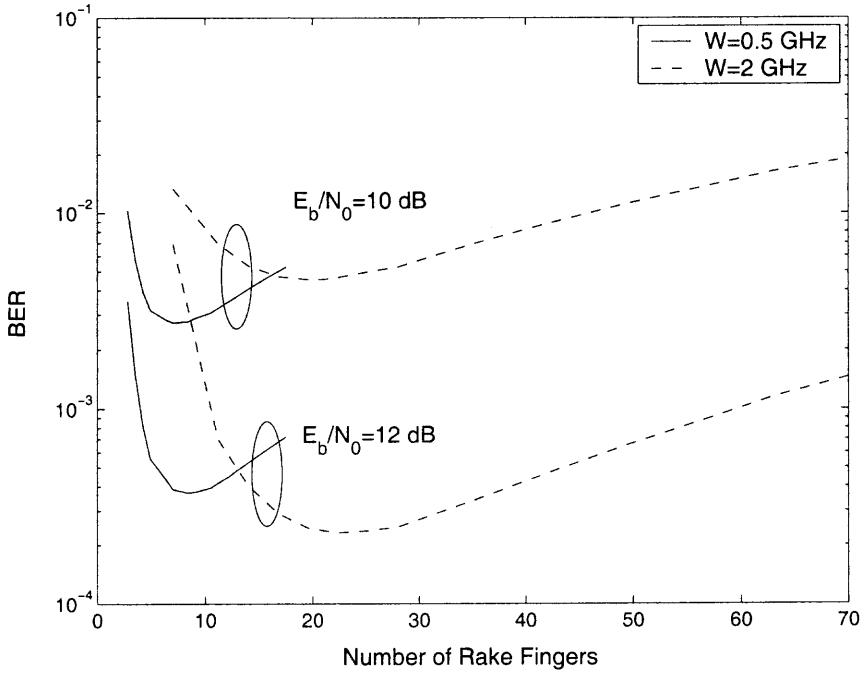

Figure 6.6 BER as a function of the number of Rake fingers for different signal bandwidths W and E_b/N_0. The number of pilot symbols $M = 5$.

The performance of selective Rake is a function of the number of combined paths L_c. Replacing L in (5.45) with L_c, the BER for the selective-Rake receiver is obtained in the presence of estimation errors for both path delays and amplitudes. The optimal value of L_c is obtained by minimizing P_e. Since no simple analytic expression is available, numerical computations are relied upon.

In Figure 6.6, the BER in (5.45) is plotted versus the number of fingers used at the Rake receiver. Various values of E_p/N_0 are obtained from (5.32) where the number of symbols per packet is $Q = 800$. It is clear that due to imperfect CSI, the performance does not improve after collecting approximately 20 paths for $W = 2$ GHz, while 8 paths are sufficient for $W = 0.5$ GHz. When E_b/N_0 increases, the BER is reduced and the optimal number of Rake fingers increases.

Further insight into the optimal number of Rake fingers can be attained by observing the E_b/N_0 required to attain a specified BER. This is shown in Figure 6.7, where the cases of two values of the signal bandwidth, $W = 0.5$ GHz and $W = 2$ GHz, are compared. The

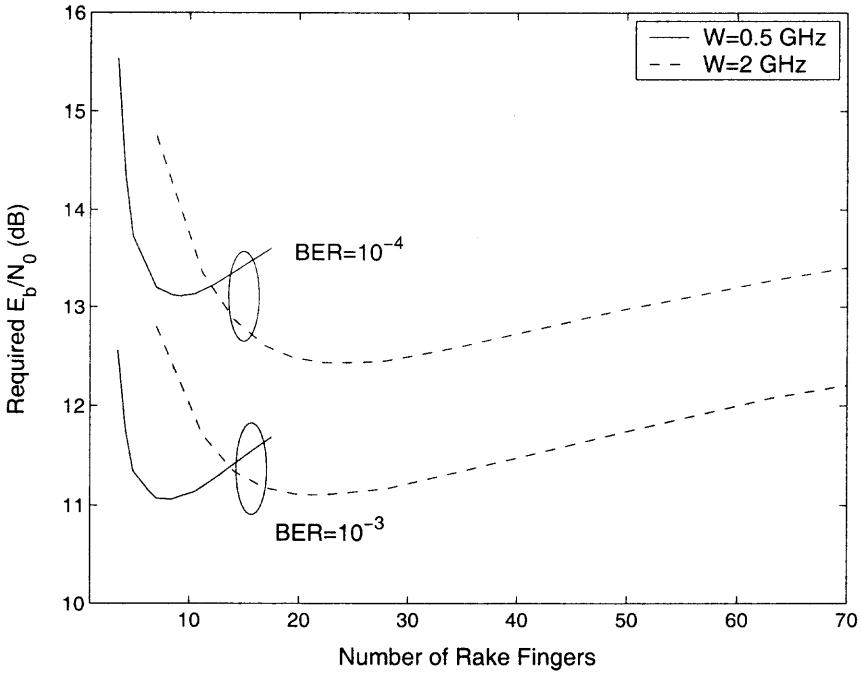

Figure 6.7 Required E_b/N_0 to attain a specified BER as a function of the number of Rake fingers, $M = 5$.

optimal L_c is obtained when the required E_b/N_0 is minimum. For a required BER of 10^{-4}, when the signal bandwidth W increases from 0.5 GHz to 2 GHz, the optimal L_c increases from 8 to 20 approximately. As the specified BER is lowered, such as from 10^{-3} to 10^{-4}, the optimal L_c increases for any value of W.

As a check, it is of interest to compare the result above with the result over a realistic UWB channel, IEEE 802.15.3a CM1. Figure 6.8 plots the required E_b/N_0 to obtain the BER 10^{-4} as a function of the number of selective Rake fingers. The signal bandwidth is chosen $W = 1.75$ GHz, and the number of pilot symbols $M = 5$ and 10. It is shown that the optimal L_c is approximately 12 when $M = 5$. This is consistent with the result in Figure 6.7.

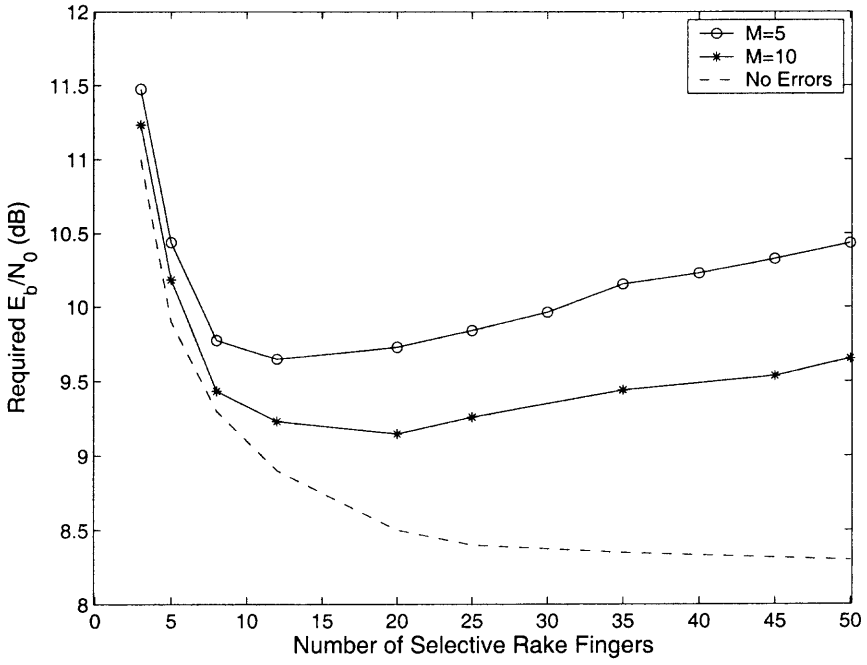

Figure 6.8 Required E_b/N_0 to obtain BER 10^{-4} as a function of the number of selective Rake fingers. The signal bandwidth is chosen $W = 1.75$ GHz, and the number of pilot symbols $M = 5$ and 10.

6.4 Chapter Summary

The impact of channel estimation errors has been investigated for the design of UWB systems employing Rake receivers. The BER was used to characterize a BSC and the achievable capacity was evaluated. The optimum fraction of symbols allocated to the pilot signal was then determined analytically to maximize the capacity. The gap between the capacity curves with and without path delay errors indicated that path delay estimation errors are an important factor, particularly at the low SNR.

Transceiver parameters were designed with imperfect CSI. The estimation errors of both path delays and amplitudes were taken into account for determining the optimal signal bandwidth and the number of paths to be combined. With a small number of pilot symbols (< 10 in a packet of 800 symbols), the optimal bandwidth was smaller than 1 GHz. For a given bandwidth, the optimum number of paths to be processed by the Rake receiver was determined to attain minimum error rate in the presence of imperfect CSI. For

the 2 GHz signal bandwidth, the optimal number of paths processed by Rake receivers was approximately 20 for a given number of pilot symbols $M = 5$.

CHAPTER 7

SUMMARY AND SUGGESTIONS FOR FUTURE WORK

7.1 Summary of the Dissertation

This dissertation has been focused on the transceiver design and system optimization for ultra-wideband communications. Novel contributions are the following.

UWB pulse waveform design:

- Invented UWB pulses satisfying the emission mask imposed by the regulatory restrictions;
- Designed parameters to possibly implement the proposed UWB pulse meeting the FCC's spectrum mask;
- Devised the link budget based on an accurate frequency-dependent path loss calculation to account for variations across the ultra-wide bandwidth of the signal.

Coding, spreading, and rate scaling:

- Quantified the UWB information rates as a function of transmission distance over AWGN and multipath channels constrained on the regulatory spectral mask and specific modulations;
- Determined the effect of self and intersymbol interference on UWB channel capacity, and identified modulation formats that mitigate against this effect;
- Evaluated spreading gains of familiar UWB signaling formats, and proved UWB signals are spread spectrum;
- Formulated conditions for trading coding gain with spreading gain with only a small impact on performance;
- Demonstrated that spreading is actually beneficial in reducing the self and intersymbol interference resulting in higher information rates.

Narrowband interference suppression and optimum combining:

- Applied reduced-rank adaptive filtering techniques to the problem of interference suppression and optimum combining in UWB Rake receivers;

- Evaluated the performance of UWB Rake receivers employing MMSE and reduced-rank eigenanalysis based optimum combining techniques.

Performance of Rake receivers with channel estimation:

- Formulated the Cramér-Rao bound expression for the variance of path delay and amplitude estimates using maximum likelihood estimation;
- Devised effective SNR for UWB Rake receivers employing MRC in the presence of channel path delay and amplitude errors;
- Derived an exact expression of the BER for UWB Rake receivers employing MRC in the presence of channel path delay and amplitude errors.

Optimal transceiver parameter design:

- Explored the optimum power allocation and number of symbols allocated to the pilot with respect to maximizing the information rate;
- Determined the signal bandwidth to be used for UWB communications in order to optimize performance in the presence of imperfect channel state information;
- Designed the number of multipath components to be collected by Rake receivers to optimize performance with non-ideal channel estimation.

It is indicated that the work in this dissertation has been cited by books [91, 92], journal papers [18, 93], dissertations and theses [94, 95, 96], and conference papers [38, 97, 98, 99, 100, 101, 102, 103, 104, 105].

7.2 Suggestions for Future Work

The promises of UWB communications systems are far from being fully explored. Anticipated future research topics may contain the following.

- Impact of multiple access interference on transceiver design.

All topics in this dissertation are in the single user case. In multi-user environment, a link has to deal with multiple access interference (MAI). It might be interesting to explore the coding-spreading tradeoff, channel estimation, and optimal transceiver parameter design with MAI.

- Design of low-rate codes suitable for UWB communications.

The large bandwidth enables the use of low coding rates. Limiting the coding to a low rate such as 1/4 and applying the rest of the bandwidth expansion to spreading incurs only a small loss. It was shown that in the low SNR regime, binary codes are optimal [106]. Using known results from [106], it is interesting to discuss binary codes with low complexity that might be suitable for UWB.

- Analysis of eigencanceler performance with imperfect channel estimation.

The reduced-rank EC is superior to MMSE when short data records are used. Analytical results of EC were provided in [107] with perfect CSI. In the presence of imperfect CSI, simulation results of the EC performance were presented in Chapter 4 for UWB. With non-ideal CSI, the analysis of the EC performance is to be investigated, particularly with UWB constraints.

- Application of trellis-coded PPM to UWB.

A high-rate UWB system suffers from ISI due to delay spread of the multipath channel. An M-PPM is one choice for UWB communications. A trellis-coded (TC) PPM might be an effective way to mitigate the ISI effects in UWB. The TC-PPM has been proposed for optical/infrared communications [108]. It would be interesting to design TC-PPM for the UWB ISI channel characterized by much longer delay spread than the infrared channel. A high-order PPM is a multidimensional modulation which can increase the distance of the signal point, and offer high average power efficiency. Potential topics include: analysis of the minimum Euclidean distance as a function of delay spread over the realistic UWB multipath channels, evaluation of BER on coded TC-PPM in high data rate over the multipath ISI channel, search for and analysis of the code for TC-PPM codes in UWB channels, and application of turbo TC-PPM for higher coding gain.

- Investigation regarding the effect of both multipath fading and channel estimation errors when increasing a signal bandwidth.

As the signal bandwidth increases, the number of resolvable multipath components increases while the energy per path decreases. At the same time, the distribution of the envelope of a resolvable path evolves from approximately a Rayleigh distribution to perhaps a Rician distribution or Nakagami-*m* distribution ($m > 1$). The evolution of the fading statistics as a function of signal bandwidth has not been fully characterized [79]. It is important to take into account both the evolution of the fading distribution, as perceived by a Rake receiver, and the effect of imperfect channel estimation (both delay and amplitude) for increasing spreading bandwidths. In addition, it might also be interesting to check the improvement of EC over MMSE when the signal bandwidth increases.

- Performance analysis of Rake receivers with selective maximal-ratio combining when the multipath delay and amplitude are jointly estimated.

The BER for a Rake receiver employing MRC was analyzed in the presence of imperfect CSI in Chapter 5. All L multipath components or the first arrival L_c out of L paths are captured. For a selective-Rake receiver, the L_c strongest branches of L diversity branches are selected and then combined coherently by MRC. Performance analysis of the selective-Rake receiver with imperfect CSI is much more complicated than the classical diversity schemes [109]. When path delays and path amplitudes are jointly estimated, no results seem to be available.

- Development of synchronization and channel estimation methods over orthogonal domains.

All search-based synchronization methods in the time domain waste power in processing slots when the signal is not present. Detecting a short pulse within a large search interval is time consuming. Sampling ultra-short pulses that occupy several gigahertz of bandwidth requires an extremely high sampling rate which cannot be met using the existing

ADC's. Sampling multipath demands more complicated circuit. By projecting the signal into an orthogonal domain, the received signal is decomposed into several components which are quantized at the end of a much longer time window [110]. This alleviates the extremely fine time resolution needed in time domain ADC's, and alleviates the bandwidth requirements of LNA's. It might be interesting to estimate the multipath delays in an orthogonal domain, particularly by spectral analysis in the frequency domain.

APPENDIX A

CHANNEL CAPACITY FOR VARIOUS MODULATIONS

Channel capacity expressions for various modulations are derived in this Appendix.

A.1 Capacity of M-ary PPM

With a restriction of an M-ary orthogonal PPM (M-PPM), the channel capacity is given by [54]

$$\mathcal{C}_{M-PPM}(\mathsf{d}) = \log_2 M - E_{\mathbf{v}|\mathbf{s}_1} \log_2 \sum_{m=1}^{M} \exp[\sqrt{\gamma(\mathsf{d})}(v_m - v_1)], \text{bits/symbol} \qquad (A.1)$$

where the random variable v_m, $m = 1, \ldots, M$, has the following distribution conditioned on the transmitted signal $\mathbf{s}_1$:

$$\begin{aligned} v_1 &\sim \mathcal{N}(\sqrt{\gamma}, 1) \\ v_m &\sim \mathcal{N}(0, 1), m \neq 1 \end{aligned} \qquad (A.2)$$

with $\gamma(\mathsf{d})$ defined in (3.9). The PPM time shift is assumed to be such that signals are orthogonal. Note that due to the symmetry of orthogonal signals, any signal can serve as the condition, and capacity is achieved with an equiprobable M-ary source distribution. Define $u_m = v_1 - v_m$, then $u_1 = 0$ and

$$u_m \sim \mathcal{N}(\sqrt{\gamma}, 2), \; m \neq 1. \qquad (A.3)$$

It follows that

$$\mathcal{C}_{M-PPM}(\mathsf{d}) = E_{\mathbf{u}|\mathbf{s}_1} \log_2 \left\{ \frac{M}{1 + \sum_{m=2}^{M} \exp\left[-\sqrt{\gamma(\mathsf{d})} u_m\right]} \right\}, \text{bits/symbol} \qquad (A.4)$$

in bits/symbol, as listed in (3.11).

In the case of $M = 2$, due to $u_2 \sim \mathcal{N}(\sqrt{\gamma}, 2)$, a closed-form expression is obtained such that

$$\mathcal{C}_{2-PPM}(\mathsf{d}) = \frac{1}{\sqrt{\pi}} \int_{-\infty}^{\infty} e^{-x^2} \log_2 \left(\frac{2}{1 + \exp[-2\sqrt{\gamma(\mathsf{d})}(x + \sqrt{\gamma(\mathsf{d})}/2)]} \right) dx \qquad \text{(A.5)}$$

in bits/symbol. Similarly, the capacity in bits/sec is $C_{2-PPM}(\mathsf{d}) = B\mathcal{C}_{2-PPM}(\mathsf{d})$, as shown in (3.13).

A.2 Capacity of Biphase

For a one-dimensional M-PAM signal with an equiprobable source distribution $p(s_m) = 1/M$,

$$\mathcal{C}_{M-PAM} = \log_2 M - E_{y|s_1} \log_2 \left(\frac{\sum_{i=1}^{M} p(y|s_i)}{p(y|s_1)} \right), \text{ bits/symbol.} \qquad \text{(A.6)}$$

When $M = 2$, it becomes

$$\mathcal{C}_{\text{biphase}} = 1 - E_{y|s_1} \log_2 \left(1 + \frac{p(y|s_2)}{p(y|s_1)} \right), \qquad \text{(A.7)}$$

where it is assumed that $s_1 = \sqrt{E_s}$ and $s_2 = -\sqrt{E_s}$. For any received symbol $y = y_m$ in any symbol duration, there is

$$\begin{aligned} y|s_1 &\sim \mathcal{N}(\sqrt{E_s}, N_0/2) \\ y|s_2 &\sim \mathcal{N}(-\sqrt{E_s}, N_0/2). \end{aligned}$$

Define $v = y/\sqrt{N_0/2}$, then

$$\begin{aligned} v|s_1 &\sim \mathcal{N}(\sqrt{\gamma}, 1) \\ v|s_2 &\sim \mathcal{N}(-\sqrt{\gamma}, 1). \end{aligned}$$

It follows that

$$\mathcal{C}_{\text{biphase}} = 1 - E_{v|s_1} \log_2 \left(1 + \frac{p(v|s_2)}{p(v|s_1)} \right). \qquad \text{(A.8)}$$

Due to

$$\frac{p(v|s_2)}{p(v|s_1)} = \exp\left(-2\sqrt{\gamma}v\right),$$

therefore, the channel capacity for biphase is given by

$$\mathcal{C}_{\text{biphase}}(\mathsf{d}) = \frac{1}{\sqrt{\pi}} \int_{-\infty}^{\infty} e^{-x^2} \log_2 \left(\frac{2}{1 + \exp\left(-2\sqrt{2\gamma(\mathsf{d})}(x + \sqrt{\gamma(\mathsf{d})/2})\right)} \right) dx \qquad \text{(A.9)}$$

in bits/symbol. The capacity in bits/sec then is (3.14).

A.3 Capacity of OOK

It is known that OOK is a one-dimensional signaling. It can follow the derivation of biphase. The capacity of OOK is given by

$$\mathcal{C}_{\text{OOK}} = 1 - E_{y|s_1} \log_2 \left(1 + \frac{p(y|s_2)}{p(y|s_1)}\right), \qquad \text{(A.10)}$$

where $s_1 = \sqrt{2E_s}$ and $s_2 = 0$, by which the average energy per symbol is the same as that for 2-PPM and biphase. It can be verified that

$$\mathcal{C}_{\text{OOK}} = 1 - E_{v|s_1} \log_2 \left(1 + \frac{p(v|s_2)}{p(v|s_1)}\right). \qquad \text{(A.11)}$$

Due to

$$\frac{p(v|s_2)}{p(v|s_1)} = \exp\left(-\sqrt{2\gamma}(v - \sqrt{\gamma/2})\right),$$

then the channel capacity for OOK is given by

$$\mathcal{C}_{\text{OOK}}(\mathsf{d}) = \frac{1}{\sqrt{2\pi}} \int_{-\infty}^{\infty} e^{-x^2/2} \log_2 \left(\frac{2}{1 + \exp(-\sqrt{2\gamma(\mathsf{d})}(x + \sqrt{\gamma(\mathsf{d})/2})} \right) dx \qquad \text{(A.12)}$$

in bits/symbol. The capacity in bits/sec then is (3.15).

APPENDIX B

EXACT BER WITH DELAY ESTIMATION ERRORS

An exact closed form of the BER of a Rake receiver employing MRC is derived in the presence of path delay estimation errors. Similar work can be found in [111,112,113,114]. Assuming $\hat{\alpha}_\ell = \alpha_\ell$, equation (5.20) becomes $D = \sum_{\ell=0}^{L-1} \alpha_\ell^2 \mu_\ell + \sum_{\ell=0}^{L-1} \alpha_\ell w_\ell$. To evaluate the BER, it is necessary to determine $P_e = \Pr(D < 0)$. Using the Inversion Theorem [115,116], the BER is given by

$$P_e = \frac{1}{2} - \frac{1}{\pi} \int_0^\infty \frac{\mathrm{Im}\left[\Psi_D(\omega)\right]}{\omega} d\omega, \tag{B.1}$$

where $\Psi_D(\omega)$ is the characteristic function (CF) of the decision statistic. Conditioned on $\{\alpha_\ell\}$, and assuming μ_ℓ and w_ℓ are mutually independent, it can be obtained that

$$\Psi_D(\omega) = E\left[e^{j\omega D}\right] = \prod_{\ell=0}^{L-1} \Psi_{s_\ell}(\omega) \prod_{\ell=0}^{L-1} \Psi_{n_\ell}(\omega), \tag{B.2}$$

where

$$\prod_{\ell=0}^{L-1} \Psi_{n_\ell}(\omega) = \exp\left[-\omega^2 \frac{\sum_{\ell=0}^{L-1} \alpha_\ell^2}{4E_p/N_0}\right] \tag{B.3}$$

is the CF of the Gaussian noise, and

$$\begin{aligned} \Psi_{s_\ell}(\omega) &= E\left[\exp\left(j\omega\alpha_\ell^2\mu_\ell\right)\right] \\ &= \int_{-\infty}^{\infty} \exp\left(j\omega\alpha_\ell^2\mu_\ell\right) p(\epsilon_\ell) d\epsilon_\ell \end{aligned} \tag{B.4}$$

is the CF of the signal for the ℓ-th path. After some manipulations, the BER conditioned on $\{\alpha_\ell\}$, can be represented by

$$\Pr(e|\{\alpha_\ell\}) = \frac{1}{2} - \frac{1}{\pi} \int_0^\infty \frac{R(\omega)\sin\Theta(\omega)}{\omega} \exp\left(-A\omega^2\right) d\omega, \tag{B.5}$$

where $A \triangleq \frac{\sum_{\ell=0}^{L-1}\alpha_\ell^2}{4E_p/N_0}$, $R(\omega) = \prod_{\ell=0}^{L-1}\sqrt{U_\ell^2(\omega)+V_\ell^2(\omega)}$, $\Theta(\omega) = \sum_{\ell=0}^{L-1}\arctan\left[\frac{V_\ell(\omega)}{U_\ell(\omega)}\right]$, and

$$U_\ell(\omega) = \int_{-\infty}^{\infty}\cos\left(\omega\alpha_\ell^2\mu_\ell\right)p(\epsilon_\ell)d\epsilon_\ell, \tag{B.6}$$

$$V_\ell(\omega) = \int_{-\infty}^{\infty}\sin\left(\omega\alpha_\ell^2\mu_\ell\right)p(\epsilon_\ell)d\epsilon_\ell. \tag{B.7}$$

An alternative expression of (B.5) can be written as

$$\Pr(e|\{\alpha_\ell\}) = \frac{1}{2}\text{erfc}\left(\sqrt{\frac{E_p}{N_0}\sum_{\ell=0}^{L-1}\alpha_\ell^2}\right) + \frac{1}{\pi}\int_0^{\infty} g(\omega)\exp\left(-A\omega^2\right)d\omega, \tag{B.8}$$

with

$$g(\omega) = \frac{\sin\left(\omega\sum_{\ell=0}^{L-1}\alpha_\ell^2\right) - R(\omega)\sin\Theta(\omega)}{\omega}. \tag{B.9}$$

The integral in (B.8) is a Gauss-Hermite format which can be calculated effectively by the Hermite formula [55]. Thus, the BER conditioned on $\{\alpha_\ell\}$ becomes a closed form

$$\Pr(e|\{\alpha_\ell\}) = \frac{1}{2}\text{erfc}\left(\sqrt{\frac{E_p}{N_0}\sum_{\ell=0}^{L-1}\alpha_\ell^2}\right) + \frac{1}{\pi\sqrt{A}}\sum_{i=1}^{\bar{N}} H_{x_i} g\left(\frac{x_i}{\sqrt{A}}\right), \tag{B.10}$$

where $\bar{N}$ is the order of the Hermite polynomial, x_i and H_{x_i} are respectively the zeros and weight factors of the i-th order Hermite polynomial.

Note that in (B.10), the first term is the error rate without estimation errors, and the second one is affected by the path delay estimation errors. It is shown that the channel path delay error diminishes the capability of the Rake receiver to capture the multipath diversity. The unconditional BER is obtained by averaging over the channel realization ensembles. It is worth stressing that this analysis is applicable to arbitrary UWB pulse waveforms.

REFERENCES

[1] *Special issue on UWB*, vol. 20, no. 9. IEEE J. Select. Areas Commun., Dec. 2002.

[2] *Special issue on UWB - state of the art*, vol. 2005, no. 3. EURASIP J. Applied Signal Processing, Mar. 2005.

[3] *Ultra Wideband Systems and Technologies, 2002. Digest of Papers.* Proc. IEEE Conf. Ultra Wideband Systems and Technology (UWBST), May 2002.

[4] *Ultra Wideband Systems and Technologies, 2003. Digest of Papers.* Proc. IEEE Conf. Ultra Wideband Systems and Technology (UWBST), Nov. 2003.

[5] *2004 International Workshop on Ultra Wideband Systems Joint with Conference on Ultra Wideband Systems and Technologies.* Proc. IEEE Conf. Joint UWBST and IWUWBS, May 2004.

[6] L. Yang and G. B. Giannakis, "Ultra-wideband communications: an idea whose time has come," *IEEE Signal Processing Mag.*, vol. 21, no. 6, pp. 26–54, Nov. 2004.

[7] S. Roy, J. Foerster, V. Somayazulu, and D. Leeper, "Ultrawideband radio design: the promise of high-speed, short-range wireless connectivity," *Proc. IEEE*, vol. 92, no. 2, pp. 295–311, Feb. 2004.

[8] K. Mandke, H. Nam, L. Yerramneni, C. Zuniga, and T. Rappaport, "Technology report: 'the evolution of ultra wide band radio for wireless personal area networks'," *High Frequency Electronics*, vol. 2, no. 5, pp. 22–32, Sept. 2003.

[9] D. Porcino and W. Hirt, "Ultra-wideband radio technology: potential and challenges ahead," *IEEE Commun. Mag.*, vol. 41, no. 7, pp. 66–74, July 2003.

[10] G. Aiello and G. D. Rogerson, "Ultra-wideband wireless systems," *IEEE Microwave Mag.*, vol. 4, no. 2, pp. 36–47, June 2003.

[11] (2002, Feb.) Revision of Part 15 of the commission's rules regarding ultra-wideband transmission systems. First Report and Order. Federal Communications Commission. ET Docket 98-153, FCC 02-48.

[12] M. Z. Win and R. A. Scholtz, "Ultra-wide bandwidth time-hopping spread-spectrum impulse radio for wireless multiple-access communications," *IEEE Trans. Commun.*, vol. 48, no. 4, pp. 679–691, Apr. 2000.

[13] UWB Forum. [Online]. Available: http://www.uwbforum.org

[14] R. Fisher, R. Kohno, H. Ogawa, H. Zhang, K. Takizawa, M. McLaughlin, and M. Welborn. (2004, July) DS-UWB Physical Layer Submission to 802.15 Task Group 3a. [Online]. Available: ftp://ieee:wireless@ftp.802wirelessworld.com/15/04/15-04-0137-03-003a-merger2-proposal-ds-uwb-update.doc

[15] Multiband OFDM Alliance (MBOA). [Online]. Available: http://www.multibandofdm.org

[16] A. Batra, J. Balakrishnan, G. R. Aiello, J. R. Foerster, and A. Dabak, "Design of a multiband OFDM system for realistic UWB channel environments," *IEEE Trans. Microwave Theory Tech.*, vol. 52, no. 9, pp. 2123–2138, Sept. 2004.

[17] A. Batra *et al.* (2004, Sept.) Multi-band OFDM Physical Layer Proposal for IEEE 802.15 Task Group 3a. [Online]. Available: ftp://ieee:wireless@ftp.802wirelessworld.com/15/04/15-04-0493-01-003a-multi-band-ofdm-cfp-document-update.zip

[18] A. F. Molisch, Y. G. Li, Y.-P. Nakache, P. Orlik, M. Miyake, Y. Wu, S. Gezici, H. Sheng, S. Y. Kung, H. Kobayashi, H. V. Poor, A. Haimovich, and J. Zhang, "A low-cost time-hopping impulse radio system for high data rate transmission," *EURASIP J. Applied Signal Processing: Special Issue on UWB - State of the Art*, no. 3, pp. 397–412, Mar. 2005.

[19] IEEE 802.15 WPAN High Rate Alternative PHY Task Group 3a (TG3a). [Online]. Available: http://www.ieee802.org/15/pub/TG3a.html

[20] IEEE 802.15 WPAN Low Rate Alternative PHY Task Group 4a (TG4a). [Online]. Available: http://www.ieee802.org/15/pub/TG4a.html

[21] IEEE P802.15 Working Group for Wireless Personal Area Networks (WPANs). (2003, Feb.) Channel modeling sub-committee report final. [Online]. Available: http://www.ieee802.org/15/pub/2003/Mar03/02490r1P802-15_SG3a-Channel-Modeling-Subcommittee-Report-Final.zip

[22] IEEE P802.15 Study Group 4a for Wireless Personal Area Networks (WPANs). (2004, Sept.) IEEE 802.15.4a channel model subgroup final report. [Online]. Available: ftp://ieee:wireless@ftp.802wirelessworld.com:/15/04/15-04-0535-00-004a-tg4a-channel-model-final-report.pdf

[23] S. S. Ghassemzadeh, L. J. Greenstein, T. Sveinsson, and V. Tarokh, "An impulse response model for residential wireless channels," in *Proc. Global Telecommun. Conf. (GLOBECOM'03)*, vol. 3, Dec. 2003, pp. 1211–1215.

[24] D. Cassioli, M. Z. Win, and A. F. Molisch, "The ultra-wide bandwidth indoor channel: From statistical model to simulations," *IEEE J. Select. Areas Commun.*, vol. 20, no. 6, pp. 1247–1257, Aug. 2002.

[25] A. A. M. Saleh and R. A. Valenzuela, "A statistical model for indoor multipath propagation," *IEEE J. Select. Areas Commun.*, vol. SAC-5, no. 2, pp. 128–137, Feb. 1987.

[26] C. Carbonelli, U. Mengali, and U. Mitra, "Synchronization and channel estimation for UWB signals," in *Proc. IEEE Global Telecommun. Conf. (GLOBECOM'03)*, vol. 2, Dec. 2003, pp. 764–768.

[27] Z. Irahhauten, H. Nikookar, and G. Janssen, "An overview of ultra wide band indoor channel measurements and modeling," *IEEE Microwave Wireless Compon. Lett.*, vol. 14, no. 8, pp. 386–388, Aug. 2004.

[28] M. Z. Win and R. A. Scholtz, "On the robustness of ultra-wide bandwidth signals in dense multipath environments," *IEEE Commun. Lett.*, vol. 2, no. 2, pp. 51–53, Feb. 1998.

[29] J. R. Foerster, E. Green, S. Somayazulu, and D. Leeper, "Ultra-wideband technology for short- or medium-range wireless communications," *Intel Technology Journal*, pp. 1–11, 2nd Quarter, 2001.

[30] L. Zhao and A. M. Haimovich, "Performance of ultra-wideband communications in the presence of interference," *IEEE J. Select. Areas Commun.*, vol. 20, no. 9, pp. 1684–1691, Dec. 2002.

[31] G. Lu, P. Spasojevic, and L. Greenstein, "Antenna and pulse designs for meeting UWB spectrum density requirements," in *Proc. IEEE Ultra Wideband Systems and Technologies (UWBST'03)*, Reston, Virginia, Nov. 2003, pp. 162–166.

[32] R. Scholtz, "Multiple access with time-hopping impulse modulation," in *Proc. IEEE Military Commun. Conf. (MILCOM'93)*, vol. 2, Oct. 1993, pp. 447–450.

[33] J. G. Proakis, *Digital Communications*, 3rd ed. New York: McGraw-Hill, 1995.

[34] L. B. Michael, M. Ghavami, and R. Kohno, "Multiple pulse generator for ultra-wideband communication using Hermite polynomial based orthogonal pulses," in *Proc. IEEE Conference on Ultra Wideband Systems and Technologies (UWBST'02)*, Baltimore, MD, May 2002, pp. 47–51.

[35] B. Parr, B. Cho, K. Wallace, and Z. Ding, "A novel ultra-wideband pulse design algorithm," *IEEE Commun. Lett.*, vol. 7, no. 5, pp. 219–221, May 2003.

[36] M. Welborn and J. McCorkle, "The importance of fractional bandwidth in ultra-wideband pulse design," in *Proc. IEEE Int. Conf. Commun. (ICC'02)*, vol. 2, New York, New York, Apr. 2002, pp. 753–757.

[37] T. S. Rappaport, *Wireless Communications: Principles and Practice*. Upper Saddle River, NJ: Prentice-Hall, 1996.

[38] N. Lehmann and A. M. Haimovich, "New approach to control the power spectral density of a time hopping UWB signal," in *37th Conference on Information Sciences and Systems (CISS'03)*, Baltimore, Maryland, Mar. 2003.

[39] Y.-P. Nakache and A. F. Molisch, "Spectral shape of UWB signals-influence of modulation format, multiple access scheme and pulse shape," in *Proc. IEEE Semiannual Veh. Technol. Conf. (VTC)*, vol. 4, Apr. Spring, 2003, pp. 2510–2514.

[40] M. Z. Win, "A unified spectral analysis of generalized time-hopping spread-spectrum signals in the presence of timing jitter," *IEEE J. Select. Areas Commun.*, vol. 20, pp. 1664–1676, Dec. 2002.

[41] S. G. Wilson, *Digital Modulation and Coding*. Upper Saddle River, NJ: Prentice-Hall, 1996.

[42] J. D. Choi and W. E. Stark, "Performance of ultra-wideband communications with suboptimal receivers in multipath channels," *IEEE J. Select. Areas Commun.*, vol. 20, no. 9, pp. 1754–1766, Dec. 2002.

[43] G. J. Foschini and M. J. Gans, "On limits of wireless communications in a fading environment when using multiple antennas," *Wirel. Pers. Commun.*, vol. 6, no. 3, pp. 311–335, 1998.

[44] L. Zhao and A. M. Haimovich, "Capacity of M-ary PPM ultra-wideband communications over AWGN channels," in *Proc. IEEE Semiannual Veh. Technol. Conf. (VTC)*, vol. 2, Atlantic City, New Jersey, Fall, 2001, pp. 1191–1195.

[45] L. Zhao, A. M. Haimovich, and M. Z. Win, "Capacity of ultra-wide bandwidth communications over multipath channels," in *Proc. IEEE International Symposium on Advances in Wireless Communications (ISWC'02)*, Victoria, Canada, Sept., 23-24 2002.

[46] L. Zhao and A. M. Haimovich, "The capacity of an UWB multiple-access communications system," in *Proc. IEEE Int. Conf. Commun.*, vol. 3, Apr. 2002, pp. 1964–1968, New York, NY.

[47] J. L. Massey, "Towards an information theory of spread-spectrum systems," in *Code Division Multiple Access Communications*, S. G. Glisic and P. A. Leppnen, Eds. Boston, Dordrecht and London: Kluwer, 1995, pp. 29–46.

[48] M. Médard and R. G. Gallager, "Bandwidth scaling for fading multipath channels," *IEEE Trans. Inform. Theory*, vol. 48, no. 4, pp. 840–852, Apr. 2002.

[49] S. Verdú, "Spectral efficiency in the wideband regime," *IEEE Trans. Inform. Theory*, vol. 48, no. 6, pp. 1319–1343, June 2002.

[50] V. V. Veeravalli and A. Mantravadi, "The coding-spreading tradeoff in CDMA systems," *IEEE J. Select. Areas Commun.*, vol. 20, no. 2, pp. 396–408, Feb. 2002.

[51] S. Verdú and S. Shamai, "Spectral efficiency of CDMA with random spreading," *IEEE Trans. Inform. Theory*, vol. 45, no. 2, pp. 622–640, Mar. 1999.

[52] D. Porrat and D. N. C. Tse, "Bandwidth scaling in ultra wideband communications," in *Proc. 41st Annual Allerton Conference on Commun., Control, and Computing*, Allerton House, Monticello, IL, Oct. 2003, pp. 1104–1113.

[53] H. Sheng, P. Orlik, A. M. Haimovich, L. Cimini, and J. Zhang, "On the spectral and power requirements for ultra-wideband transmission," in *Proc. IEEE Int. Conf. Commun. (ICC'03)*, vol. 1, Anchorage, AK., May 2003, pp. 738–742.

[54] S. Dolinar, D. Divsalar, J. Hamkins, and F. Pollara, "Capacity of pulse-position modulation (PPM) on Gaussian and Webb channels," JPL TMO, Tech. Rep. 42-142, August 15, 2000.

[55] M. Abramowitz and I. A. Stegun, Eds., *Handbook of Mathematical Functions with Formulas, Graphs, and Mathematical Tables*, 10th ed. Government Printing Office, 1972.

[56] S. Benedetto and E. Biglieri, *Principles of Digital Transmission: with Wireless Applications*. Kluwer Academic Publishers, 1999.

[57] M. Z. Win and R. A. Scholtz, "On the energy capture of ultrawide bandwidth signals in dense multipath environments," *IEEE Commun. Lett.*, vol. 2, no. 9, pp. 245–247, Sept. 1998.

[58] D. Cassioli, M. Z. Win, F. Vatalaro, and A. F. Molisch, "Performance of low-complexity rake reception in a realistic UWB channel," in *Proc. IEEE Int. Conf. Commun. (ICC'02)*, vol. 2, New York, NY., 2002, pp. 763–767.

[59] J. Bellorado, S. S. Ghassemzadeh, L. J. Greenstein, T. Sveinsson, and V. Tarokh, "Coexistence of ultra-wideband systems with IEEE-802.11a wireless LANs," in *Proc. IEEE Global Telecommun. Conf. (GLOBECOM'03)*, vol. 1, Dec. 2003, pp. 410–414.

[60] J. H. Winters, "Optimum combining in digital mobile radio with cochannel interference," *IEEE J. Select. Areas Commun.*, vol. SAC-2, no. 4, pp. 528–539, July 1984.

[61] Q. Li and L. A. Rusch, "Multiuser detection for DS-CDMA UWB in the home environment," *IEEE J. Select. Areas Commun.*, vol. 20, no. 9, pp. 1701–1711, Dec. 2002.

[62] I. Bergel, E. Fishler, and H. Messer, "Narrow-band interference suppression in time hopping impulse radio systems," in *Proc. IEEE Conf. Ultra Wideband Systems and Technology*, Baltimore, USA, May 2002, pp. 303–308.

[63] A. M. Haimovich and A. Vadhri, "Rejection of narrow-band interference in PN spread spectrum systems using an eigenanalysis approach," in *Proc. IEEE Military Commun. Conf. (MILCOM'94)*, vol. 3, Fort Monmouth, NJ, Oct. 1994, pp. 1002–1006.

[64] A. F. Molisch, Y.-P. Nakache, P. Orlik, J. Zhang, Y. Wu, S. Gezici, S. Y. Kung, H. V. Poor, Y. G. Li, H. Sheng, and A. Haimovich, "An efficient low-cost time-hopping impulse radio for high data rate transmission," in *The 6th International Symposium on Wireless Personal Multimedia Communications (WPMC)*, Yokosuka, Kanagawa, Japan, Oct. 2003.

[65] S. Verdu, *Multiuser Detection*. Cambridge University Press, 1998.

[66] J. E. Hudson, *Adaptive Array Principles*. Peter Peregrinus Ltd., 1981.

[67] R. A. Monzingo and T. W. Miller, *Introduction to Adaptive Arrays*. New York: John Wiley and Sons, 1980.

[68] A. M. Haimovich, "The eigencanceler: adaptive radar by eigenanalysis methods," *IEEE Trans. Aerosp. Electron. Syst.*, vol. 32, no. 2, pp. 532–542, April 1996.

[69] H. Sheng, A. M. Haimovich, A. F. Molisch, and J. Zhang, "Optimum combining for time hopping impulse radio UWB Rake receivers," in *Proc. IEEE Conference on Ultra Wideband Systems and Technologies (UWBST'03)*, Reston, Virginia, Nov. 2003.

[70] R. J.-M. Cramer, R. A. Scholtz, and M. Z. Win, "Evaluation of an ultra-wide-band propagation channel," *IEEE Trans. Antennas Propagat.*, vol. 50, no. 5, pp. 561–570, May 2002.

[71] A. F. Molisch, J. R. Foerster, and M. Pendergrass, "Channel models for ultrawideband personal area networks," *IEEE Wireless Commun.*, vol. 10, no. 6, pp. 14–21, Dec. 2003.

[72] V. Lottici, A. D'Andrea, and U. Mengali, "Channel estimation for ultra-wideband communications," *IEEE J. Select. Areas Commun.*, vol. 20, no. 9, pp. 1638–1645, Dec. 2002.

[73] M. J. Gans, "The effect of Gaussian error in maximal ratio combiners," *IEEE Trans. Commun. Technol.*, vol. COM-19, no. 4, pp. 492–500, Aug. 1971.

[74] B. R. Tomiuk, N. C. Beaulieu, and A. A. Abu-Dayya, "General forms for maximal ratio diversity with weighting errors," *IEEE Trans. Commun.*, vol. 47, no. 4, pp. 488–492, Apr. 1999.

[75] R. K. Mallik, D. Singh, and A. Kumari, "Analysis of Rake reception with multiple symbol weight estimation for antipodal signaling," *IEEE Trans. Commun.*, vol. 51, no. 10, pp. 1721–1729, Oct. 2003.

[76] R. Annavajala and L. B. Milstein, "On the performance of diversity combining schemes on Rayleigh fading channels with noisy channel estimates," in *Proc. IEEE Military Commun. Conf. (MILCOM'03)*, vol. 1, Oct. 2003, pp. 320–325.

[77] W. M. Gifford, M. Z. Win, and M. Chiani, "Diversity with pilot symbol assisted channel estimation," in *Proc. the 38th Annual Conf. Inform. Sciences and Systems (CISS'04)*, Princeton, New Jersey, Mar. 2004, pp. 101–105.

[78] L. Yang and G. B. Giannakis, "Optimal pilot waveform assisted modulation for Ultrawideband communications," *IEEE Trans. Wireless Commun.*, vol. 3, no. 4, pp. 1236–1249, July 2004.

[79] J. D. Choi and W. E. Stark, "Performance of UWB communications with imperfect channel estimation," in *Proc. IEEE Military Commun. Conf. (MILCOM'03)*, vol. 2, Oct. 2003, pp. 915–920.

[80] C. Carbonelli, S. Vedantam, and U. Mitra, "Sparse channel estimation with zero tap detection," in *Proc. IEEE Int. Conf. Commun. (ICC'04)*, vol. 6, Paris, France, June 2004, pp. 3173–3177.

[81] J. R. Foerster, "The effects of multipath interference on the performance of UWB systems in an indoor wireless channel," in *Proc. IEEE 53rd Veh. Technol. Conf. (VTC Spring'01)*, vol. 2, May 2001, pp. 1176–1180.

[82] S. M. Kay, *Fundamentals of Statistical Signal Processing: Estimation Theory.* Upper Saddle River, New Jersey: Prentice-Hall, 1993.

[83] J. G. Proakis, "Probabilities of error for adaptive reception of M-phase signals," *IEEE Trans. Commun. Technol.*, vol. COM-16, no. 1, pp. 71–81, Feb. 1968.

[84] M. K. Simon and M.-S. Alouini, *Digital Communication over Fading Channels: A Unified Approach to Performance Analysis.* John Wiley & Sons, Inc., 2000.

[85] R. Price, "Error probabilities for adaptive multichannel reception of binary signals," *IRE Trans. Inform. Theory*, vol. 8, no. 6, pp. 387–389, Oct. 1962.

[86] M. Z. Win, G. Chrisikos, and N. R. Sollenberger, "Performance of Rake reception in dense multipath channels: Implications of spreading bandwidth and selection diversity order," *IEEE J. Select. Areas Commun.*, vol. 18, no. 8, pp. 1516–1525, Aug. 2000.

[87] D. Cassioli, M. Z. Win, F. Vatalaro, and A. F. Molisch, "Effects of spreading bandwidth on the performance of UWB Rake receivers," in *Proc. IEEE Int. Conf. Commun. (ICC'03)*, vol. 5, Anchorage, AK., May 2003, pp. 3545–3549.

[88] W. C. Lau, M.-S. Alouini, and M. K. Simon, "Optimum spreading bandwidth for selective RAKE reception over Rayleigh fading channels," *IEEE J. Select. Areas Commun.*, vol. 19, no. 6, pp. 1080–1089, June 2001.

[89] M. Z. Win and Z. A. Kostić, "Impact of spreading bandwidth on Rake reception in dense multipath channels," *IEEE J. Select. Areas Commun.*, vol. 17, no. 10, pp. 1794–1806, Oct. 1999.

[90] I. E. Telatar and D. N. C. Tse, "Capacity and mutual information of wideband multipath fading channels," *IEEE Trans. Inform. Theory*, vol. 46, no. 4, pp. 1384–1400, July 2000.

[91] J. H. Reed, *An Introduction to Ultra Wideband Communication Systems.* Prentice Hall PTR, 2005.

[92] M.-G. D. Benedetto and G. Giancola, *Understanding Ultra Wide Band Radio Fundamentals*, 1st ed., ser. Prentice Hall Communications Engineering and Emerging Technologies Series. Prentice Hall PTR, June 2004. [Online]. Available: http://authors.phptr.com/dibenedetto

[93] H. Kim, D. Park, and Y. Joo, "All-digital low-power CMOS pulse generator for UWB system," *Electronics Letters*, vol. 40, no. 24, pp. 1534–1535, Nov. 2004.

[94] N. Lehmann, "Approaches for ultra-wide bandwidth data transmission," Master's thesis, University Karlsruhe and New Jersey Institute of Technology, May 2003.

[95] A. Taha, "Performance considerations of wireless multiple-access digital impulse radio under realistic multipath channels," Ph.D. dissertation, University of South California, May 2003.

[96] C.-H. Tsai, "Ultra-wideband technologies and their performance analysis," Master's thesis, National Sun Yat-Sen University, Aug. 2004.

[97] J. Bellorado, S. S. Ghassemzadeh, A. Kavčić, B. Tarokh, and V. Tarokh, "Time-hopping sequence design for narrowband interference suppression," in *IEEE Vehicular Technology (VTC'04)*, Los Angeles, CA, Sept. 2004.

[98] Y. Chen, J. Chen, and T. Lv, "A high order bi-phase modulation scheme for UWB transmission," in *IEEE Vehicular Technology (VTC'04)*, Los Angeles, CA, Sept. 2004.

[99] M. P. Green and P. Wang, "Ultra-wideband: Principles, practices and potential," in *Proceedings of SPIE - The International Society for Optical Engineering*, vol. 5284, Apr. 2004, pp. 83–94.

[100] N. Lehmann and A. M. Haimovich, "The power spectral density of a time hopping UWB signal: A survey," in *IEEE Conference on Ultra Wideband Systems and Technologies (UWBST'03)*, Reston, Virginia, Nov. 2003, pp. 234–239.

[101] L. D. Nardis, G. Giancola, and M.-G. D. Benedetto, "Power limits fulfillment and MUI reduction based on pulse shaping in UWB networks," in *IEEE International Conference on Communications*, vol. 6, June 2004, pp. 3576–3580.

[102] A. Taha and K. M. Chugg, "On the power spectral density of wireless multiple-access UWB impulse radio under realistic propagation conditions," in *IEEE 58th Vehicular Technology Conference (VTC 2003-Fall)*, vol. 2, Oct. 2003, pp. 1298–1302.

[103] T. Wang and Y. Wang, "Capacity of M-ary PAM impulse radio with various derivatives of Gaussian pulse subject to FCC spectral masks," in *International Symposium on Computers and Communications*, vol. 2, 2004, pp. 696–702.

[104] J.-Y. Lee and S. Choi, "Through-material propagation characteristic and time resolution of UWB signal," in *2004 International Workshop on Ultra Wideband Systems; Joint with Conference on Ultra Wideband Systems and Technologies, Joint UWBST and IWUWBS*, May 2004, pp. 71–75.

[105] E. Cano and S. McGrath, "TH-UWB and DS-UWB in lognormal fading channel and 802.11a interference," in *IEEE International Symposium on Personal, Indoor and Mobile Radio Communications (PIMRC)*, vol. 4, Sept. 2004, pp. 2978–2982.

[106] G. D. Forney and G. Ungerboeck, "Modulation and coding for linear Gaussian channels," *IEEE Trans. Inform. Theory*, vol. 44, no. 6, pp. 2384–2415, Oct. 1998.

[107] A. M. Haimovich, A. Shah, and X. Wu, "Reduced-rank array processing for wireless communications with applications to IS-54/IS-136," *IEEE Trans. Commun.*, vol. 48, no. 5, pp. 743–747, May 2000.

[108] D. C. M. Lee, J. M. Kahn, and M. D. Audeh, "Trellis-coded pulse-position modulation for indoor wireless infrared communications," *IEEE Trans. Commun.*, vol. 45, no. 9, pp. 1080–1087, Sept. 1997.

[109] A. Annamalai and C. Tellambura, "Analysis of hybrid selection/maximal-ratio diversity combiners with Gaussian errors," *IEEE Trans. Wireless Commun.*, vol. 1, no. 3, pp. 498–511, July 2002.

[110] S. Hoyos, B. M. Sadler, and G. R. Arce, "High-speed A/D conversion for ultra-wideband signals based on signal projection over basis functions," in *Proc. IEEE Int. Conf. Acoustics, Speech, and Signal Processing (ICASSP'04)*, vol. 4, May 2004, pp. iv–537–540.

[111] H. Sheng, R. You, and A. M. Haimovich, "Performance analysis of ultra-wideband Rake receivers with channel delay estimation errors," in *Proc. the 38th Annual Conference on Information Sciences and Systems (CISS'04)*, Princeton, New Jersey, Mar. 2004, pp. 921–926.

[112] I. Guvenc and H. Arslan, "Performance evaluation of UWB systems in the presence of timing jitter," in *Proc. IEEE Conference on Ultra Wideband Systems and Technologies (UWBST'03)*, Reston, Virginia, Nov. 2003.

[113] W. Lovelace and J. K. Townsend, "The effects of timing jitter and tracking on the performance of impulse radio," *IEEE J. Select. Areas Commun.*, vol. 20, no. 9, pp. 1646–1651, Dec. 2002.

[114] Y. Yin, J. P. Fonseka, and I. Korn, "Sensitivity to timing errors in EGC and MRC techniques," *IEEE Trans. Commun.*, vol. 51, no. 4, pp. 530–534, Apr. 2003.

[115] J. Gil-Pelaez, "Note on the inversion theorem," *Biometrika*, vol. 38, no. 3/4, pp. 481–482, Dec. 1951.

[116] Q. T. Zhang, "Probability of error for equal-gain combiners over Rayleigh channels: some closed-form solutions," *IEEE Trans. Commun.*, vol. 45, no. 3, pp. 270–273, Mar. 1997.